

# **BRANCHING RATIO MEASUREMENT FOR RARE ANNIHILATION DECAY**

**Thesis**

**Submitted to Punjab Agricultural University  
in partial fulfillment of the requirements  
for the degree of**

**MASTER OF SCIENCE  
in  
PHYSICS  
(Minor subject: Mathematics)**

**By  
Titiksha Dua  
(L-2016-BS-302-M)**

**Department of Mathematics, Statistics and Physics  
College of Basic Sciences and Humanities  
PUNJAB AGRICULTURAL UNIVERSITY  
LUDHIANA-141004**

**2019**

## **CERTIFICATE-I**

This is to certify that the thesis entitled, “**Branching ratio measurement for rare annihilation decay**”, submitted for the degree of M.Sc. in the subject of **Physics** (Minor Subject: **Mathematics**) of the Punjab Agricultural University, Ludhiana, is a bonafide research work carried out by **Titiksha Dua (L-2016-BS-302-M)** under my supervision and that no part of this thesis has been submitted for any other degree.

The assistance and help received during the course of investigation has been fully acknowledged.

---

**Dr Rajeev Kumar**

**(Major Advisor)**

Assistant Professor of Physics  
Dept of Math., Stat. and Physics  
Punjab Agricultural University  
Ludhiana-141004

## **CERTIFICATE-II**

This is to certify that the thesis entitled, “**Branching ratio measurement for rare annihilation decay**”, submitted by **Titiksha Dua** (Admn. No. **L-2016-BS-302-M**) to the Punjab Agricultural University, Ludhiana, in partial fulfilment of the requirements for the degree of **M.Sc.** in the subject of **Physics** (Minor Subject: **Mathematics**) has been approved by the Student’s Advisory Committee after an oral examination on the same.

---

**Dr Rajeev Kumar**  
(Major Advisor)

---

**Dr Vipin Bhatnagar**  
(External Examiner)  
Professor of Physics  
Department of Physics  
Panjab University  
Chandigarh-160014

---

**Dr Sukhjinder Singh Sidhu**  
(Head of the Department)

---

**Dr (Mrs) Gurinder Kaur Sangha**  
(Dean, Postgraduate Studies)

## ACKNOWLEDGEMENT

*I take this opportunity to thank God for granting me the capability to proceed this work, and some important people in my life who made immense contribution in shaping me to who I am, which essentially made possible the successful completion of this thesis.*

*Firstly, I'd like to express my gratitude and sincerest thanks to my Major Advisor Asst. Prof. Dr Rajeev K.Sharma for opening the doors of beautiful field of High Energy Physics to me and giving me the opportunity to carry out this research. Sir has superb insight on physics; without his invaluable guidance and patience, it wouldn't have been possible to carry out the analysis. I'd like to mention that he is a very refined person and has been very polite and gave me ample space to work at my pace, but also encouraged me when my progress slowed. His hard work and dedication towards research is hugely motivating.*

*I am thankful to Dr. Paramjit Singh, Professor and Dean PGS nominee and Dr Kiran Jeet, Asst. Prof of Nanotechnology, PAU for their motivation and invaluable suggestions during the tenure of my research.*

*I wish to thank Belle Group, KEK, Japan for allowing us to work on this analysis and fruitful comments.*

*I would like to thank Dr. Kavita Lalwani (MNIT, Jaipur) for giving me the great opportunity to attend the BAW-2017, held at MNIT, Jaipur during which I learnt a lot from the Belle Indian Group. This short visit proved to be great experience and I cannot forget to thank Dr. Saurabh Sandilya (University of Cincinnati), Renu di (PU) and all others for their guidance.*

*A person is nothing without family and friends. I owe the most to my parents who instilled in me the learning spirit and the necessary morals; my siblings who have always supported me by all means. My school, Kundan Vidya Mandir, holds a bigger credit for shaping me. Thanks to all my teachers, friends and cousins, for I am nothing without them. My cousin, Ashish Ahuja deserves a special mention, who has been my constant guide in all ways and also helped me adopt the computer skills needed for the research.*

*I am thankful to Punjab Agricultural University for introducing research at the Master's level. I am grateful to all the worthy faculty members of the Dept. of Mathematics, Statistics and Physics, PAU, Ludhiana for their unending support and welcoming behaviour. My sincere thanks are due to Mrs. Arvinder Kaur for she helped me in every way for the thesis and otherwise.*

**Place :**

**Date :**

**Titiksha**

Title of the Thesis	: Branching ratio measurement for rare annihilation decay
Name of the Student and	: Titiksha Dua
Admission No.	: L-2016-BS-302-M
Major Subject	: Physics
Minor Subject	: Mathematics
Name and Designation of Major Advisor	: Dr. Rajeev Kumar (Assistant Professor)
Degree to be Awarded	: Master of Science
Year of award of Degree	: 2019
Total Pages in Thesis	: 77
Name of University	: Punjab Agricultural University, Ludhiana – 141004, Punjab, India

### ABSTRACT

The research is based on study of the rare radiative decay  $B^0 \rightarrow J/\psi\gamma$ , using data collected (corresponding to  $772 \times 10^6 B\bar{B}$  pairs) by the Belle detector at  $Y(4S)$  resonance at asymmetric  $e^+e^-$  collider at KEK, Japan during its long run. In this annihilation decay, there is potential sign of New Physics from the possibility of (V+A) charged current admixture to the standard (V-A) current. Branching ratio measurement will help test the validity of various QCD models. A large Monte Carlo sample is generated to determine the signal reconstruction efficiency, which is obtained as  $33.9 \pm 0.19\%$ . The energy difference,  $\Delta E = E_B^* - E_{beam}^*$ , the beam-constrained mass  $M_{bc} = \sqrt{E_{beam}^{*2} - p_B^{*2}}$  and helicity ( $\cos \theta$ ) of  $J/\psi$  are used for signal extraction, where  $E_{beam}^*$  is the run dependent beam energy,  $E_B^*$  and  $p_B^*$  are the reconstructed energy and momentum, respectively of the  $B$  meson candidates in the center-of-mass frame. The peaking background in the signal region is dominated by  $B^0 \rightarrow J/\psi \pi^0$  ( $\pi^0 \rightarrow \gamma\gamma$ ),  $B^0 \rightarrow J/\psi \eta$  ( $\eta \rightarrow \gamma\gamma$ ) mainly and also  $B^0 \rightarrow J/\psi K_L$  ( $K_L \rightarrow 3\pi^0$  or  $6\gamma$ ) and  $B^0 \rightarrow J/\psi K_S$  and other combinatorial backgrounds. To suppress these backgrounds, we vetoed these photons that when combine with another photon of energy  $E_\gamma > 60 \text{ MeV}$  and form a  $\pi^0(\eta)$  candidate. Whereas,  $B \rightarrow J/\psi K_S$  and  $B \rightarrow J/\psi K_L$  are not peaking in  $\Delta E$  but are peaking in  $M_{bc}$  signal region. The peaking backgrounds  $B \rightarrow J/\psi \eta$  and  $B \rightarrow J/\psi \pi^0$  correspond to  $103.56 \pm 3.29$  events.

**Keywords:** Belle detector, KEK,  $B$  mesons, V+A current, helicity.

---

Signature of Major Advisor

---

Signature of the Student

ਬੀਸਿਸ ਦਾ ਟਾਈਟਲ	: ਬਰਾਂਚਿੰਗ ਰੇਸ਼ੇ ਮੇਅਸੂਰੇਮੈਂਟ ਰੇਅਰ ਅੰਨਿਹਿਲੇਸ਼ਨ ਡਿਕੇਅ ਲਈ
ਵਿਦਿਆਰਥੀ ਦਾ ਨਾਮ ਅਤੇ ਪ੍ਰਵੇਸ਼ ਨੰਬਰ	: ਤਿਤਿਕਸ਼ਾ ਦੂਆ ਐਲ-2016-ਬੀ ਐਸ-302-ਐਮ
ਮੇਜਰ ਵਿਸ਼ਾ	: ਭੌਤਿਕੀ
ਮਾਮੂਲੀ ਵਿਸ਼ਾ	: ਗਣਿਤ
ਮੁੱਖ ਸਲਾਹਕਾਰ ਦਾ ਨਾਮ ਅਤੇ ਅਹੁਦਾ	: ਡਾ. ਰਾਜੀਵ ਕੁਮਾਰ (ਸਹਾਇਕ ਪ੍ਰੋਫੈਸਰ)
ਦਿੱਤੀ ਜਾਣ ਵਾਲੀ ਡਿਗਰੀ	: ਮਾਸਟਰ ਆਫ਼ ਸਾਇੰਸ
ਡਿਗਰੀ ਮਿਲਣ ਦਾ ਸਾਲ	: 2019
ਬੀਸਿਸ ਵਿੱਚ ਕੁੱਲ ਪੰਨੇ	: 77
ਯੂਨੀਵਰਸਿਟੀ ਦਾ ਨਾਂ	: ਪੰਜਾਬ ਖੇਤੀਬਾੜੀ ਯੂਨੀਵਰਸਿਟੀ, ਲੁਧਿਆਣਾ – 141004, ਪੰਜਾਬ, ਭਾਰਤ

#### ਸਾਰਾਂਸ਼

ਇਹ ਰਿਸਰਚ ਰੇਅਰ ਰੇਡੀਏਟਿਵ ਡਿਕੇਅ  $B^0 \rightarrow J/\psi \gamma$  ਦੇ ਅਧਿਐਨ ਤੇ ਅਧਾਰਿਤ ਹ ਜੋਕਿ ਕੇ. ਈ. ਕੇ., ਜਪਾਨ ਦੇ ਏਸਮਿਟ੍ਰਿਕ  $e^+e^-$  ਕੋਲਾਇਡਰ ਸਥਿਤ ਬੈਲ ਡਿਟੈਕਟਰ ਤੇ  $\Upsilon(4S)$  ਰੈਜ਼ੋਨੈਂਸ ਤੇ ਆਪਣੇ ਲੰਮੇ ਸਮੇਂ ਦੌਰਾਨ ਕੱਠੇ ਕੀਤੇ ਡਾਟੇ ਦੇ ਅਧਾਰ ਤੇ ਕੀਤੀ ਗਈ ਹੈ (ਜਿਸ ਵਿੱਚ  $772 \times 10^6 B\bar{B}$  ਜੋੜੇ ਹਨ)। ਇਸ ਅੰਨਿਹਿਲੇਸ਼ਨ ਡਿਕੇਅ ਵਿੱਚ ਮੌਜੂਦਾ ਪ੍ਰਧਰਾਗਤ (V-A) ਕਰੰਟ ਦੇ ਨਾਲ (V+A) ਚਾਰਜ ਕਰੰਟ ਦੀ ਸੰਭਾਵਨਾ ਤੋਂ ਨਵੇਂ ਭੌਤਿਕ ਵਿਗਿਆਨ ਦਾ ਸੰਭਾਵੀ ਸੰਕੇਤ ਹੈ। ਬਰਾਂਚਿੰਗ ਰੇਸ਼ੇ ਮਾਪਣ ਨਾਲ ਵੱਖ-ਵੱਖ QCD ਮਾਡਲਾਂ ਦੀ ਪ੍ਰਮਾਣਿਕਤਾ ਦੀ ਜਾਂਚ ਕਰਨ ਵਿੱਚ ਮਦਦ ਮਿਲੇਗੀ। ਇੱਕ ਵਿਸ਼ਾਲ ਸਿਗਨਲ ਮੋਟੋ ਕਾਰਲੋ ਦਾ ਨਮੂਨਾ ਰੀਕੰਸਟ੍ਰਕਸ਼ਨ ਕੁਸ਼ਲਤਾ ਨੂੰ ਨਿਰਧਾਰਤ ਕਰਨ ਲਈ ਤਿਆਰ ਕੀਤਾ ਗਿਆ ਹੈ, ਜਿਸ ਨਾਲ ਕੁਸ਼ਲਤਾ  $33.9 \pm 0.19\%$  ਪ੍ਰਾਪਤ ਹੋਈ। ਊਰਜਾ ਫਰਕ,  $\Delta E = E_B^* - E_{beam}^*$ , ਬੀਮ-ਕੱਸਟਰੈਨਡ ਮਾਸ  $M_{bc} = \sqrt{E_{beam}^{*2} - p_B^{*2}}$  ਅਤੇ  $J/\psi$  ਦੀ ਹੈਲੀਸਿਟੀ ( $\cos \theta$ ) ਨੂੰ ਸਿਗਨਲ ਐਕਸਟਰੈਕਸ਼ਨ ਲਈ ਇਸਤੇਮਾਲ ਕੀਤਾ ਹੈ, ਜਿੱਥੇ  $E_{beam}^*$  ਰਨ ਨਿਰਭਰ ਬੀਮ ਊਰਜਾ ਹੈ,  $E_B^*$  ਅਤੇ  $p_B^*$  ਸੈਟਰ-ਆਫ-ਮਾਸ ਫਰੇਮ ਵਿੱਚ ਰੀਕੰਸਟ੍ਰਕਟਿਡ  $B$  ਮੇਸੋਨ ਦੇ ਊਰਜਾ ਤੇ ਮੋਮੈਂਟਮ ਹਨ। ਸਿਗਨਲ ਏਰੀਏ ਵਿੱਚ ਵੱਧ ਪੀਕਿੰਗ ਬੈਕਗਰਾਊਂਡ  $B^0 \rightarrow J/\psi \pi^0$  ( $\pi^0 \rightarrow \gamma\gamma$ ),  $B^0 \rightarrow J/\psi \eta$  ( $\eta \rightarrow \gamma\gamma$ ) ਮੁੱਖ ਤੌਰ ਤੇ ਹੈ ਅਤੇ  $B^0 \rightarrow J/\psi K_L$  ( $K_L \rightarrow 3\pi^0$  or  $6\gamma$ ) ਅਤੇ  $B^0 \rightarrow J/\psi K_S$  ਸਮੇਤ ਹੋਰ ਬੈਕਗਰਾਊਂਡਾਂ ਸ਼ਾਮਲ ਹਨ। ਇਹਨਾਂ ਨੂੰ ਦਬਾਉਣ ਲਈ ਅਸੀਂ ਉਨ੍ਹਾਂ ਫੋਟੋਨਾਂ ਨੂੰ ਕੱਟਿਆ ਹੈ ਜੋ ਦੂਜੇ  $E_\gamma > 60 \text{ MeV}$  ਵਾਲੇ ਫੋਟੋਨਾਂ ਨਾਲ ਜੋੜਨ ਤੇ  $\pi^0(\eta)$  ਉਮੀਦਵਾਰ ਬਣਾਉਂਦੇ ਹਨ। ਜਦਕਿ  $B \rightarrow J/\psi K_S$  ਅਤੇ  $B \rightarrow J/\psi K_L$   $\Delta E$  ਵਿੱਚ ਨਹੀਂ ਵਧ ਰਹੇ ਪਰ  $M_{bc}$  ਸਿਗਨਲ ਖੇਤਰ ਵਿੱਚ ਵਧ ਰਹੇ ਹਨ। ਬੈਕਗਰਾਊਂਡ  $B \rightarrow J/\psi \eta$  ਅਤੇ  $B \rightarrow J/\psi \pi^0$   $103.56 \pm 3.29$  ਸਮਾਗਮਾਂ ਦੇ ਅਨੁਸਾਰੀ ਹਨ।

**ਮੁੱਖ ਸ਼ਬਦ:** ਬੈਲ ਡਿਟੈਕਟਰ, ਕੇ. ਈ. ਕੇ.,  $B$  ਮੇਸੋਨ, (V+A) ਕਰੰਟ, ਹੈਲੀਸਿਟੀ।

## CONTENTS

Chapter	Title	Page
<b>I</b>	<b>INTRODUCTION</b>	<b>1-11</b>
1.1	The Standard Model	2-4
1.2	Symmetries and Conservation Laws	4-5
1.3	Broken Symmetries in Nature	5-8
1.4	$B$ mesons and $B$ -factories	8-10
1.5	Physics of the decay $B^0 \rightarrow J/\psi\gamma$	10-11
1.6	Objectives	11
<b>II</b>	<b>REVIEW OF LITERATURE</b>	<b>12-23</b>
<b>III</b>	<b>MATERIALS AND METHODS</b>	<b>24-47</b>
3.1	Path to KEKB	24
3.2	KEKB Collider	24-28
3.3	The Belle Detector	29-44
3.4	Trigger System	45
3.5	Data Acquisition System (DAQ)	45
3.6	Computer System and Software	45-47
3.7	Roadmap of Analysis	47
<b>IV</b>	<b>RESULTS AND DISCUSSION</b>	<b>48-69</b>
4.1	Hadronic Event Selection	48-50
4.2	Continuum Background Suppression	50-52
4.3	Monte Carlo Data	52
4.4	Particle Identification (PID)	52-58
4.5	Reconstruction Procedure for $B^0 \rightarrow J/\psi\gamma$	58-64
4.6	Background Study	64-68
4.7	Conclusion	69
<b>V</b>	<b>SUMMARY</b>	<b>70-72</b>
	<b>REFERENCES</b>	<b>73-77</b>

## CHAPTER I

### INTRODUCTION

In the early twentieth century, the “elementary” particles known were proton, electron and photon. For about a century now, physicists have been occupied with fracturing out atoms and sorting out the elementary particles that are produced. A wealth of energetic subatomic particles were found in cosmic rays and have been observed in cloud chambers and other detectors. Particle physics is the field of study of these elementary particles and their interactions. Goal is to understand basic laws of nature that govern the entire universe. Standard Model (SM) of particle physics has been developed over several decades to describe the properties and interactions/decays of elementary particles. Some observations also indicate New Physics (NP) beyond the SM. The search for universal laws of elementary particles results in greater understanding of the universe.

The field is commonly known as High Energy Physics (HEP) because many elementary particles do not exist under normal conditions, but at very high energies. Such high energy scale existed when the universe began, according to the Big Bang model. Experimentalists designed enormous accelerating machines to create high energy beams of subatomic particles and smash them into a chosen target or into each other and analyze the collisions. These particle accelerators combined with detectors can also be thought of as very powerful microscopes with the basic principle of operation being same as that of an electron microscope. At high energies, we are able to produce particles of high mass, according to the famous relation  $E = mc^2$ , where energy (or mass, setting  $c = 1$ ) is measured in the units MeV or GeV, etc. To have a fair idea of the scale of the energy, a flying mosquito, weighing about 2.5 mg has energy of a few TeV. Now imagine how great GeV scale of energy for a bunch of electrons (incredibly smaller than a mosquito) is, enough to create heavier particles. Also, Boltzmann taught us  $E = k_B T$ , so high energy ( $E$ ) means high temperature ( $T$ ). With high energy we can recreate the conditions at a tiny scale what had happened just after the Big Bang. In a tiny volume at the collision point, temperatures one billion times hotter than the centre of the sun are reached. So HEP help us infer about the early universe.

The smallest constituents that form matter are called elementary particles. For every particle, there is a corresponding antimatter particle or antiparticle, which has the same properties but opposite charge. For example, the antiparticle of the electron ( $e^-$ ) is called positron ( $e^+$ ). When a particle meets an antiparticle, they annihilate, giving energy. On the other hand, a pair of a particle and corresponding antiparticle can be created from pure energy, the process being called pair production.



## 1.1 The Standard Model

As Modern Periodic table is to a chemist, the Standard Model (SM) is to a particle physicist. But the SM lists the fundamental particles that make up the atoms along with other elementary particles. It classifies the interaction forces into electromagnetic, weak and strong forces—keeping aside the force of gravity, which is irrelevant on the scale of elementary particles. In the SM, the elementary particles are classified into *fermions* and *bosons*. Fermions are half-integral spin particles, like electron, etc., and they build up the matter. The spin, measured in units of angular momentum, is quantized and is as intrinsic to a particle as mass or charge. Fermions are divided into *quarks* and *leptons*. The protons and neutrons which form the nuclei, are no longer regarded as elementary particles but are found to be made of quarks. These ultimate units of matter were identified as the fractionally charged, forever-confined particles. Quarks come in six “flavors” (labeled  $u, d, s, c, b$  and  $t$ ) and three “colors” (red, green and blue). The quarks that form matter are only  $u$  and  $d$  quark, the stable ones (and the lightest). Heavier quarks do not exist naturally in today’s temperature and pressure conditions of the universe but they can be produced using particle accelerators. These heavy quarks decay into lighter ones immediately after they are produced. The properties of quarks are listed in the Table 1.1 below.

**Table 1.1. Properties of quarks.**

Quarks	Symbol	Mass $GeV/c^2$	Quantum number	Charge $Q/e$	Spin- parity $J^P$	Baryon number $B$
down	d	$\sim 0.3$	–	$-1/3$	$1/2^+$	$1/3$
up	u	$\sim 0.3$	–	$+2/3$	$1/2^+$	$1/3$
strange	s	0.5	$S = -1$	$-1/3$	$1/2^+$	$1/3$
charm	c	$1.25 \pm 0.09$	$C = +1$	$+2/3$	$1/2^+$	$1/3$
bottom	b	$4.20 \pm 0.07$	$B = -1$	$-1/3$	$1/2^+$	$1/3$
top	t	$174.2 \pm 3.3$	$T = +1$	$+2/3$	$1/2^+$	$1/3$

The second set of fermions, i.e., leptons are the light particles and hence named so. The most familiar example is electron, others being muon ( $\mu$ ) and tau ( $\tau$ ) leptons. These can be thought of as the massive versions of electrons ( $m_e = 0.51 MeV/c^2$ ). Muons ( $m_\mu = 105.7 MeV/c^2$ ) mostly decay into electron and neutrinos. The tau lepton ( $m_\tau = 1777 MeV/c^2$ ), however, is heavy enough to decay into hadrons and there is a large spectrum of decay channels for the tau. Leptons also contain three types of neutrinos ( $\nu_e, \nu_\mu$  and  $\nu_\tau$ )

corresponding to flavors  $e$ ,  $\mu$  and  $\tau$ . Neutrinos are charge neutral and massless according to the SM. However, neutrino oscillations suggest that neutrinos also have a small mass.

### 1.1.1 Standard Model Interactions

Other class of particles of SM, bosons, are the carrier of forces and they are integral spin particles.  $W^\pm$ ,  $Z^0$ ,  $\gamma$ , and gluons are the gauge bosons that carry weak, electromagnetic and strong forces respectively. Higgs boson (Chatrchyan *et al* 2012, Aad *et al* 2012), the last piece to enter SM, is a scalar boson responsible for providing mass to the particles. Photons and gluons are massless but the ones responsible for weak interaction are massive bosons. QCD—based on the SU(3) (special unitary) gauge symmetry—describes the strong interactions of colored quarks and gluons. According to this, there are three color-charge states and there are eight massless gluons. The colors are just a degree of freedom for the quarks, just like the charge, and have nothing to do with the visible colors. Quarks are always found bound to other quarks, confined in *mesons* (quark-antiquark pairs) or *baryons* (quark triplets) in a way that they are color neutral or white. The residual color force between quarks in nucleons is responsible for strong nuclear force and binds nucleons inside the nucleus. Quarks also feel weak and electromagnetic forces. Most particles classified as mesons or baryons have finite lifetimes. For instance, a neutron will decay into a proton and an electron in about 10 minutes when extracted from the nucleus. Massive particles tend to decay into less massive particles. Stable particles—proton, electron and photon have infinite lifetimes.

Talking about weak nuclear force, there is no particular ‘stuff’ that causes weak forces, as in electric charge for electromagnetic or color charge for strong force. It is sometimes simply called the ‘weak charge’; it is carried by all quarks and leptons. The leptons have no color charge, and hence they don’t undergo strong interaction. Similarly, neutrinos have no electric charge, hence they don’t undergo electromagnetic interaction. They just appear in the weak interaction. The weak interaction is of two types—charged (mediated by  $W^+$  and  $W^-$ ) and neutral (mediated by  $Z^0$ ). When the quarks change flavor, it is caused by  $W^\pm$  exchange. The properties of bosons are listed in Table 1.2 below.

**Table 1.2. Properties of force mediating particles, gauge bosons.**

Gauge Bosons	Symbol	Mass $GeV/c^2$	Width $GeV$	Decay Mode
photon	$\gamma$	0	stable	—
Gluon	$g$	0	Stable	—
weak boson	$W^\pm$	$80.40 \pm 0.03$	$\Gamma = 2.14 \pm 0.04$	$e\nu/\mu\nu/\tau\nu/\text{hadrons}$
weak boson	$Z^0$	$91.19 \pm 0.002$	$\Gamma = 2.49 \pm 0.002$	$l^+l^-/\nu\bar{\nu}/\text{hadrons}$

Summing up, fermions are divided into six quarks and six leptons, grouped into three generations each, in order of increasing mass (also their order of discoveries, think why!) and in the category of bosons, there are four gauge bosons and a Higgs boson. Figure 1.1 summarizes the SM particles.

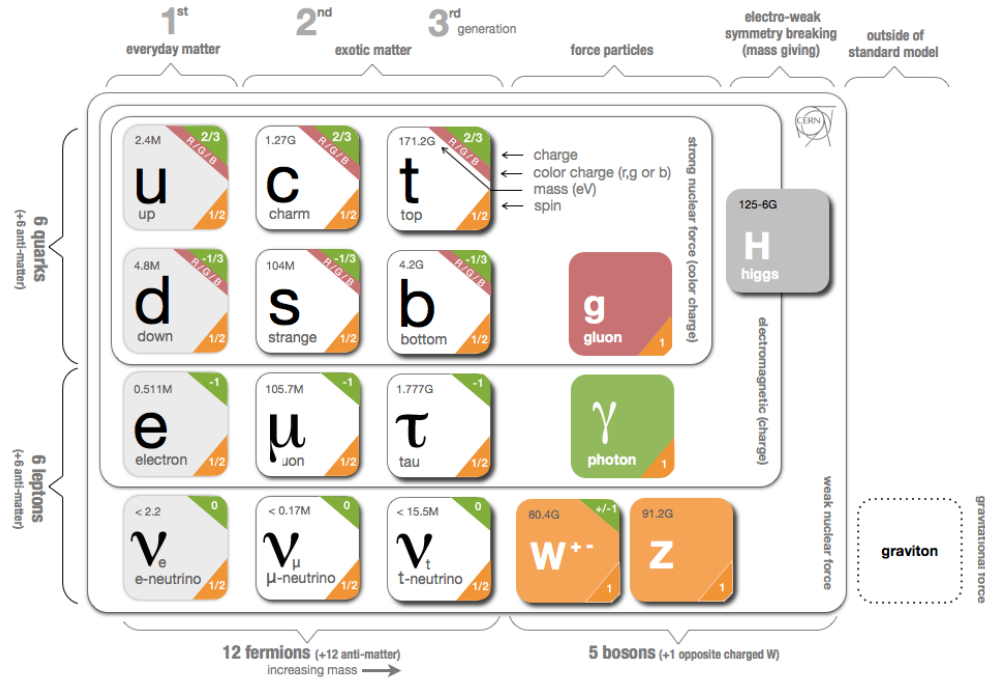


Figure 1.1. The Standard Model of particle physics.

## 1.2 Symmetries and Conservation Laws

In 1917, Noether gave this theorem: Every symmetry of nature yields a conservation law; conversely, every conservation law reveals an underlying symmetry. For example, translational invariance of space implies conservation of linear momentum, gauge transformation symmetry ensures charge conservation. Of great interests in theoretical physics are the symmetries of the physical laws. An object is said to be symmetric with respect to a given operation (such as translation, rotation or reflection), if it remains unchanged by the application of this operation on the object, i.e., the object is invariant under that particular operation. Particle physicists, for a long time believed that all fundamental interactions were symmetric under three discrete operations of parity ( $P$ ), time reversal ( $T$ ) and charge conjugation ( $C$ ), defined as follows:

### Parity Symmetry ( $P$ )

Parity operation means reflection through the origin, i.e. inverting the sign of all coordinates. This can be done by reflecting in the y-axis followed by a  $180^\circ$  rotation about x-

axis. The parity operation  $P$  changes the sign of any polar vector,  $P(x) \rightarrow -x$ ,  $P(p) \rightarrow -p$ . Axial vectors, however, remain unchanged under  $P$ . An example is the orbital angular momentum,  $L = r \times p$ . Under  $P$ , both  $r$  and  $p$  change sign, and  $L$  consequently remains unchanged. If  $P\psi(x) = \psi(-x) = \psi(x)$  then we regard  $\psi$  as a positive parity eigenfunction (even function) of parity operator and if  $P\psi(x) = \psi(-x) = -\psi(x)$ , then parity of  $\psi$  is negative (odd function).

The polarization of a spin  $\frac{1}{2}$  particle is described by helicity operator ( $\mathcal{H}$ ) defined as

$$\mathcal{H} = 2 \frac{\mathbf{J} \cdot \hat{p}}{\hbar} \quad (1.1)$$

where  $\hat{p}$  is a unit vector in the direction of the momentum. Helicity is defined as the projection of spin on momentum. The expectation value of helicity ( $\langle |\mathcal{H}| \rangle$ ) for a particle having its spin along the momentum is +1 and such a particle is said to be right-handed (RH); and a particle whose spin is opposite to  $\hat{p}$  is called a left-handed (LH) particle with helicity -1. It is important to note that the helicity of a particle is not a Lorentz invariant for a massive particle. An observer moving faster than the particle will see its helicity in the opposite direction. The parity transformation turns a negative-helicity particle into a positive-helicity particle.

### Charge Conjugation ( $C$ )

Under charge conjugation operation, the sign of charge on the particle is reversed. Along with this, all the internal quantum numbers, baryon number, lepton number, isospin, flavor charges-strangeness, charm, etc., also get inverted. Spin is left unchanged. The name is a little ambiguous because charge conjugation can also be applied to neutral particles like photons and neutrinos. Since photon is a candidate of electromagnetic radiation, the internal  $C$  parity is taken to be negative. Even  $C$ -parity refers to even symmetry under charge conjugation, e.g.  $C\psi(q) = C\psi(-q)$ , and odd  $C$ -parity which refers to antisymmetry under charge conjugation, e.g.  $C\psi(q) = -C\psi(-q)$ .

### Time reversal ( $T$ )

This simply means that the laws of physics will not change if time runs backwards.

## 1.3 Broken Symmetries in Nature

Up to 1957, the  $C, P, T$  discrete symmetries were assumed unbroken for all kinds of interaction, but then some observations indicated that the symmetries are not exact in the weak interactions, which led physicists to formulating a new theory. The first problem was concerning the parity violation in weak interactions in the so called  $\theta - \tau$  puzzle.  $\theta$  and  $\tau$  were the names given to two weakly decaying particles with the same mass, lifetime, charge, spin and production cross section, but decaying to two different final states of opposite parity. Now, either the two particles

were different, because they decayed into states of different parities, or they were actually the same particles, which means violation of parity. Lee and Yang (1956) boldly suggested that the latter was true. They also suggested some experiments to confirm parity violation in weak decays. Later it was confirmed that the  $\theta$  and  $\tau$  were actually the same particle  $K^+$ , decaying into  $2\pi$  violating parity and into  $3\pi$ , conserving it. The first experiment to confirm parity violation was carried out by Madame Wu and others (Wu *et al* 1957). The experiment studied  $\beta$  transitions of polarized cobalt nuclei, involving a change in nuclear spin  $J$  from 5 to 4 in the decay

$$Co^{60} \rightarrow Ni^{60*} + e^- + \bar{\nu} \quad (1.2)$$

One unit of angular momentum, lost from the nucleus in the direction of the initial polarization, must be carried away by the leptons. Thus, the spin projections of the two leptons onto the z-axis have to be  $+1/2$  each. For an electron emitted at an angle  $\theta$  relative to the z-axis, the positive or negative helicity states  $|\theta_{\pm}\rangle$  can be expressed as linear combinations of spin-up and spin-down states along the z-axis  $|\pm\rangle$  (Sakurai 1994).

$$|\theta_+\rangle = \cos \theta/2 |+\rangle - \sin \theta/2 |-\rangle \quad (1.3)$$

$$|\theta_-\rangle = \sin \theta/2 |+\rangle + \cos \theta/2 |-\rangle \quad (1.4)$$

For electrons in the negative-helicity state  $|\theta_-\rangle$ , the probability of finding the  $+1/2$  spin projection onto the z-axis is  $\sin^2 \theta/2$ . Thus, the probability per solid angle  $dP/d\Omega$  of emitting such an electron is given by:

$$\frac{dP}{d\Omega} = \frac{\sin^2(\theta/2)}{2\pi} = \frac{1 - \cos\theta}{4\pi} \quad (1.5)$$

And for positive helicity electrons by,

$$\frac{dP}{d\Omega} = \frac{\cos^2(\theta/2)}{2\pi} = \frac{1 + \cos\theta}{4\pi} \quad (1.6)$$

Under the assumption of parity conservation the emitted leptons from  $Co^{60}$  should show no preference for either helicity state. The sum of the distributions in Eq. 1.5 and Eq. 1.6 with equal weights does not depend on  $\theta$ . Thus, one would expect the electrons to be emitted uniformly in all directions. The nuclear spins in the sample of  $Co^{60}$  were aligned by an external magnetic field, the emitted electrons were found to be in a preferred direction antiparallel to nuclear spin. This asymmetry was found to change sign upon reversal of magnetic field such that the electrons prefer to be emitted in a direction parallel to that of nuclear spin. So, decay

picture and the one under parity inversion was not found to be identical, confirming parity violation.

Coming to  $C$  violation, we know that neutrinos exist in nature as left handed particles and anti-neutrinos as right handed, i.e. opposite polarization states. Charge conjugation operation would transform a left handed neutrino into a left handed anti-neutrino. But such a particle does not exist in SM. This is called ‘maximal violation’ of  $C$  symmetry. These violations were separately maximal and thus combined  $CP$  operation was assumed an unbroken symmetry until a long time.

### 1.3.1 $CP$ Violation

The  $CP$  transformation combines charge conjugation  $C$  with parity  $P$ . This results in, for example, transforming a left-handed electron  $e_L^-$  into a right-handed positron,  $e_R^+$ , i.e. changing a particle into antiparticle and inverting the coordinates. For  $CP$  to be an exact symmetry, the laws of nature should be the same for matter and for antimatter. While weak interactions violate  $C$  and  $P$  separately, combined  $CP$  symmetry is, however, violated only in certain rare processes, as discovered in neutral kaon decays in 1964 (Christenson *et al* 1964), and observed in recent years in  $B$  meson decays. However, such broken symmetries in nature buy us a little extra matter than antimatter. It is that little extra that we are all made of and the universe is made of. Observational evidence from radio astronomy and cosmic ray detection indicate that the universe is made up of matter (and not antimatter). Physicists seek to explain this asymmetry. There are a few possibilities for how the universe turned out this way (Perepelitsa 2008):

- The universe has been baryon-asymmetric ever since.
- The universe actually is baryon-symmetric (antimatter concentrated elsewhere).
- The universe was baryon-symmetric in the beginning but now isn’t. Nature has somehow generated excess of baryons. This idea is called *baryogenesis* since the matter excess is generated after the Big Bang by some process.

Andrei Sakharov (1967) postulated three minimum properties of nature which are required for any baryogenesis to occur, regardless of the exact mechanism. Sakharov conditions are as follows:

1. At least one baryon number ( $B$ ) violating process (necessary to produce an excess of baryons over anti-baryons).
2.  $C$ - and  $CP$ -violation.  $C$ -symmetry violation is required so that the interactions which produce more anti-baryons than baryons shall not be counterbalanced by interactions which produce more baryons than antibaryons. Similarly,  $CP$ -symmetry violation is necessary as otherwise,

left-handed baryons and right-handed antibaryons would be produced in equal numbers as that of left-handed antibaryons and right-handed baryons.

3. Interactions outside of thermal equilibrium. Without this, *CPT* symmetry would assure compensation between processes increasing and decreasing the baryon number.

The above conditions must be met by any explanation in which  $B=0$  at the time of Big Bang but is very high in the present day.

According to the Standard Model, *CP* violation occurs in the weak interaction, more specifically, when quarks of one flavor change into quarks with different electric charge under weak interactions. All of the possible transitions of quarks are constituted in a matrix of numbers, known as the CKM (Cabibbo-Kobayashi-Maskawa) matrix (Cabibbo 1963, Kobayashi and Maskawa 1973).

But the combined *CPT* symmetry holds till date. G. Luders, in 1954, published the first demonstration that in a local quantum field theory, the combined operation *CPT* must be a good symmetry. The validity of the *CPT* theorem is examined by looking for a difference between particles and antiparticles in terms of lifetime or mass. At the moment, the best measurement of the validity of the *CPT* theorem arrives from measurement in the neutral kaon system of  $|m_{K^0} - m_{\bar{K}^0}|/m_{K^0}$  which is smaller than one part in  $10^{18}$  (Carosi *et al* 1990). The *CPT* violation experiments are a useful test for the SM and serve as a means to look for physics beyond the SM since several models which include gravity (like the String Theory) are not locally gauge invariant and so they are not subjected to the *CPT* theorem.

#### 1.4 *B* mesons and *B*-factories

*B* mesons are a bound state of *b* quark and a light anti-quark (*u* or *d*), e.g.,  $B^0$  constitutes  $d\bar{b}$ . They have spin  $J = 0$ , isospin  $I = 1/2$  and negative parity ( $P = -1$ ) and mass of  $B^0$  is  $5.279 \text{ GeV}/c^2$ . *B* mesons contain quarks of the third generation and thus their decays offer great opportunity to measure the CKM matrix elements  $V_{cb}, V_{ub}, V_{ts}$  and  $V_{td}$  which describe the couplings of the third generation of quarks to the quarks of first and second generations.  $B^0 - \bar{B}^0$  mixing occurs through second order weak interactions via “box diagrams” as shown in Figure 1.2. Due to mixing, an arbitrary neutral *B* meson state is defined as the admixture of  $B^0$  and  $\bar{B}^0$ . They have almost identical lifetimes of approximately  $1.5 \times 10^{-12} \text{ s}$ .  $K_L$  meson decays more often to  $\pi^- e^+ \nu_e$  than to  $\pi^+ e^- (\bar{\nu}_e)$ , thus permitting electrons and positrons to be distinguished easily, but the decay rate asymmetry is only at 0.003 level. In the *B* system, the *CP* -violating effects observed are larger because of large mass of *B* meson compared to *K* and hence large mass difference, which accounts for oscillations.

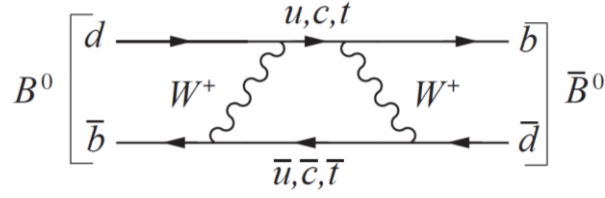


**Figure 1.2.** Example of a process that can convert  $B^0$  i.e.,  $d\bar{b}$  state into  $\bar{B}^0$  i.e  $b\bar{d}$  state.

There are three types of  $CP$  violation:  $CP$  violation in decay,  $CP$  violation in mixing, and  $CP$  violation in the interference of decays with and without mixing.

To study  $B$  meson decay,  $B$ -factories were constructed. These facilities exploit the properties of the  $\Upsilon(4S) = b\bar{b}$  resonance, which has a mass of 10.58 GeV. This is a state of *bottomium* that is just enough heavy to decay to  $B$  and  $\bar{B}$  by mechanism shown in the Figure 1.3. Further details on  $\Upsilon(4S)$  are given in chapter II. The  $\Upsilon(4S)$  resonance decays only to  $B^0\bar{B}^0$  or to  $B^+\bar{B}^-$  pairs, while heavier states such as  $B_c$  or  $B_s$  mesons and  $b$ -flavored baryons are not accessible.

Two such  $B$  factories have been constructed to study  $CP$  violation in  $B$  decays: the PEP-II facility at SLAC, California, in which a 3.1 GeV positron beam is collided with a 9.0 GeV electron beam, and the KEKB facility in Japan, in which a 3.5 GeV positron beam is collided with an 8 GeV electron beam. The KEKB accelerator produces 10  $B$  mesons in a second and 100 million  $B$  mesons a year! It looks like a factory that produces a huge number of  $B$  mesons, and therefore called  $B$ -factory. In the accelerator, packets of electrons and positrons are energized with powerful electric and magnetic fields, which steer and guide them. They are made to go faster and faster until they have extremely high energy. These beams are sent into two vacuum rings, one in clockwise direction and other in counterclockwise direction. These two counter-rotating packets of beams are on a collision course at 99% the speed of light. The high vacuum ensures that the beam doesn't encounter anything on the way. The beams crash into each other, recreating a bang with energies approaching that of Big Bang, be it at a minute fraction of its ferocious energy. The collision is recorded by Belle detector. This harmless version of the Big Bang can tell us about the birth of all matter and infact the universe itself. In this sense, such machines are both time machines, taking us back to the Big Bang, and the most powerful microscopes as well.

KEKB started operation in 1998 and collected huge data for nearly 10 years, which I shall use in the current analysis. Then it underwent a huge upgrade and has started operation recently again as SuperKEKB (Akai *et al* 2018) with even higher collision rate and promising outcomes, and suspected to probe physics beyond the SM. The center-of-mass energy corresponds to the  $\Upsilon(4S)$  mass, while the asymmetric beam energies ensure that  $B$  mesons are produced with enough momentum to travel a measurable distance before decaying. This is



important, because studies of  $CP$  violation require the measurement of the time difference between the decay of the  $B$  and anti- $B$  mesons. These decays probe the small CKM matrix element  $V_{ub}$ , whose magnitude sets bounds on  $(\bar{\rho}^2 + \bar{\eta}^2)$  in the Wolfenstein parameterization (Wolfenstein 1983) of the CKM matrix. Further details of the KEKB accelerator and the Belle detector can be found in chapter III.

#### 1.4.1 Physics at KEKB

Electrons and positrons are accelerated in the KEKB accelerator to nearly speed of light and collided at the center of Belle detector. Electron-positron pair mostly produce  $Y(4S)$  resonance which decays into a pair of  $B$  mesons, instantaneously. While the  $B$  mesons have moved only slightly, they decay quickly into several lighter particles. For each collision, the measured momenta and energies of the particles are recorded as data. The data for a single collision is called an event. Production of  $B$  meson pairs in  $e^+e^-$  collisions is shown in the figure below.

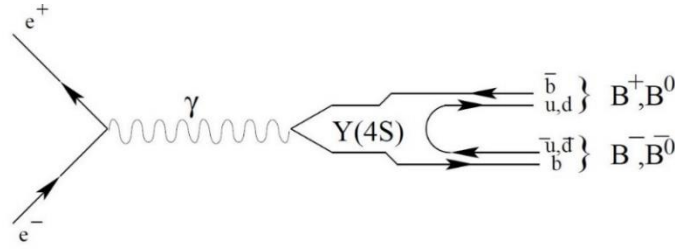
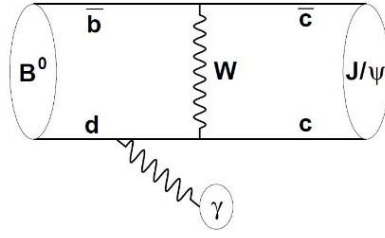


Figure 1.3. Production of  $B$  mesons in  $e^+e^-$  collision through  $Y(4S)$ .

#### 1.5 Physics of the decay $B^0 \rightarrow J/\psi\gamma$

Radiative  $B^0 \rightarrow J/\psi\gamma$  is a very rare decay, which is sensitive probe of physics beyond the SM. Charmonium ( $J/\psi$ ) meson is the bound state of  $c$  and  $\bar{c}$  quarks.  $J/\psi$  is a vector meson with spin 1 and photon ( $\gamma$ ) also has spin 1. So the decay is a pseudoscalar to vector-vector ( $S \rightarrow VV$ ) kind. In the decay, a  $W$  boson is exchanged between the quarks and a photon is radiated from  $d$  (light quark) of the  $B$  meson. The mechanism of decay (tree level) in the SM is shown in the Feynman diagram, Figure 1.4. The possibility of photon being radiated from other quarks is suppressed by power of  $O(\Lambda_{QCD}/m_b)$  because  $J/\psi$  meson must be transversely polarized (Lu, Wang and Yang 2004).

In the annihilation decay  $B \rightarrow J/\psi\gamma$ , there is possibility of admixture of (V+A) charged current (Lu, Wang and Yang 2004) to the SM (V-A) current, which can be a possible indication of New Physics. Also, CKM suppressed decay mechanisms involving possibility of



**Figure 1.4.** Leading order Feynman diagram for the decay  $B \rightarrow J/\psi\gamma$ .

non-spectator intrinsic charm in the  $B$  meson (Brodsky and Gardner 2002) points towards NP. Although the main objective of the  $B$ -factories is the study of flavor physics and weak decays, the study of decays of  $B$  mesons are important to test the different calculations of the QCD interactions within these decays, which helps to identify the most appropriate theoretical approaches for predicting observables. A typical approach for predicting the branching fractions of such decays is to factorize the decay into a short-distance contribution which can be computed with perturbative QCD and a long-distance contribution for which non-perturbative QCD is required.

## 1.6 Objectives

- a) Event selection and identification of possible backgrounds.
- b) Modelling of various background components and to estimate the reconstruction efficiency for branching ratio measurement of rare annihilation decay under study.

## CHAPTER II

### REVIEW OF LITERATURE

Ask a layman whether matter is continuous, he'd most likely answer affirmatively. We rarely bear the intuition that matter can't be divided infinitely. If sand is ground very finely, it still remains sand. We have no experience on why we can't keep on dividing it further and further. This is the continuous view of matter. The same notion was proclaimed by the best-known philosopher of ancient Greece, Aristotle and it seemed logical at that time.

Much later, in the early nineteenth century, John Dalton explained atomic theory of matter, building upon Lavoisier's quantitative scientific laws: law of conservation of mass and law of definite proportions. This is indeed the discrete nature of matter. According to Richard P. Feynman, establishing the atomic nature of matter is the most important scientific fact ever expressed in a single sentence. While atomic nature of matter seems obvious today, when Dalton's theory came out, it took no less than a century for the scientific community to fully accept it. The urge to have better knowledge of what we are made of, what the universe is made of, and to 'see' beyond our 'common observations' has directed scientists to dig deeper and deeper and has landed to the field of what is now at the front end research of 21<sup>st</sup> century—high energy physics. The field derives from nuclear physics, where people like Rutherford, who gave the nuclear model, were the great leaders. The discovery of electron by J.J. Thomson in 1897 can be marked as the first step toward this modern field. In the year 1900, Max Planck necessitated that electromagnetic radiation is quantized, and light was in fact coming in little packages called 'photons', is now the electromagnetic field particle of the SM. With years of discovering subatomic particles, and many of them often leading to a Nobel Prize, the last leg of discoveries of particles of the Standard Model was that of Higgs boson (Aad *et al* 2012, Chatrchyan *et al* 2012) made in the year 2012 by the Large Hadron Collider (LHC) experiment group. Historical synopsis of the development of SM is given in detail in this section. But SM is not the end of the story. Any model in particle physics cannot be fully accepted until the experiments verify it completely. Standard model too has some flaws; there are certain things which it is unable explain. The *CPT* violation experiments, etc, look beyond the SM, and there are other theories which act as an extension to it, like the Supersymmetry (SUSY), left-right symmetric models, models with extra  $Z'$  bosons, scenarios with extra dimensions, or "little Higgs" models. There are several other theories like the String theory, which are built on motive of incorporating gravity as well. For now, let's see through the important events in development of sub-nuclear world of quarks and leptons which gave rise to the most successful theory till date, i.e. the Standard Model.

Particle physics deals with small particles, to which we now know, the rules of Newtonian physics do not apply. When we are working with high energy physics, we need a theoretical framework that deals with the ‘small’ and the ‘fast’. Fortunately, theories for the small—quantum mechanics and the fast—Einstein’s special relativity theory started developing in the early 1900’s. But a combined theory of quantum mechanics and special relativity was needed. One of the most prominent scientists in the making of these compound theories was Paul Dirac. He formulated around 1930, a great theory ranking with the Maxwell’s theory of electromagnetism (the physical theory that describes electromagnetism is called electrodynamics or ED). Dirac’s theory described electrons moving at relativistic speed and this accounted for Einstein’s special relativistic considerations. His relativistic equation incorporated the spin property of electrons and that they behave like tiny magnets. He also concluded from the results of his relativistic equation that electron has an anti-matter partner, which made in for the first ever proposition of anti-matter. The first successful theory thus developed is known as Quantum Electrodynamics (QED) and this theory encompasses the electromagnetic interactions. In this amalgamated theory, the special relativity adds the mass-energy equivalence; quantum mechanics, on the other hand, adds the energy-time uncertainty principle. In combination, the number of particles can no longer be considered constant, quite contrary to special relativity or quantum mechanics alone. Also, the interactions between particles is seen differently in this theory. There are virtual particles responsible for mediating the interactions, as opposed to potential in classical physics.

Another noted theorist following the Dirac’s generation is Richard P. Feynman. His theory acquired accuracy to a level higher than that of Dirac. He also invented a visual approach to aid the lengthy calculations, called Feynman diagrams. For their contributions to the development of QED, Sinitiro Tomonaga (1946), Julian Schwinger (1954), and Richard Feynman (1948) shared the Nobel Prize in Physics in 1965. One of the many noteworthy achievements of QED thus developed is the precise calculation of the electron’s magnetic moment, which agrees with experimental measurements to 10 decimal places.

Antimatter discovery: Many particles were discovered in cosmic rays, giving a great push to the particle physicists. Carl Anderson in 1932 observed a track in a cloud chamber placed in a magnetic field and exposed to cosmic rays which he proved to be that of anti-electron or positron (Anderson 1933). This was the first ever antimatter particle discovered. Anti-electrons, as we know, were proposed earlier, in 1931 by Dirac as an alternative to negative energy solutions of his relativistic equations describing an electron. This discovery brought triumph to Dirac’s theory. In modern particle physics, the most complete theoretical approach to the calculations (such as transition rates and particle interaction cross sections) is to use quantum field theory (QFT).

Coming to the nucleus, there was one big question—what holds the nucleus together? After all, the positive protons in the nucleus must repel each other by the electrical repulsion. This indicated that there was some other force, which is operative inside the nucleus, holding it together. This was simply called the ‘strong’ nuclear force. The first significant theory in this regard was put forward by Yukawa in 1934. Yukawa (1934) proposed that there must be some quantum particle, in analogy with photon, responsible for strong interaction. He suggested that such a particle must mediate in small range (since we don’t experience it in our daily lives) and hence it must be massive. He even calculated that the mass should be about 300 times that of electron, and he named it ‘meson’. Such a particle, matching Yukawa’s description was found in the cosmic rays in 1937 by two groups: Neddermeyer and Anderson (1937) on the West Coast, and Street and Stevenson (1937) on the East. But there was some confusion because the lifetime and mass did not match the Yukawa particle. The confusion was later resolved by Powell and his co-workers when they found that there were in fact two types of middle-weight particles in the cosmic rays: the pion ( $\pi$ ), the real Yukawa particle, and another was muon ( $\mu$ ). Later, it was found that the strong force between two protons, which Yukawa took to be a fundamental and irreducible process, must be regarded as a complicated interaction of six quarks, laid down under the theory of strong interactions or the Quantum Chromodynamics (QCD).

Let’s carry the discussion of ‘forces’ a little forward before coming back to the matter particles of the SM. Consider the electromagnetic interaction. In classical physics, this interaction is propagated by electromagnetic waves, which are continuously emitted and absorbed. While this is an adequate description at long distances, at short distances the quantum nature of the interaction must be taken into account. In quantum theory, the interaction is transmitted discontinuously by the exchange of spin-1 photons, which are the ‘force carriers’, or gauge bosons, of the electromagnetic interaction and, as we know presently, the long-range nature of the force is related to the fact that photons have zero mass. The use of the word ‘gauge’ refers to the fact that the electromagnetic interaction possesses a fundamental symmetry called *gauge invariance*. QED, QCD and the unified electroweak theory are all examples of gauge theories, with somewhat different forms of gauge invariance in each case. Each of these forces is mediated by the exchange of a particle, which is the quantization of the field. The strong forces are mediated by the gluon and weak forces by the intermediate vector bosons,  $W$  and  $Z$ . These mediators transmit the force between one quark or lepton and another.

The first theory of the weak forces was presented by Fermi in 1933; it was refined by Lee and Yang, Feynman and Gell-Mann, and many others, in the fifties, and put into its present form by Glashow, Weinberg, and Salam (GWS), in the sixties. The theory proposed by C.N. (Frank) Yang and Robert Mills (1954) required three massless gauge bosons: one with positive

electric charge, one with negative electric charge, and one electrically neutral. The introduction of additional gauge bosons implied the existence of a force that is capable of transforming particles from one type to another. At the time, this seemed to describe the characteristics of the weak force, which, among other things, converted protons to neutrons in nuclear  $\beta$ -decay. Then in 1961, Sheldon Glashow (1961) aimed to unify the weak and electromagnetic interactions into a single theoretical system, in which they would appear *not* as unrelated phenomena, but rather as different manifestations of one fundamental “electroweak” interaction. But Glashow and others recognized a problem—the theory could be accounted for only if the weak interactions were mediated by extremely massive particles. But for the combination to be one basic interaction, it was not clear how the electromagnetic mediator ( $\gamma$ ) is massless, while the weak mediators ( $W$  and  $Z$ ) are so heavy. This needed to be resolved.

It turns out that in many cases, a system that has some symmetry existing in the Lagrangian may have a ground state that does *not* satisfy the same symmetry. When a situation like this exists, we say that the system has undergone *spontaneous symmetry breaking*. This effect is known as the Higgs Mechanism (Higgs 1966), named after its discoverer Peter Higgs in 1964. In analogy, think of the marble sitting on top of the bowl as a ground state, which is clearly unstable. Now suppose that the marble is perturbed and rolls off the bowl. It is destined to roll in one particular direction and will come to rest below on the flat ground. So, the perturbation has *spontaneously broken* the symmetry that existed before. In fact, the true ground state of potential energy exists when the symmetry is broken and the marble finds itself resting on the ground below.

Weinberg (1967) and Salam (1968) provided the solution to the problem faced by Glashow in the form of “Higgs mechanism”, which accounts for the mass of the  $W$ ’s and  $Z$  bosons. In 1979 Sheldon L. Glashow, Abdus Salam, and Steven Weinberg got Nobel Prize for developing the unified electroweak theory. The unified theory can be understood as—at sufficiently high energies, the difference between the electromagnetic and weak interactions becomes negligible and the two act together as a single, unified electroweak interaction. Carlo Rubbia bagged Nobel Prize in 1984 for discovering the  $W$  and  $Z$  particles, hence verifying the electroweak unification. The UA1 and UA2 collaborations in 1983 made the first measurements of the  $W$  and  $Z$  boson masses based on a few of events from  $ppN$  collisions at the CERN SPS collider (Ansari *et al* 1987).

As for the strong forces, beyond the pioneering work of Yukawa in 1934 there really was no theory until the emergence of QCD in the mid-seventies. In 1965, Moo-Young Han, Yoichiro Nambu (1979), and Oscar Greenberg laid the foundation for QCD. The strong interaction is mediated by massless gauge bosons called gluons, the field quanta that carry a unique kind of charge, called color, for which the theory is named.

The set of fermions called leptons also set out to be discovered by the scientists. The most famous of these, the electron formed the member of lightest doublet of the lepton family. The muon,  $\mu$ , the heavier version of electron was discovered in cosmic rays by Carl Anderson and Seth Neddermeyer in 1936. The heaviest known lepton, the tau ( $\tau$ ), was discovered decades later in 1975 by Martin Perl (Perl *et al* 1975) with colleagues at SLAC. The muon and tau are unstable and can exist for only fractions of a second before they decay into electron and neutrinos, in a reaction conserving lepton number. The leptons, as we now know, also contain three partner neutrinos of  $e, \mu$  and  $\tau$ . For this strand in the story, let's return back to the year 1930. Continuous energy spectrum of the electrons in the nuclear beta decay was observed, as opposed to alpha or gamma decay, which was waiting for an explanation. This implied that there should be a missing particle which carried the energy. So, Wolfgang Pauli in 1930 postulated an electrically neutral, mass-less spin  $\frac{1}{2}$  particle. Enrico Fermi coined the name neutrino for it in 1933 and postulated theory for  $\beta$  decay (weak interaction). It was mysterious particle because it was difficult to observe, it hardly interacts with anything. Neutrinos can pass through light years of lead; compare to gamma rays which can be stopped in just 1.3 feet of lead. Clyde Cowan and Fred Reines observed the interactions of electron antineutrinos with protons in a huge instrumented tank of water (Reines and Cowan 1953). After this indirect evidence of neutrinos, a group led by Melvin Schwartz, Leon Lederman, and Jack Steinberger (Danby *et al* 1962) developed a neutrino beam at Brookhaven National Laboratory, in 1961, which even resulted in the discovery of the second species of neutrino: the muon neutrino ( $\nu_\mu$ ), and Nobel Prize for them in 1988. The tau neutrino ( $\nu_\tau$ ) was ultimately discovered at Fermilab in 2000 (Kodama *et al* 2001).

### Discovery of heavy quarks

The stable matter of today is made up of nuclei consisting of  $u$  and  $d$  quarks only. A wealth of energetic particles was found in cosmic rays but heavier quarks needed to be created in labs. Rochester and Butler observed a 'V' event in a cloud chamber that was probably due to  $K^0 \rightarrow \mu^+ + \mu^-$ . With this, the year 1946 saw the first evidence for *strange* particles. They were called strange because these particles were produced in strong interactions and were expected to decay by strong interactions with a timescale of  $10^{-23}$  sec, but they decayed quite slow in comparison to it, indicating weak interactions. Such discoveries led to building of high energy accelerator machines in the 1950's.

With the discovery of so many particles, the garden which seemed so tidy before 1950's had grown into a jungle by 1960. There was dire need to organize the chaotic hadron physics. In order to understand and classify the jungle of hadronic (not elementary) particles, an Eightfold way was proposed by Gell-Mann. The plethora of strongly interacting particles was

divided into two great families-the baryons and the mesons-and the members of each family were distinguished by charge, strangeness, and mass. That is, in 1963, Murray Gell-Mann and George Zweig (Gell-Mann 1964, Zweig 1964) independently proposed that observed hadrons could be simply interpreted as bound states of three fundamental spin-  $\frac{1}{2}$  particles. These particles were required to have fractional electric charges of  $\frac{2}{3}$ ,  $-\frac{1}{3}$  and  $-\frac{1}{3}$ , in units of  $e$ , and were called *quarks* by Gell-Mann. The quarks come in three types (or “flavors”), forming a triangular “Eightfold-Way” pattern. These quarks inside the hadrons (protons, etc.) were discovered much like the nucleus in the atom was, in the alpha scattering experiment. In a SLAC experiment performed in 1968 by a team (Islam and Rosen 1969), electrons with energies 20 GeV, with corresponding wavelength  $6 \times 10^{-15}$  cm were smashed at protons and the scattered electrons were detected. These electrons probed structures to  $1/15^{\text{th}}$  of the size of the proton. The results of the experiment indicated existence of pointlike particles with masses inside the proton. This is the discovery of quarks. In fact, Gell-Mann’s classification of elementary particles bagged him Nobel Prize in the year 1969. Now, let’s delve in a bit more and see what the theoreticians contributed that time which led to prediction of the *charm* and *bottom* quarks. We shall proceed to the experimental part of it after the following two sections which lay the theoretical groundwork for their discoveries.

**Kaons system and CP violation:** Kaons are strange particles. They are produced in pairs by non-strange particles but can decay to non-strange particles only via weak interaction. In 1964, Jim Cronin and Fitch studied the neutral kaon system at Brookhaven National Laboratory (BNL).  $K^0$  and  $\bar{K}^0$  are not *CP* eigenstates but their linear combinations do. These are called  $K$  –short ( $K_S$ ) and  $K$  –long ( $K_L$ ). As the name suggests,  $K_S$  has shorter lifetime as compared to  $K_L$ . We detect kaons as  $K_S$  ( $CP = +1$ ) and  $K_L$  ( $CP = -1$ ) which are *CP* self-conjugate states. These states,  $K_S$  and  $K_L$  decay to  $2\pi$  and  $3\pi$  respectively, conserving *CP* in the process. *CP* eigenstate of bosonic systems  $\pi^0\pi^0$  and  $\pi^+\pi^-$  is  $+1$ . And for the  $3\pi$  systems,  $\pi^+\pi^-\pi^0$  and  $\pi^0\pi^0\pi^0$ ,  $CP = -1$ . In an experiment in 1964 by Christenson, Cronin, Fitch and Turlay (Christenson *et al* 1964) first demonstrated that the long-lived kaon state could also decay to  $\pi^+\pi^-$  with a branching ratio of order  $10^{-3}$ . It normally decayed into three pions, conserving *CP* symmetries, but decay into two pions does not conserve the *CP* symmetry. For their groundbreaking discovery, Cronin and Fitch received the 1980 Nobel Prize in physics, but back then, it was hard for the scientific community to accept the discovery of *CP* violation because it led to unsettling conclusion that the microscopic laws of physics indeed allow absolute distinctions between left-and right-handed co-ordinate systems, between particles and anti-particles and time running forwards and backwards.

The support to *CP* violation can be seen in the set of three conditions given by physicist Andrei Sakharov in 1960s, which gave necessary conditions that could explain the appearance



of our matter-dominated universe.  $CP$  violation is one of Sakharov's conditions (Sakharov 1967) for matter dominated universe to exist. Apart from this, today we recognize that the existing sources of  $CP$  violation cannot explain the amount of matter dominance in the observable universe. The amount of  $CP$  violation explained by weak force is so little (Rubakov and Shaposhnikov 1996) that it is not even enough to leave matter for a single galaxy. We need to at least look for sources of  $CP$  violation beyond the quark sector such as in “leptogenesis”, where new  $CP$  violating effects appear in decays of heavy Majorana neutrinos (Buchmuller *et al* 2005), decay of Higgs boson, etc.

**GIM mechanism and CKM matrix:** It was experimentally observed that semi-leptonic decay rates of strange particles (kaons, etc.) involving a change in strangeness  $\Delta S = 1$  were suppressed as compared to  $\Delta S = 0$  decays. This and some other factors were accounted for in the Cabibbo theory, in which  $d$  and  $s$  quarks were not taken as pure states but occurred in a mixed state, with the amount of mixture being contained in the Cabibbo angle  $\theta_c$ . Note that, at that time, only  $u, d$  and  $s$  quarks were known. Quarks naturally occurred as a mixture but leptons as pure states because of *lepton universality*. Cabibbo model could not explain the absence of  $\Delta S = 1$  neutral currents. The remedy to this problem was provided by Glashow, Iliopoulos and Maiani (GIM) in 1970. They proposed the existence of another quark with charge  $+\frac{2}{3}e$  and labelled it ‘charm’. The Cabibbo-GIM mixing matrix specifying the quark states involved in weak interaction is written as

$$\begin{pmatrix} d' \\ s' \end{pmatrix} = \begin{pmatrix} \cos \theta_c & \sin \theta_c \\ -\sin \theta_c & \cos \theta_c \end{pmatrix} \begin{pmatrix} d \\ s \end{pmatrix} \quad (2.1)$$

The GIM mechanism (Glashow 1961, Weinberg 1967, Salam 1968) removed the unwanted  $\Delta S = 1$  neutral currents at the cost of additional quark (charm). The details of how it works can be found in any particle physics textbook. When the charm was discovered in  $J/\psi$  resonance in 1974 (Augustin *et al* 1974, Aubert *et al* 1974), the GIM mechanism was certainly proved. Cabibbo, Kobayashi and Maskawa (1973) extended this concept in 1972. They gave first theory which included  $CP$  violation in the SM. They proposed the third generation of quarks,  $b$  and  $t$  and a  $3 \times 3$  unitary matrix, called CKM matrix. The  $2 \times 2$  Cabibbo matrix contained one real parameter  $\theta_c$ , but the  $3 \times 3$  matrix contained three Euler angles and one phase,  $\delta$ . This phase will enter the wavefunction  $e^{i(\omega t + \delta)}$ , and is not invariant under time reversal, or equivalently, the  $CP$  operation. Hence, this phase which is only possible in a  $3 \times 3$  matrix, accounted for the required  $CP$  violation. So, Kobayashi and Maskawa boldly predicted that there must be at least six quarks in nature. The subsequent discoveries of  $c, b$  and  $t$  quarks in several experiments and the occurrence of  $CP$  violation in the KM model led to its inclusion in the SM. Kobayashi and Maskawa received Nobel Prize in 2008 for their explanation of origin

of  $CP$  violation, which predicted large  $CP$  violation in decays of particles containing  $b$  quarks, when it was verified by the  $B$ -factories, KEK and PEP-II. The weak currents are described by unitary transformations among the three doublets as

$$\begin{pmatrix} d' \\ s' \\ b' \end{pmatrix} = V \begin{pmatrix} d \\ s \\ b \end{pmatrix}, \quad (2.2)$$

where  $V$  is the  $3 \times 3$  CKM (Cabibbo, Kobayashi-Maskawa) matrix,

$$V = \begin{vmatrix} V_{ud} & V_{us} & V_{ub} \\ V_{cd} & V_{cs} & V_{cb} \\ V_{td} & V_{ts} & V_{tb} \end{vmatrix} \quad (2.3)$$

The values of the matrix elements represent the relative tendencies of quarks to transform into quark of other flavor. Each quark has preference to transform into its own generation and so  $V_{ud}$ ,  $V_{cs}$  and  $V_{tb}$  have values close to one, and others have value close to zero; a decay involving decay of quark from one generation to other is Cabibbo suppressed decay. The elements of the CKM matrix are fundamental parameters of the SM and are determined in the analysis of various experiments. For example,  $V_{ub}$  can be measured by selecting semi-leptonic decays of  $B$  mesons to non-charmed particles. The precise measurement of CKM elements is an important task of flavor physics and can be conveniently displayed in the  $\rho\eta$  plane.

Now, let's resume the experimental determination of the quarks predicted by the KM theory. In November 1974, a series of  $\psi$  resonances were observed at SPEAR collider at SLAC, Stanford (Augustin *et al* 1974), first at the  $e^+e^-$  annihilation centre-of-mass energy of 3.1 GeV and then at 3.7 GeV and other higher broad states. Due to discovery of the series of resonances, this event is known as the 'November revolution'. The fine structure of energy levels of these states were quite similar to those of positronium ( $e^+e^-$  non-relativistic bound state). Naturally, it was inferred that these meson states were also bound states of fermion-antifermion. The  $\psi$  was interpreted as lowest bound state of a new heavy quark, *charm*, and its antiquark ( $c\bar{c}$  or *charmonium*). The  $c\bar{c}$  spectra showed that the difference in energy levels is much smaller than the quark mass i.e., charmonium are non-relativistic systems. The resonance was independently observed at Brookhaven alternating gradient synchrotron (AGS), where the experimentalists called it ' $J$ ' (Aubert *et al* 1974). The state is therefore referred to as  $J/\psi$ . This new quark, with new quantum number C, for *charm*, was the one postulated in 1970 by Glashow, Iliopoulos and Maiani, in connection with the non-existence of strangeness-changing neutral weak currents (GIM mechanism). The large mass of  $J/\psi$  implied that they contained such charmed quarks. Soon after that Goldhaber *et al* (1992) discovered charmed  $D$  mesons, containing single  $c$  quarks.

OZI (Okubo, Zweig and Iizuka) rule: The broadness of higher mass  $J/\psi$  states are associated with decay to hadrons containing  $c$  and  $\bar{c}$  quarks, while the lower states, which were

sharp resonances such as  $J/\psi$  (3100) and  $J/\psi$  (3700) were because they decayed only to lighter quarks and antiquarks with a change of flavor of quarks. I'll refer back to this rule in a moment.

The discovery of charmonium was followed by observation of similar narrow resonances in the  $9.5 - 10.5 \text{ GeV}$  region (Herb *et al* 1977, Innes *et al* 1977). These were realized as the bound state of even heavier bottom-antibottom quarks, named *bottomonium*, from the generic name *quarkonium* for quark-antiquark, leading to discovery of *bottom* quark in the year 1977. The bottomonium ( $b\bar{b}$ ) was denoted as  $\Upsilon$  (Upsilon). Just as for the charmonium, the OZI rule explains why the  $1S, 2S$  and  $3S$  states are narrow. Also, the state which decayed to a pair of  $b$  and  $\bar{b}$  containing mesons, is a broad state, should be above the threshold  $10.558 \text{ GeV}$ . This is why the  $B$ -factories operate at  $\Upsilon(4S)$  state, which is just above the threshold of producing  $B\bar{B}$  pairs. Infact, the  $B^0$  mesons were discovered in 1983 in the decay of  $\Upsilon(4S)$  resonance (Andrews *et al* 1980, Behrends *et al* 1983). The decay branching ratio to a  $B$  meson pair is larger than 96% (Barish *et al* 1996). The lifetime of the  $B$  meson was found to be an unexpectedly long, 91.6 psec (Bartel *et al* 1982, Fernandez *et al* 1983, Nakamura *et al* 2010) considering its heavy mass. The energy level diagram (Eichten *et al* 2008) of bottomonium is illustrated in Figure 2.1. The various levels are labelled by charge and space parities,  $C$  and  $P$ . For the non-relativistic system, the charge conjugation symmetry is  $C = (-1)^{L+S}$  and space parity is  $P = (-1)^{L+1}$ . The horizontal axis is labelled by the values of  $J^{PC}$  for different states.  $S$  and  $P$  indicate the values for orbital momentum  $L$ , upper index gives  $2S + 1$ , and lower index gives  $J = L + S$ , where the symbols have their usual meaning.

Heavy quarkonia, systems which compose of heavy quark and antiquark of the same flavor, have mass much larger than the QCD confinement scale. Due to this, the systems are non-relativistic and are affected by physical processes of broad range of energies. These are good probes to test all regimes of QCD—expansion in the coupling constant at high energies and non-perturbative effects of the low energy domain, and also spans the intermediate energy. Thus, quarkonium offers a good laboratory for controlled testing of non-perturbative QCD and its interplay with perturbative QCD.

The sixth and final quark, *top*,  $t$ , anticipated in the KM model, was observed 20 years after discovery of  $b$  quark. It took much time essentially because its mass is too high ( $M \simeq 175 \text{ GeV}$ ) that exceeded the center of mass energies of earlier accelerators and hence could not be produced in those. Top quark was finally discovered in 1995 at Fermilab  $p\bar{p}$  collider with  $1.8 \text{ TeV}$  cms energy, by both the CDF (Abe *et al* 1995) and DØ (Abachi *et al* 1995) collaborations. All six quarks anticipated in the KM model are now at hand.

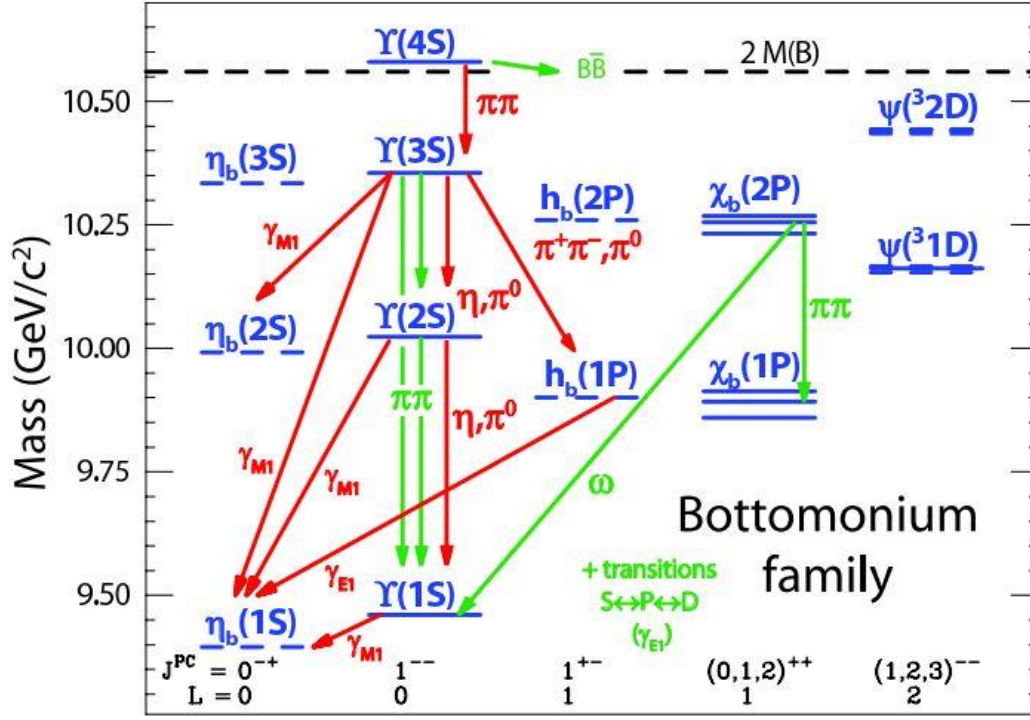


Figure 2.1. The energy-level diagram for bottomonium. Only states with  $J^{PC} = 1^{--}$  can be accessed in  $e^+e^-$  annihilation experiments.

### Measuring $CP$ violation in $B$ system

The KM model predicts two types of  $CP$  violation in  $B$  meson decays. The first one is indirect  $CP$  violation which involves mixing between  $B^0$  and  $\bar{B}^0$ . In 1983, MAC and MarkII collaborations at SLAC found that lifetime of  $b$  flavored mesons was unexpectedly long  $\sim 10^{-12}$  sec (Peruzzi 1983). Following this, in 1980-1981, Ashton B. Carter, Ikaros Bigi and Ichiro Sanda showed that  $CP$  violating effects are observable in the  $B^0\bar{B}^0$  system within the KM framework (Carter and Sanda 1981), if the  $B$  lifetime is long and  $B^0\bar{B}^0$  mixing is large. They also suggested ways to measure it.  $B^0\bar{B}^0$  mixing means that  $B^0$  can change itself to a  $\bar{B}^0$  in sometime and viceversa. Actually, mixing depends on the mass difference between  $B^0$  and  $\bar{B}^0$ , hence greater amounts of mixing can be found in this system as compared to kaons.  $B^0\bar{B}^0$  mixing allows two separate routes from initial  $B$  meson to the final  $CP$  self-conjugate state, one without mixing and other with mixing. The decay processes corresponding to these two separate paths interfere with each other. If the interference between these two paths is different, depending on whether one starts with  $B^0$  or  $\bar{B}^0$ , potentially measurable differences in the decay time are generated. Such asymmetry in mixing is called indirect  $CP$  violation. I.I. Bigi and A.I. Sanda (Bigi and Sanda 1984) found that  $CP$  violation appears in the form of a difference in the time-dependent decay rate of a  $B^0$  meson to the specific final state to which both  $B^0$  mesons

and  $\bar{B}^0$  mesons can decay. Large  $B^0\bar{B}^0$  mixing was discovered in 1987 by ARGUS collaboration at DESY (Albrecht *et al* 1987).

The second one is direct  $CP$  violation in the decay of each  $B$  meson. The KM model allows the decay rate of a  $B$  meson to a specific channel to be different from the corresponding decay rate of  $\bar{B}^0$  meson. The difference between the decay rates of a particle and its anti-particle is called direct  $CP$  violation. Let's understand this with an example, the Belle experiment observed  $1856 \pm 52$  events of  $B^0 \rightarrow K^+\pi^-$  and  $2241 \pm 57$  events of  $\bar{B}^0 \rightarrow K^+\pi^-$ , where 52 and 57 represent statistical errors. The difference between the number of observed  $\bar{B}^0 \rightarrow K^-\pi^+$  events versus  $B^0 \rightarrow K^+\pi^-$  events, normalized to the sum of these events is called direct  $CP$  violating decay rate asymmetry ( $A^{CP}$ ). The  $CP$  violating asymmetry in  $B \rightarrow K^\pm\pi^\mp$  is measured as

$$A^{CP} \equiv \frac{N(\bar{B}^0 \rightarrow K^-\pi^+) - N(B^0 \rightarrow K^+\pi^-)}{N(\bar{B}^0 \rightarrow K^-\pi^+) + N(B^0 \rightarrow K^+\pi^-)} = -0.094 \pm 0.018 \pm 0.008 \quad (2.4)$$

where the first error is statistical and second is schematic error from fitting and bias due to detector response. The ratio of  $CP$  violating asymmetry and its error is called ‘significance’. The total error is obtained by the square root of the quadratic sum of the statistical and systematic errors. The significance is calculated to be  $\frac{0.094}{\sqrt{(0.018^2 + 0.008^2)}} = 4.8 \sigma$ . This value of significance indicates that a probability of no asymmetry is less than  $1.8 \times 10^{-6}$ . In 2001,  $CP$  violation in decay of  $B$  meson was discovered by two experiments: the Belle experiment (Abe *et al* 2001) at KEK and the Babar experiment (Aubert *et al* 2001) at SLAC. Then in 2004, Chao *et al* (2004) found evidence for direct  $CP$  violation in the decay  $B^0 \rightarrow K^+\pi^-$ .

### Earlier work on $B^0 \rightarrow J/\psi\gamma$

$B^0 \rightarrow J/\psi\gamma$ , the decay under my study, is a rare decay and such decays are sensitive of possible New Physics (NP) beyond the SM. This decay occurs predominantly via a  $W$  boson exchange and radiation of gamma from the lighter quark of  $B^0$ . This decay includes the possibility of right handed charge current or V+A weak current (Lu, Wang and Yang 2004) which is not possible in the realm of the SM. This could also signal non-spectator intrinsic charm in the  $B^0$  meson (Brodsky and Gardner 2002). BaBar first sought the radiative decay  $B \rightarrow J/\psi\gamma$  at PEP-II, SLAC from a dataset of 123 million  $Y(4S) \rightarrow B\bar{B}$  decays (Aubert 2004). No evidence for the signal was found and they placed an upper limit of  $\mathcal{B}(B^0 \rightarrow J/\psi\gamma) < 1.6 \times 10^{-6}$  at 90% confidence level.

Recently, LHCb came out with a paper on search of the rare decay. They performed their analysis using data collected by the experiment at  $\sqrt{s} = 7$  and 8 TeV corresponding to integrated luminosity of  $3 \text{ fb}^{-1}$ . They have set an upper limit of branching fraction value  $1.5 \times$

$10^{-6}$  for the  $B^0 \rightarrow J/\psi\gamma$  decay, at 90% confidence level (Aaij *et al* 2015). This limit is in good agreement with the BaBar value. Study of  $B$  meson decays are a good laboratory for verifying the QCD predictions. Precise experimental measurements are therefore crucial to test the QCD calculations within these decays. Since the decay is quite rare, statistics must be very high for conducting a fruitful analysis. As Belle has collected large amount of data of  $772 \times 10^6 B\bar{B}$  pairs, we have a good opportunity to use this to find an evidence of the decay or to put a precise upper limit.

## CHAPTER III

### MATERIALS AND METHODS

In this section, I'll first describe the need for accelerators and then move to details of KEKB accelerator and Belle detector. It is important to understand the characteristics of the detector well in order to carry out good analysis. Subsequently, software tools and research analysis workflow will be discussed.

To understand the structure at very small scale, we require probes of very small wavelength and hence very high energy (according to QM, the de-Broglie wavelength of a particle of momentum  $p$  is  $\lambda = h/p$ ). To study structure of the atom ( $\sim \text{\AA}$ ) we need energy  $\sim \text{KeV}$  ( $10^3 \text{ eV}$ ). At a smaller scale, say, to probe proton structure ( $10^{-3} \text{ fm}$ ), energy  $\sim \text{GeV}$  ( $10^9 \text{ eV}$ ) is required. To “look” inside the protons, we need even higher energies. Such high energy beam particles are not emitted from any radioactive sources and so must be produced artificially in the accelerators. Accelerators are nothing but machinery for generating electric and magnetic fields, operated in high vacuum. Charged particles are accelerated using the electric fields and magnets are used to bend and steer the particles in the accelerator tunnels.

#### 3.1 Path to KEKB

In the early 1980's, Bigi, Sanda and Carter published papers exploring the possibilities of using  $B$  meson decays to test the KM six-quark mechanism for  $CP$  violation. In 1987, in a workshop which focused on possibilities of using linear colliders for  $B$  physics, Pier Oddone proposed a novel concept of circular, asymmetric energy  $e^+e^-$  collider for  $B$  physics. This would operate at the  $Y(4S)$  and produce  $B$  mesons with a lab-frame boost decent enough to enable decay time dependent measurements (Oddone, 1987). The experiment to observe  $CP$  violation in  $B$  decays would require enormous data on  $B$  mesons. So in the year 1994, the SLAC and KEKB factories were approved. The data used to perform this analysis has been collected at the KEKB asymmetric  $e^+e^-$  collider and the Belle detector at High Energy Accelerator Research Organization, KEK, Japan. The accelerator construction was completed in 1998 and it collected huge data in its long run. Belle carried out experiments almost continuously except for several months of summer and New Year holidays. The facility has now been upgraded to SuperKEKB and Belle II in the past years and has restarted its functioning.

#### 3.2 KEKB Collider

KEKB (Kurokawa and Kikutani 2003, Toge *et al* 1995) is a two-ring, asymmetric-energy, electron-positron collider, shown in Figure 3.1. The rings, 3 km in circumference, are installed side by side in a tunnel 11 m underground. The electrons and positrons are accelerated to 8 GeV and 3.5 GeV, respectively, in the linear accelerator and then injected into the rings,

HER (high energy ring) and LER (low energy ring). Beam particles lose energy during circulation by emitting synchrotron radiation; RF cavities supply energy to the particles to recover lost energy. Copper vacuum chambers are used for the rings since they can sustain a high heat load of synchrotron radiation. The electrons and positrons tunnel in the rings in bunches. In KEKB, hundreds of billions of electrons and positrons are contained in one bunch, and more than 1000 bunches circulate in one ring. Beams accelerated to nearly the speed of light are made to collide (some of them annihilate) at the *interaction point* (IP) in Tsukuba experimental hall, where Belle detector (records the behavior of particles produced in the collision) is placed. Even with a high number of particles in a bunch, most of them do not collide but just pass each other. The beam crossing angle is  $\pm 22 \text{ mrad}$ . This helps in avoiding the complications of the machinery required to produce head-on collisions, as well as bunches, are easily separated after the collision.

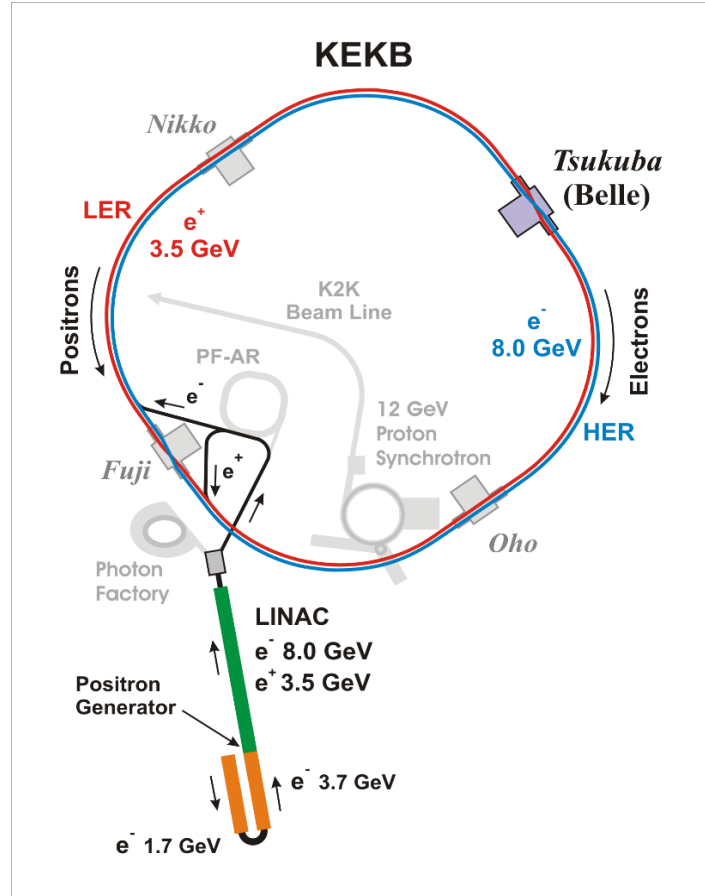


Figure 3.1. Schematic of layout of KEKB.

The collision of 8 GeV electron and 3.5 GeV positron amounts to centre-of-mass (CM) energy,

$$\sqrt{s} = \sqrt{(4E_+ E_-)} = 10.58 \text{ GeV} \quad (3.1)$$



This corresponds to the mass of  $Y(4S)$  resonance and these are mostly produced in these collisions.  $Y(4S)$  immediately decays nearly exclusively into  $B\bar{B}$  pairs ( $Br(Y(4S) \rightarrow B\bar{B}) > 96\%$  (Beringer *et al* 2012) ) because its mass is just a little north of sum of masses of  $B$  and  $\bar{B}$ . Although  $B$  and  $\bar{B}$  are produced almost at rest in the CM frame, but they have finite velocities in the lab frame. This is because of the Lorentz boost provided by the asymmetric energies of the two particles. Lorentz boost factor is given by

$$\beta\gamma = \frac{E_{e^-} - E_{e^+}}{\sqrt{s}} = 0.425 \quad (3.2)$$

We have deliberately created this boost so that we can measure the difference between decay times (and hence positions) of  $B$  and  $\bar{B}$  mesons, in order to study time dependent  $CP$  asymmetries. The difference between decay times is too small to be measured and therefore we measure the distance between decay vertices, using  $\Delta z \sim c\beta\gamma\Delta t$ . The boost displaces the  $B$  meson decay vertices for approximately  $200 \mu m$  in the laboratory frame.

Using a DC voltage source to generate the electric field needed to accelerate particles is quite intuitive. But high energies cannot be achieved using such an accelerator. In 1930, accelerators with radio frequency (RF) cavities were developed, which employed a high voltage AC source to produce high-frequency electromagnetic waves. In this case, particles are grouped together so that they are accelerated in accordance with the high frequency. The electric fields change signs with time inside cavities, and so the particles must traverse cavities such that they are always accelerated. To achieve high energy in circular accelerators, we need large radius as there are synchrotron losses at smaller radii. Also, if we use colliding beams, there is high center of mass energy (compared to the fixed target accelerator). To look at rare decays, we need to look at as many as possible particle decays. For this, we require high-luminosity machines. Luminosity  $L$  is given by

$$L = f \frac{n_1 n_2}{4\pi\sigma_x\sigma_y} \quad (3.3)$$

where  $n_1$  and  $n_2$  particles collide with frequency  $f$ . Here,  $\sigma_x$  and  $\sigma_y$  represent transverse beam sizes in the horizontal and vertical directions respectively. To increase the luminosity, beam current must be increased and the size of beams must be decreased. Simply putting, highly focused beam containing a large number of particles leads to greater number of collisions. To achieve a high luminosity, the KEKB underwent some detector upgrades during its operation:

**Continuous injection and crab cavities:** During beam injection, the detector high voltage was turned off in Belle which slashed the average luminosity. In order to reduce this loss, a continuous injection scheme was adopted in Belle from January, 2004. Under this scheme, the

detector high voltage was not turned off but the trigger signals, just after beam injection, were vetoed for 3.5 ms. This improved stability and peak luminosity due to constant beam currents.

Then in 2007, another major upgrade took place, introducing Crab cavities (Yamamoto *et al* 2010). These are RF-deflectors and they provided a rotational kick to the electron-positron just bunches before the collision, which despite of 22 *mrad* beam crossing angle, led to a head-on collision. After incorporating crab cavities, though the increase in the luminosity was modest, the beam induced backgrounds were reduced. The schematic principle of the Crab cavities operation is shown in Figure 3.2.

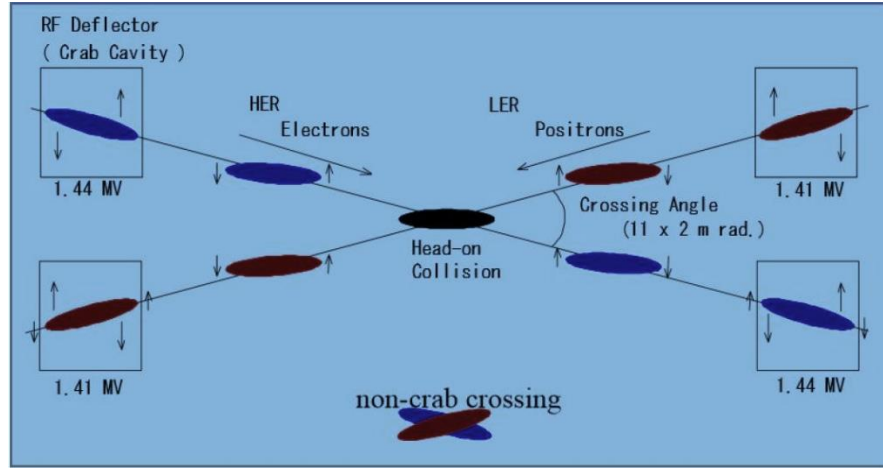


**Figure 3.2.** Principle of operation of crab cavities is shown which led to head-on collisions in KEKB despite the finite crossing-angle of electron and positron bunches.

Luminosity times the cross section provides the rate of interaction per second:

$$R = \frac{dN}{dt} = \sigma L \quad (3.4)$$

Hence luminosity is measured in  $cm^{-2}s^{-1}$ . KEKB achieved the world's highest luminosity of  $1.7 \times 10^{34} cm^{-2}s^{-1}$ . The creation of a  $B\bar{B}$  meson pair has a cross section (implying probability of collision) 1.1 nb ( $1 nb = 10^{-33} cm^2$ ). The cross sections in  $e^+e^-$  collision at the  $\Upsilon(4S)$  resonance are summarized in Table 3.1. If the luminosity is integrated over time, we obtain the integrated luminosity,

$$N = \int L \cdot \sigma dt \quad (3.5)$$

which is proportional to the total amount of collected data. KEKB produces 10  $B\bar{B}$  pairs per second,  $10^6 B\bar{B}$  per day and hence it gives out 100 million  $B$  mesons annually. KEKB currently holds the record for peak luminosity:  $2.11 \times 10^{34} cm^{-2}s^{-1}$  and one day integrated luminosity of  $1.47 fb^{-1}$ , both achieved in 2009.

In addition to  $B\bar{B}$ , KEKB produces other particles as well. Other interactions that occur include quark jets from  $q\bar{q}$  ( $q = u, d, s \text{ or } c$ ),  $\tau$  pair events, as well as two-photon interactions and other higher order QED processes. In order to study  $B$  meson decays, Belle collected most data at the energy of  $\Upsilon(4S)$  resonance. For the purpose of the background estimation arising from the non- $B$  meson events, off-resonance data was collected at 60 MeV below the  $\Upsilon(4S)$  peak energy, approximately every two months. Data taking was also performed at other  $\Upsilon$  resonances. The cross section of  $e^+e^-$  annihilations in the region of different  $\Upsilon$  resonances is shown in Figure 3.3.

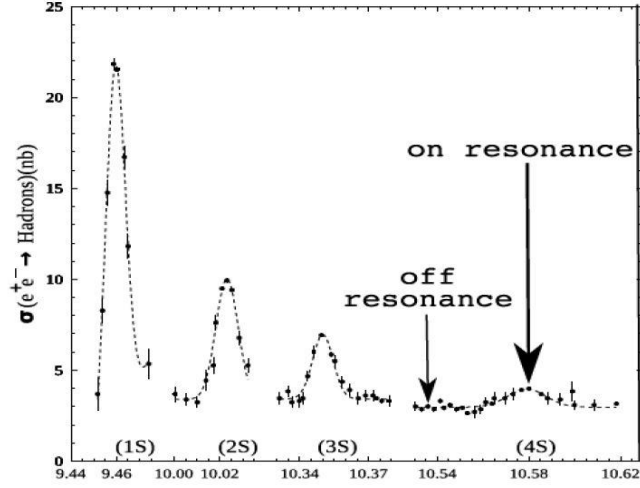


**Figure 3.3.** Cross-section in  $e^+e^- \rightarrow \text{hadrons}$  at CM energies near  $\Upsilon$ .

The last  $\Upsilon(4S)$  resonance data was taken in June 2008 after which, energy scans at  $\Upsilon(1S)$ ,  $\Upsilon(2S)$  and  $\Upsilon(5S)$  resonances were taken. During the last two years of operation, energy scans between the  $\Upsilon(4S)$  and  $\Upsilon(6S)$  were carried out. The beam background did not change much when running at different energies. The final beam abort ceremony of KEKB/Belle took place at KEK on June 30, 2010. The integrated luminosity collected by Belle for  $\Upsilon(4S)$  resonance, calculated using Bhabha events, where the final state electrons are detected in the barrel part of the detector, corresponds to  $772 \times 10^6 B\bar{B}$  pairs.

**Table 3.1.** Cross-section in  $e^+e^- \rightarrow \text{hadrons}$  at  $\sqrt{s} = 10.58 \text{ GeV}$ . QED refers to Bhabha and radiative Bhabha events.

Process	$\sigma$ [nb]
$B\bar{B}$	1.1
$c\bar{c}$	1.3
$q\bar{q}$ ( $q = u, d, s$ )	2.1
$\tau\bar{\tau}$	0.93
QED( $25.551^\circ < \theta < 159.94^\circ$ )	37.8
$\gamma\gamma$	11.1

### 3.3 The Belle Detector

The interaction region is surrounded by a giant detector consisting of several sub-detectors, known as the Belle detector. The debris erupting from the collision of particles move through the layers of Belle detector which records them, of course, in electronic form. The detector has a superconducting magnet (1.5 T) which curves the path of particles traversing through the detector layers. The more energetic particles manage to reach outermost layers of detectors and the low energy ones stop in the inner layers. The sub-detectors trace the particle's track (hence curvature) and record their momentum, energy, etc. We use this information to identify the particles.

Since the  $B$  mesons produced have a very small lifetime (one-trillionth of a second), they decay almost instantaneously. Therefore the Belle detector cannot detect  $B$  mesons directly and we detect the secondary particles of  $B$  mesons decay, and reconstruct  $B$  mesons from them. The final state particles (the ones which are recorded in the layers of the detector) of any decay in the Belle experiment are electrons ( $e^+, e^-$ ), muons ( $\mu^+, \mu^-$ ), pions ( $\pi^+, \pi^-$ ), kaons ( $K^+, K^-, K_L$ ), protons ( $p, \bar{p}$ ) and photons ( $\gamma$ ). Now let us look at the detector in detail. The sub-detectors, in the order from innermost to outermost, are:

**SVD** (Silicon Vertex Detector), **EFC** (Extreme Forward Calorimeter), **CDC** (Central Drift Chamber), **ACC** (Aerogel Cherenkov Counter), **TOF** (Time of Flight), **ECL** (Electromagnetic Calorimeter), **KLM** ( $K_L$  and muon detector). A superconducting solenoid—generating a field of 1.5 Tesla, applied in the direction of the beam—is placed between ECL and KLM. SVD and CDC are the tracking detectors. Details of each sub-detector part is described in the following sections. We measure trajectories of particles and determine their momenta using hit data and also measure velocities from the magnitude of hit signals. ECL and EFC measure energy; CDC, ACC, TOF are used for particle identification of charged particles except for electrons. ECL performs the task of identifying electrons and gamma, while KLM is used for  $K_L$  and muon separation, as clear from its name. Figure 3.4 shows the dissected diagram of the Belle detector showing its sub-detectors. The photograph of Belle detector is shown in Figure 3.5. The Belle detector is described in much detail elsewhere (Abashian *et al* 2002).

For the description of the sub-detectors, the z-axis is taken to be the direction of the magnetic field within the solenoid, which is anti-parallel to the  $e^+$  beam. The x-axis is the horizontal axis and y-axis is vertical, forming a right handed coordinate system. In the polar coordinate representation, the polar angle,  $\theta$ , is subtended from the positive z-axis. The azimuthal angle,  $\phi$ , is subtended from the positive x-axis and lies in the x-y plane. The radius ( $r = \sqrt{x^2 + y^2}$ ) is measured from the origin (position of the nominal interaction) in the x-y plane.

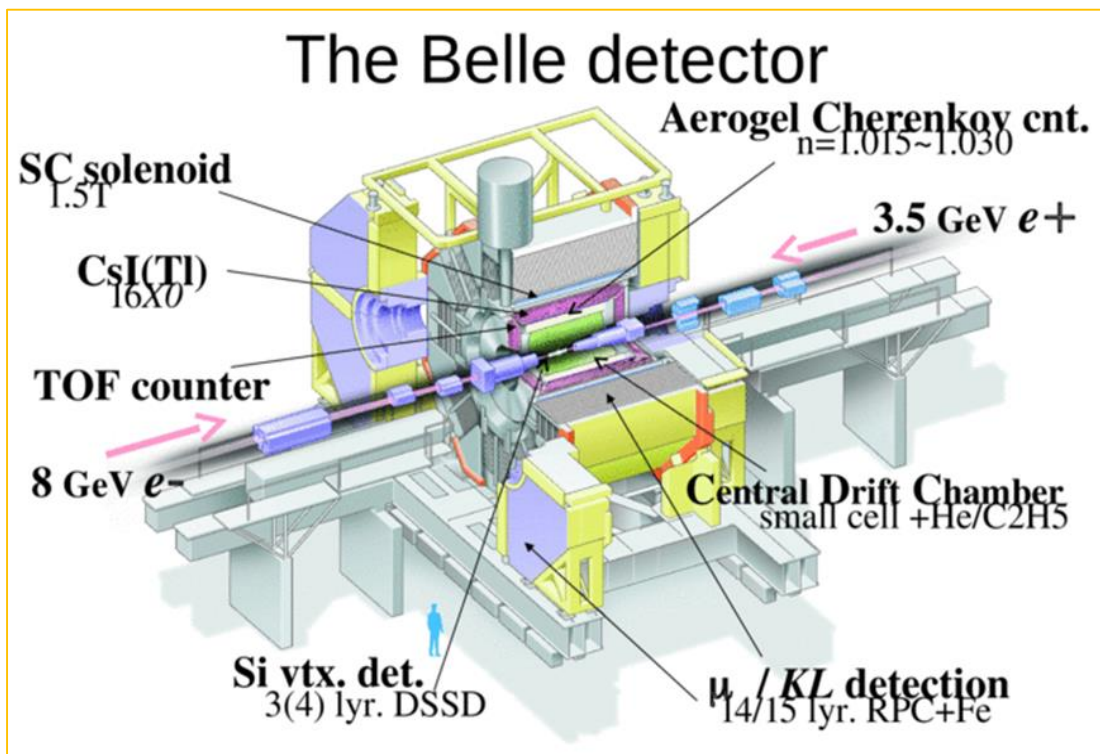


Figure 3.4. Dissected diagram of the Belle detector.

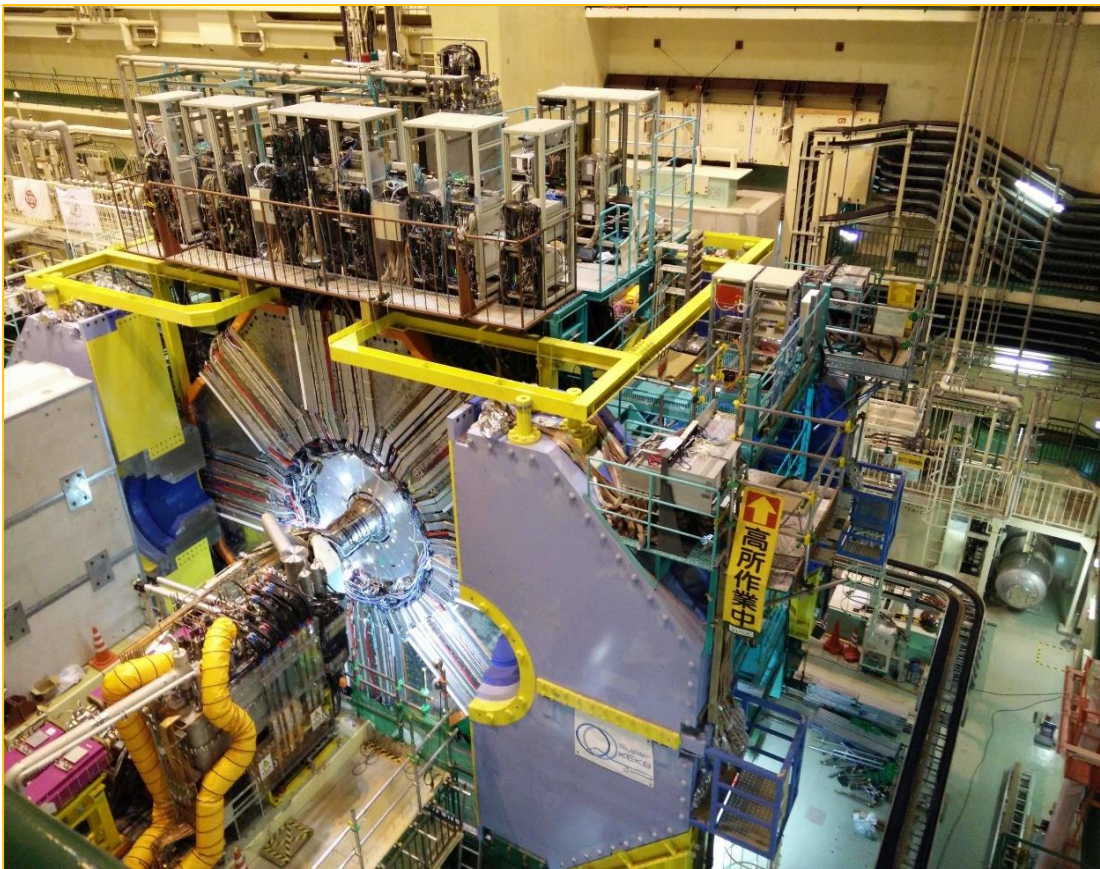


Figure 3.5. The Belle Detector, KEK, Japan.



The detector has a wide angle coverage of  $17^\circ < \theta < 150^\circ$ . The polar angle coverage of barrel section (parallel to the beam axis) is  $34^\circ < \theta < 127^\circ$ . Two endcaps, which extend radially from the beam axis at the forward and backward ends of the detector have coverages  $17^\circ < \theta < 34^\circ$  and  $127^\circ < \theta < 150^\circ$  respectively. The design requirements of detector, driven by the physics goals, are as follows:

**Vertexing capability:** Precise determination of decay vertex of each  $B$  meson in an event is crucial for measuring  $CP$  violating asymmetries. For this, silicon-strip based vertex detector, SVD (Kawasaki 2002) is employed and it forms the innermost detector layer.

**Particle identification:** To classify the final state particles, Central Drift Chamber (Hirano *et al* 2000) was constructed with good specific energy loss ( $dE/dx$ ) measuring capability. In addition to this, a time-of-flight system (Kichimi *et al* 2000), and an aerogel-based Cherenkov counter (Iijima *et al* 2000) was also constructed which in unison perform the task of identification of charged particles over a broad momentum range.

**Electromagnetic calorimetry:** For final states of any decay, for example, electrons in  $J/\psi \rightarrow e^+e^-$ , it is necessary to measure the energy of both neutral particles ( $\gamma$ ) and electrons, for which electromagnetic calorimeter (Ikeda *et al* 2000) was adopted.

**$K_L$  and muon identification:** The  $K_S$  mesons are expected to decay in the beam pipe or SVD owing to their short lifetime, whereas most  $K_L$  mesons pass through the inner part of the detector due to longer lifetime. Detection requirements of  $K_L$  and muons are identical and KLM is designed for it (Abashian *et al* 2000). Belle employed float-glass based Resistive Plate Chambers (RPCs) for this, placed in the iron yoke which renders the magnetic flux return.

### 3.3.1 Beam Pipe

The beam pipe is the innermost region of the Belle detector and the particles traverse through it before entering SVD. Beam pipe in the active region of the detector is made of beryllium. This material was chosen because it is light and we wish to minimize the amount of material in order to reduce energy loss of particles crossing the beam pipe and multiple coulomb scattering. Also, it should be able to withstand beam induced heating. The beam pipe consists of two concentric cylinders (each 0.5 mm thick) with different radii, 20.0 mm and 23.0 mm respectively, see Figure 3.6. Helium gas is used as coolant and is cycled between the inner and outer walls.

### 3.3.2 Silicon Vertex Detector (SVD)

Silicon vertex detector is a solid state detector and it forms the first layer of sub-detectors surrounding the interaction point. This is ideal for measuring the decay vertices of particles ( $B$  mesons decay immediately after production and hence SVD must be placed closest

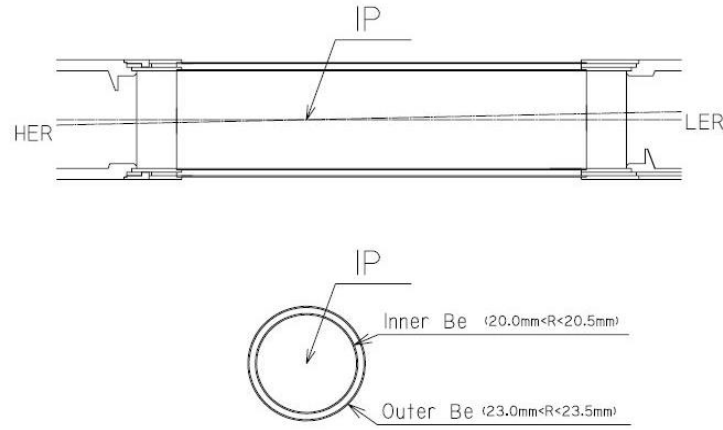


**Figure 3.6. Cross-section of the beryllium beam pipe at the interaction point.**

to IP). The SVD also helps to improve the momentum resolution of particles and also contributes to the track reconstruction of particles. It covers a solid angle  $23^\circ < \theta < 139^\circ$ . The working of a solid state detector can be compared to that of a gas detector, and is quite similar, except that in a gas detector there is ionization of the gas whereas in a solid state detector, electrons and holes are formed in the silicon material as a charged particle traverses the detector. Signals are detected and amplified to measure the coordinates of particle's hit positions.

SVD consists of double-sided silicon strip detectors (DSSD), called ladders, which are installed with IC chip for reading out signals. Three layers (SVD1) of ladders (later increased to four (SVD2)) are placed in a cylindrical fashion around the beam pipe at the IP. The innermost layer, containing 8 ladders, is at 3 cm from the collision point, second with 10 ladders is at 4.55 cm, and the outermost layer with 14 ladders has radius of 6 cm. The total length is about 30 cm. Figure 3.7 shows illustrates the side and endcap view of SVD. The image of SVD can be seen in Figure 3.8.

The DSSD is basically a p-n junction. A bias voltage is supplied to the n-side, while the p-side is grounded. When a charged particle passes through n-bulk silicon, it creates electron-hole pairs. These are then separated due to external field and collected at the strip electrodes on the opposite sides of DSSD, as illustrated in Figure 3.9. Since the strips on one side are perpendicular to the strips on the other, collecting the charge from both layers makes it possible to determine the position of the particle crossing the DSSD plane. Each DSSD module consists of 1280 sensitive strips. The precision of z-axis measurement is about  $100 \mu\text{m}$ , though it can be worsened by multiple scattering of particles before entering SVD. Wondering how this precision is achieved? Imagine a particle crossing a point in space and thereby creating ionization. Now the electrons will drift towards the nearing signal strips. Magnitude of pulse on the strip closer to the point of crossing will be greater in than the one far from it. By taking

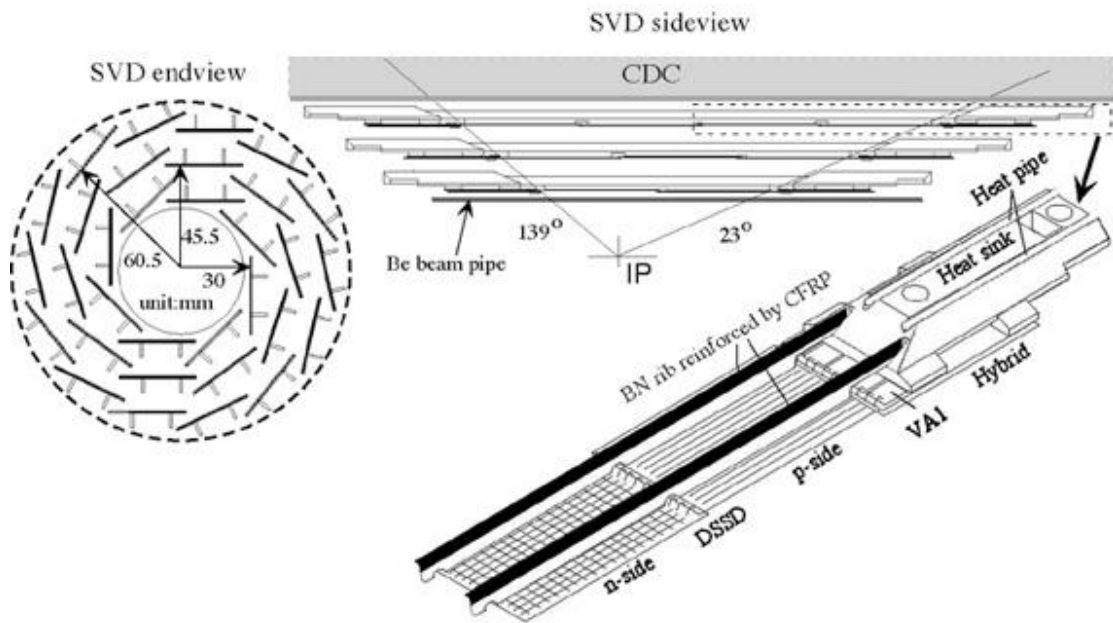


Figure 3.7. Endview and sideview of SVD1.

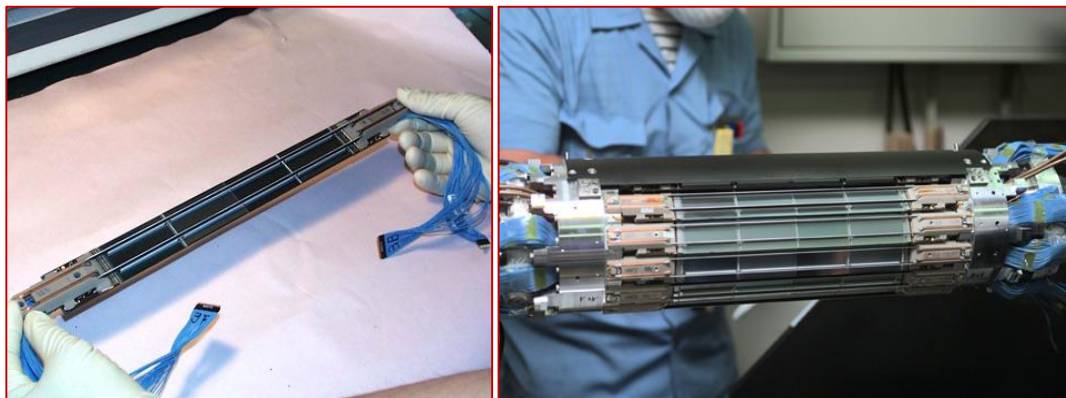


Figure 3.8. Left image shows a 'ladder' and right image shows assembled SVD. One can notice the cables connected to each sensor, needed to electronically record the hits along with the other cables attached to sensors to monitor various physical factors during the experiment run.

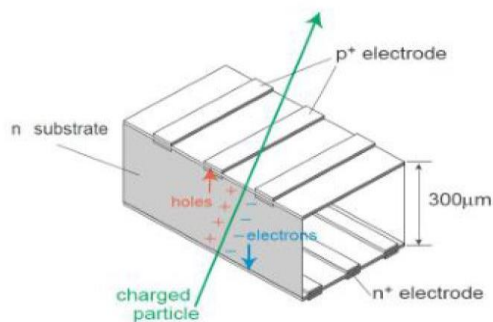
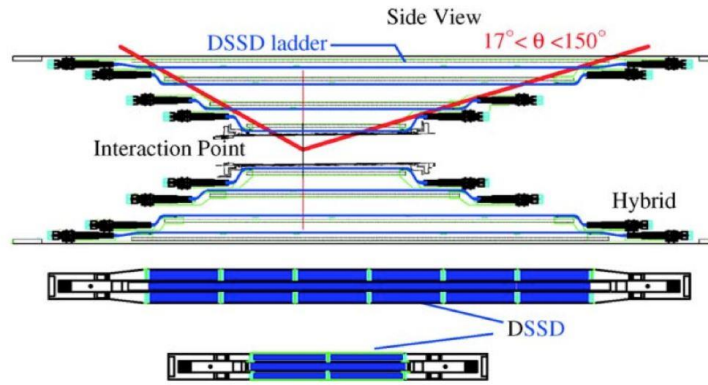


Figure 3.9. Charged particle position determination with DSSD.



weighted average, we can determine up to some accuracy the precision of particle's position. 128 channel VA1 chips (Toker *et al* 1994) are placed on both sides of the ladder which read signals from DSSDs. Signals are amplified using VA1 chips and sent to shaping circuits, where the shaping time is adjusted to about  $1 \mu\text{s}$ . Then, the outputs of the shaper are taken when TOF triggers a Level-0 (L0) trigger to the VA1 chips. This information is passed to fast analog-to-digital converters (FADC) in the electronic hut if a Level-1 (L1) trigger occurs. There are 81920 readout channels in total.

SVD1 was upgraded to SVD2 (Ushiroda 2003) in 2003. It consisted of four layers of 20.0 mm, 43.5 mm, 70.0 mm and 88.0 mm radii. The geometrical configuration is shown in Figure 3.10. At the same time, the inner part of the central drift chamber was also replaced with a compact small cell type drift chamber in order to make space for four SVD layers and along with this, the inner radius of beam pipe was reduced 15 mm from 20 mm. In SVD1, the chips were read sequentially, but in SVD2 the chips are read in parallel, in order to reduce readout deadtime.



**Figure 3.10.** Longitudinal cross section of Belle SVD2. It covers full Belle acceptance angle  $17^\circ < \theta < 150^\circ$ .

### 3.3.3 Central Drift Chamber (CDC)

CDC is the detector responsible for tracking the charged particles with  $p < 0.8 \text{ GeV}/c$  and  $p > 2.0 \text{ GeV}/c$ . About 10,000 wires are stretched in a gas-filled cylindrical chamber, 1 m in diameter. The wires are of two types- field wires (to set up strong electric field) and sense wires (for receiving electronic signal). The combination of signal wires and field wires form a cell structure, shown in Figure 3.11. The principle of drift chamber is: as the charged particles pass through the gas mixture of 50 %  $\text{He}$  and 50 %  $\text{C}_2\text{H}_6$ , they ionise the gas and generate ions and electrons along its track. On an average, 100 ionized electrons/cm are produced. These accelerating electrons even cause more ionizations on their way, causing gas amplification. These electrons move towards the nearest signal wire and accumulate, giving out an electric pulse. The larger the pulse, more the ionization, meaning more is the charge on the ionizing

particle. In this instrument, we know to a good accuracy the speed of electrons (about 4 cm/μs). By measuring the time taken by the electrons to move to the sense wire, we can find out the distance of the point where the electrons were generated i.e. from where the charged particle crossed in the vicinity of signal wire. We can determine the distance with a precision of 150 μm. CDC has 50 layers of sense wires, so one can reconstruct the tracks by connecting the dots (signal positions). The position resolution is about 100 μm in a direction perpendicular to the central axis. Not to forget, the apparatus is placed in a large magnet which curves the trajectory of the traversing charged particle. After reconstructing the tracks, we can find out, by the curvature, the momentum of the particle.

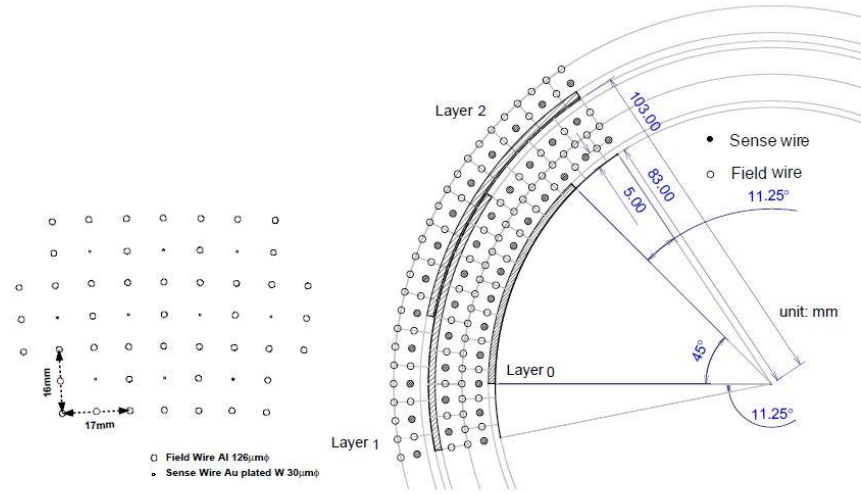


**Figure 3.11. Cell structure of CDC and cathode sector configuration.**

There are two types of signal wires—axial and stereo wires. The axial wires are strung parallel to the beam direction (taken z-direction) and are used to measure coordinates of the particles in the  $r - \phi$  plane, i.e. plane perpendicular to the beam. The stereo wires are tilted a bit with respect to the beam direction, used to measure the z coordinate. The diagram and images of CDC are shown in Figures 3.12 and 3.13.

The energy loss of a particle per 1 g of a material due to ionization, namely  $dE/dx$ , is given by Bethe-Bloch equation,

$$-\frac{dE}{dx} = KZ^2 \frac{Z}{A} \frac{1}{\beta^2} \left[ \frac{1}{2} \ln \frac{2m_e c^2 \beta^2 \gamma^2 T_{max}}{I^2} - \beta^2 - \frac{\delta(\beta\gamma)}{2} \right] \quad (3.6)$$

where,  $K = 0.30 \text{ MeV } g^{-1} cm^2$ ,  $\gamma = \frac{1}{\sqrt{1-\beta^2}}$ ,  $\delta$ = Density effect correction,  $A$ = Atomic mass,  $Z$ = Atomic number,  $I$ = Excitation energy,  $T_{max}$ = Maximum kinetic energy.

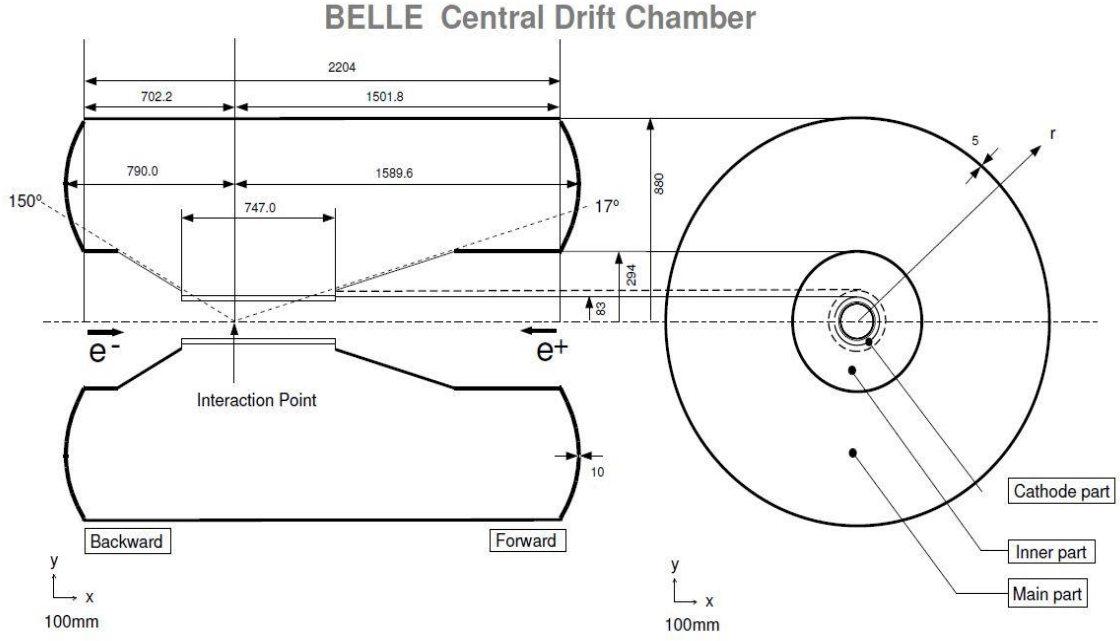


Figure 3.12. Detailed configuration of Central Drift Chamber of Belle.

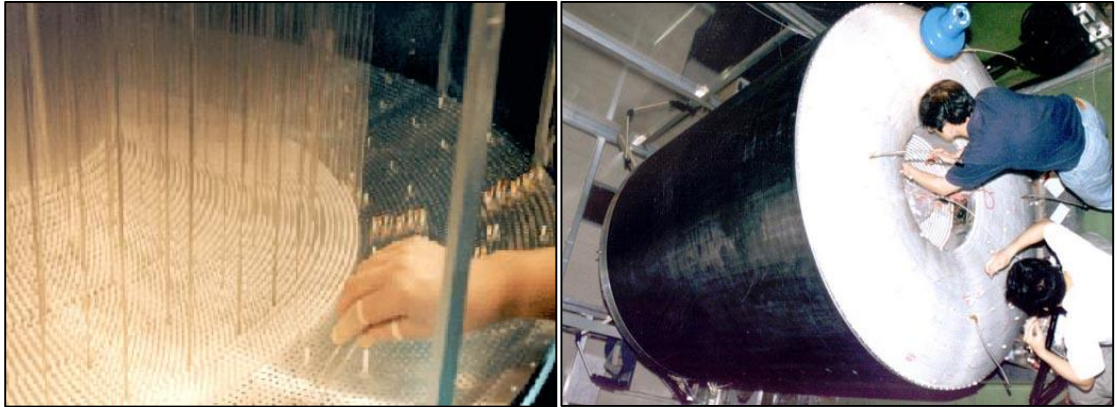
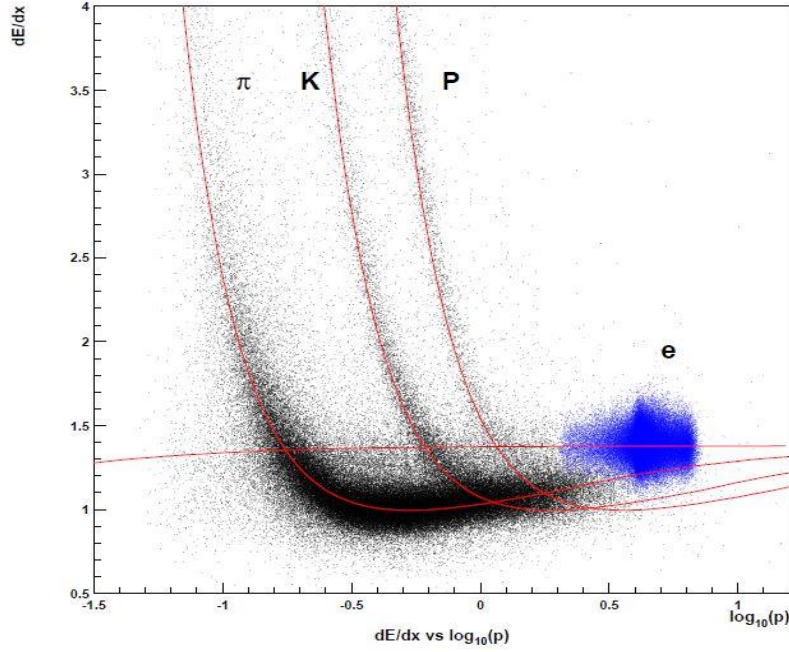


Figure 3.13. The image on the left shows a portion of the inside of CDC, showing the signal and field wires. The image on the right shows the outer body of CDC. One can see that the detector is about 1 m in diameter.

The energy loss in the same gas depends only on the mass  $m$  and velocity  $\beta$  normalized by the velocity of light. Measurement of the pulse of the hit is equivalent to measuring  $dE/dx$ . Figure 3.14 shows plots of  $dE/dx$  versus  $\log_{10} p$  ( $p$  is in  $GeV/c$ ), corresponding to  $\pi, p, K$  and  $e^-$ . The magnitude of momentum  $p$  ( $p = m\beta\gamma$ ) depends only on mass  $m$  and velocity  $\beta$ . The curves for particles with different masses are separated and so we can identify particles by combining measurements of  $dE/dx$  and momentum (from ACC measurements).



**Figure 3.14.** Scatter plot for momentum versus  $dE/dx$  (energy loss) at Belle CDC. Expected relation for  $\pi$ ,  $K$ ,  $p$  and  $e$  are shown by solid curves. One can see how this parameter can be used to identify charged particles.

### 3.3.4 Aerogel Cherenkov Counter (ACC)

Cherenkov light is a light emitted in the blue or ultraviolet region when a charged particle travels in a medium with a speed greater than the speed of light in that medium ( $= c/n$ ,  $n$  is the refractive index of the material). The phenomenon of Cherenkov light, shown in Figure 3.15, is analogous to a sonic boom, i.e. when a jet flies with a speed greater than the speed of light in that medium. The light and its emission angle hold certain information of the particle responsible for it. Angle  $\theta$  at which Cherenkov lights are emitted with respect to the direction of given angle is given by  $\cos \theta = 1/n\beta$ , where  $\beta = v/c$ . We take advantage of this phenomenon to retrieve information about the particle, i.e. its momentum. The number of photons,  $N$  is given by  $N = 490L\sin^2\theta$ ; so it is proportional to  $L \times \sin^2\theta$ ,  $L$  (cm) is the distance that particle travelled through the material.

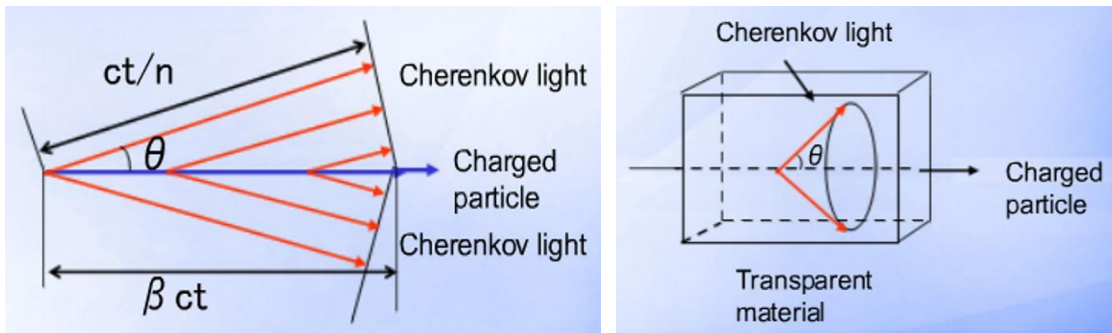


**Figure 3.15.** These diagrams show emission of Cherenkov radiation in a suitable medium with emission angle  $\theta$ . Geometry shows the formation of cone shaped emission of light.



Silica aerogel, a very light, transparent, porous material (made of silicon dioxide and about 90% of it is actually air) is used as the medium for Cherenkov light emission. Hence the detector got the name, Aerogel Cherenkov counter. Photomultiplier tubes (PMTs) are used to detect Cherenkov lights and are recorded as electric signals. An ACC module is shown in Figure 3.16.

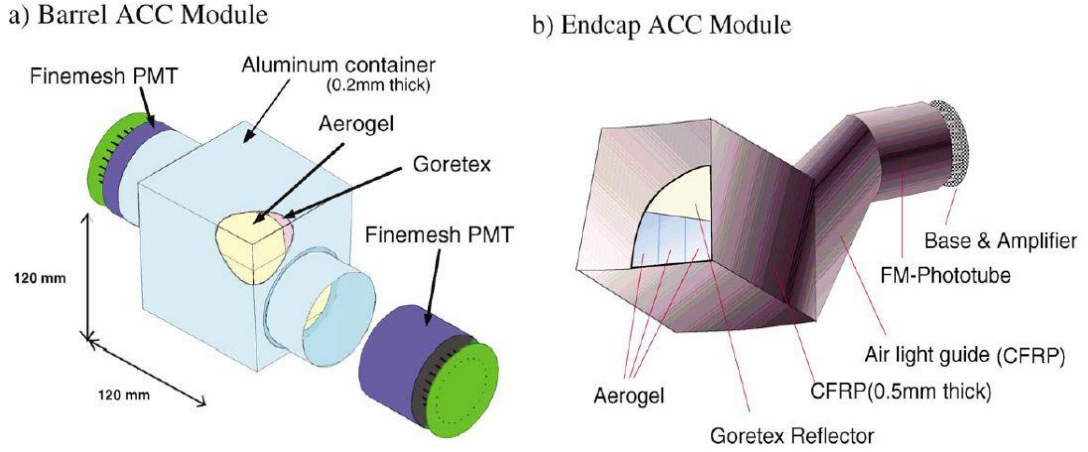


**Figure 3.16. Schematic drawing of a typical barrel and endcap ACC module.**

In ACC, particles are identified by measuring whether Cherenkov lights are emitted or not. It is a great way to distinguish between pions and kaons. Figure 3.17 shows a plot of amount of Cherenkov light emitted by kaons and electrons. Silica aerogel, used as the radiator material has refractive index between 1.01 and 1.03, for good  $K/\pi$  separation. The ratio of energy to momentum  $E/p$ , where energy is taken from ECL, is ideal for identification of electrons.

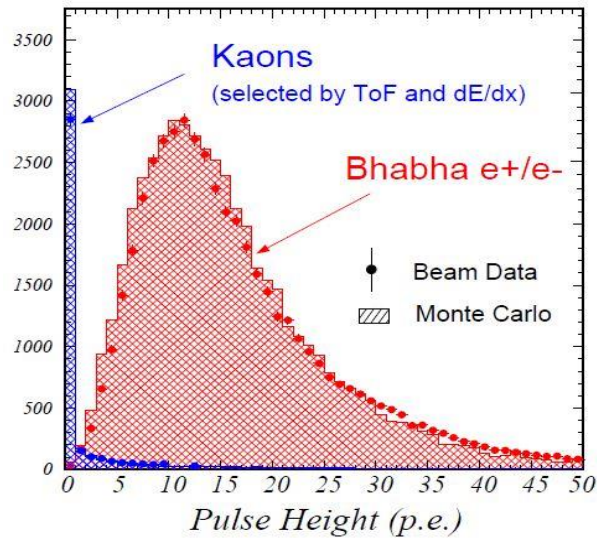


**Figure 3.17. The plot for  $K$  and  $e$  showing the amount of light absorbed (in units of photoelectrons, p.e.) by barrel ACC. Electron (owing to small mass) emits Cherenkov light but  $K$  does not emit Cherenkov light.**

### 3.3.5 Time-of-flight (TOF)

Time-of-flight is the time difference between a hit at the TOP (time-of-propagation) counter and the time of creation of particle. TOF consists of long, thin cuboidal shaped plastic scintillation counters which have a very good timing resolution, and measure time-of-flight of a particle and identify the particle. A typical module is shown in Figure 3.18. Many such counters are assembled in the form of a cylinder of radius 1.2 m. When a charged particle enters a plastic scintillation counter, scintillation lights are created. The photomultiplier tubes connected at the ends of the counter detect the lights. TOF has a precision of 100 ps. This helps in identifying particles of same momenta, as different particles (different mass) travelling with different speeds can carry same momentum ( $=\text{mass} \times \text{speed}$ ), and to measure their speed, we obviously need the information of time of flight. We can work out the speed if we measure the time when particles fly a certain distance (known from CDC measurements) since collision of electrons and positrons, so we can calculate the mass (that is, the type of particles) when combined with the measurement of momentum taken from CDC. The Time of Flight counter (TOF) is used to measure the velocity of charged particles in an intermediate momentum range  $0.8 \text{ GeV}/c$  to  $1.2 \text{ GeV}/c$ .

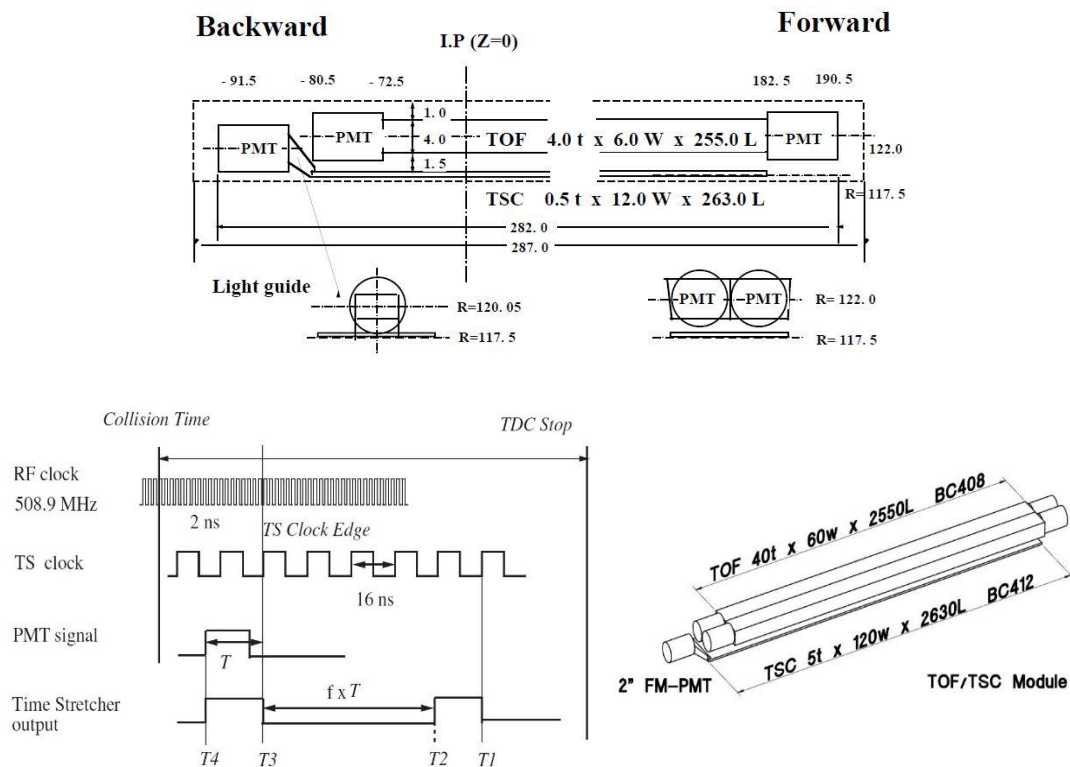


**Figure 3.18.** Top figure shows dimensions of a TOF/TSC module. The Bottom left diagram shows scheme for time stretcher and bottom right shows arrangement of a TOF module consisting of two TOF counters and one TSC.

In the case of particles with momentum  $1 \text{ GeV}/c$ ,  $\pi^\pm$  (mass approximately  $140 \text{ MeV}/c^2$ ), it will take  $4.0 \text{ ns}$  to pass through  $1.2 \text{ m}$ , and  $K^\pm$  (mass  $500 \text{ eV}/c^2$ ) will take  $4.3 \text{ ns}$ . Since Belle's TOF detector has a time resolution of  $0.1 \text{ ns}$ , it has  $K/\pi$  discrimination ability, as shown in Figure 3.19.

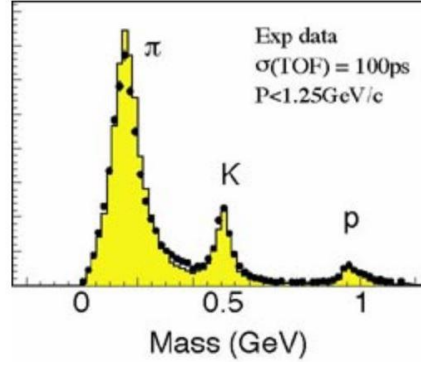


Figure 3.19. A plot of particle mass calculated based on the time information from TOF detector combined with momentum calculated from CDC. Dots and the histogram show data and MC distributions, respectively;  $K/p/\pi$  are clearly identified.

### 3.3.6 Electromagnetic Calorimeter (ECL): Detection of gamma and $e^+e^-$ .

ECL is a barrel-shaped detector for detecting photons ( $\gamma$ ) and electrons with good precision. When a photon enters a crystal of Caesium iodide (CsI), it creates an electron and positron by pair production and these create photons by bremsstrahlung process. Multiplication of this process creates a so-called ‘electromagnetic shower’. An electron gives a shower in a similar way. A large number of electrons and positrons create high yield of scintillation lights in tarium doped CsI crystals, shown in Figure 3.20 (left). Belle combines about 8000 CsI crystals into a barrel shape detector (Figure 3.20, right) surrounding the collision point. By measuring the shower with photomultiplier tubes, we measure the energy of particle. Light yield is proportional to the energy of the initial particle.

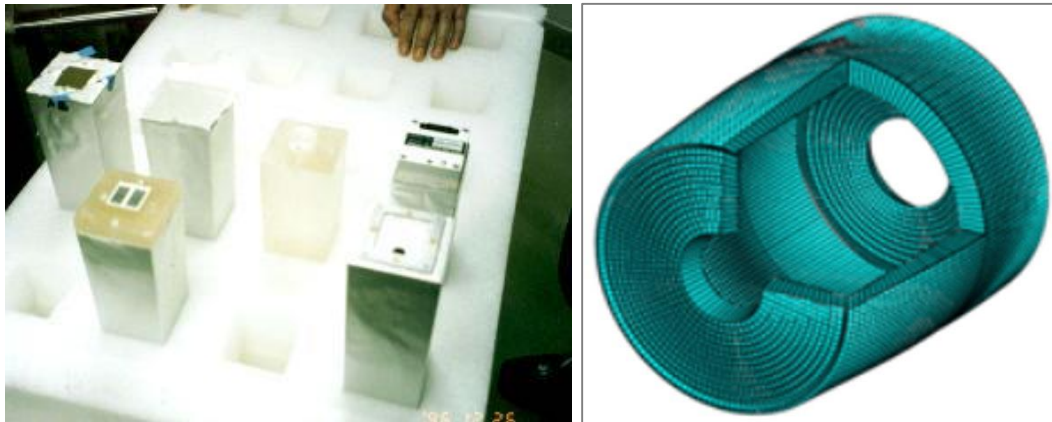
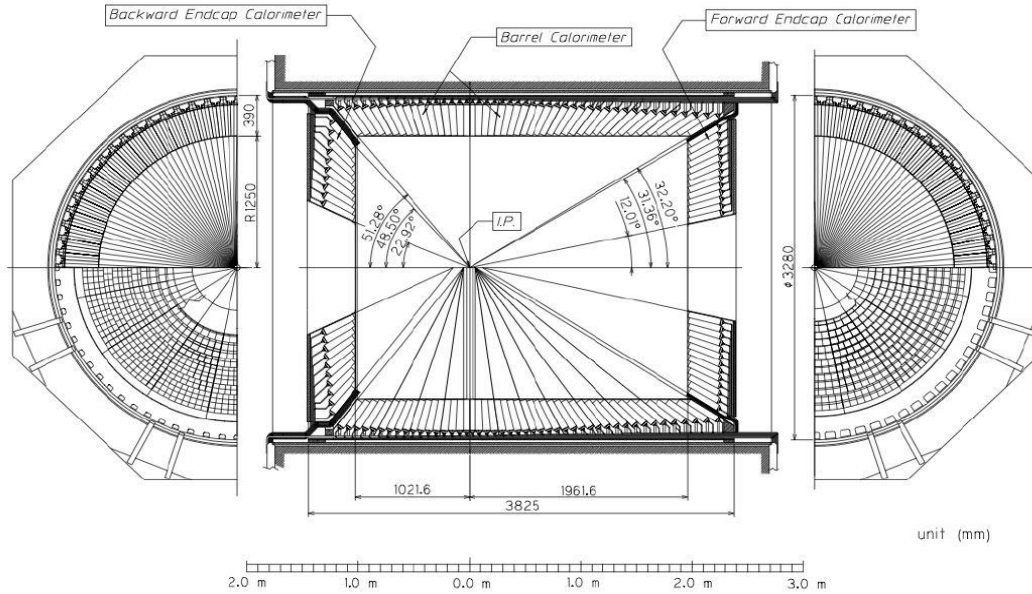


Figure 3.20. Image on the left shows CsI crystals for electromagnetic interaction. Right image shows about 8000 of these components are arranged into the barrel shaped ECL detector or Belle.

An electron is differentiated from other types of particles by comparing the magnitude of momentum measured in CDC. Also, kaons and pions give much less bremsstrahlung (since energy emitted by bremsstrahlung is inversely proportional to square of mass) so their light yield is negligible. The barrel section of ECL is 3.0 m in length with inner radius of 1.25 m and annular endcaps at  $z = +2.0$  m and  $-1.0$  m from the IP. The overall configuration of ECL with barrel and endcap regions are shown in Figure 3.21, showing the angular coverage for each region.



**Figure 3.21. Overall configuration of ECL.**

### 3.3.6 Solenoid Magnet

The superconducting solenoid, surrounding ECL, provides a magnetic field of 1.5 T in the cylindrical volume of 3.4 m in diameter and 4.4 m in length. The magnetic field bends charged particle into helical tracks, allowing for momentum determination. The superconducting coil consists of a single layer niobium-titanium-copper alloy that is embedded in the high purity aluminium stabilizer. It is wound around the inner surface of the aluminium support cylinder. Liquid helium, circulating through the cooling tubes on the inner side of the support cylinder, is used for cooling.

### 3.3.7 KLM

Muons do not interact strongly and they are 200 times heavier than electrons, so they do not lose much energy in ECL by bremsstrahlung. So they manage to reach outer part of the detector. This makes it obvious to build KLM detector as the outermost layer of the Belle detector. Most of the particles except for  $K_L$  and muons are absorbed before entering KLM or in the inner layers of KLM. In KLM, charged particles are detected by glass-electrode resistive



plate counters or RPCs. RPCs are alternated with iron plates. Three dimensional space point and timing information of the particles is catered by RPCs.

In order to be detected,  $K_L$  (neutral particle) has to first undergo some interaction;  $\pi^\pm$  are usually the secondary particles of  $K_L$ , which are formed by interaction with detector layers. On the outermost side of Belle, there is a structure of iron for returning magnetic flux. By sandwiching 14 to 15 particle detectors in between,  $K_L$  can be detected. If there is no trace corresponding to CDC for a signal in KLM, it becomes a candidate for  $K_L$ ; whereas, if extrapolated tracks from CDC hits are matching with RPC hit signals, muon is confirmed.

Resistive plate counters have parallel glass-plate electrodes separated by gas-filled gaps. High voltage is applied between the two electrodes. When a charged particle passes through the gap, the gas is ionized and initiates a discharge of plates due to the high voltage. The discharge induces a signal on the external pickup strips, which is used to record the location and time of ionization. The two dimensional space point information is obtained using a super-layer, shown in Figure 3.22, in which two RPCs are sandwiched between orthogonal  $\theta$  and  $\phi$  pickup-strips.

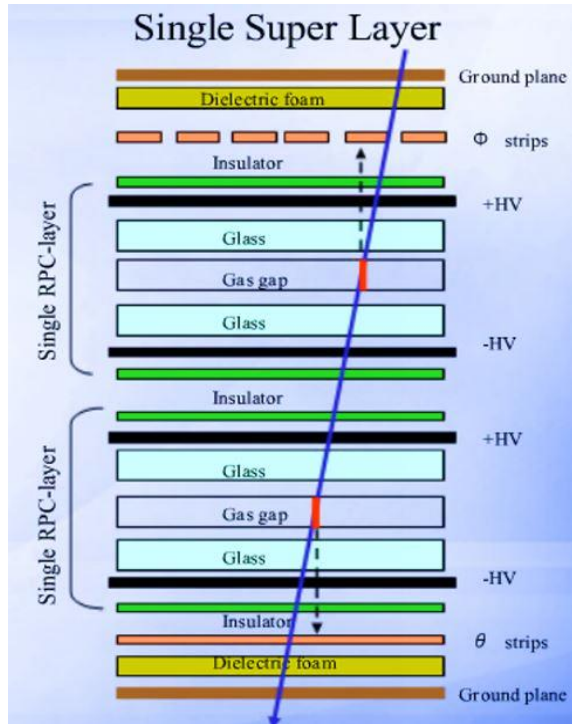
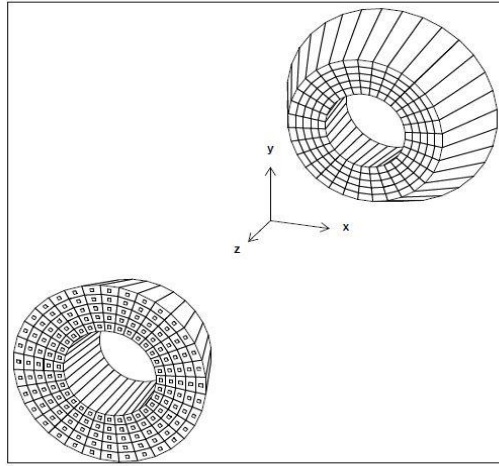


Figure 3.22. Magnified cross section of a Belle super layer double-gap RPC module.

### 3.3.8 Extreme Forward Calorimeter (EFC)

EFC is needed to extend the polar angle coverage in order to improve the experimental sensitivity. The EFC covers angular range from  $6.4^\circ < \theta < 11.5^\circ$  in the forward direction and  $163.3^\circ < \theta < 171.2^\circ$  in the backward direction. The EFC is attached to front faces of cryostats

of the KEKB accelerator compensation solenoid magnets surrounding the beam pipe. The EFC is also used for beam monitoring in the KEKB accelerator and as a luminosity monitor for the Belle experiment. EFC configuration is shown in Figure 3.23. Since the EFC is placed in the very high radiation level region around the beam pipe near the IP, so it is required to be able to sustain the radiation. So, the BGO crystal has been adopted which has the property of radiation hardness at a  $Mrad$  level and has excellent  $e/\gamma$  energy resolution. Both forward and backward EFC consist of BGO crystals segmented into 5 regions in  $\theta$  –direction and 32 regions in the  $\phi$  –direction which provides good position resolution.



**Figure 3.23. EFC Configuration.**

The particle identification role of each sub detector is summarized in Table 3.2 and the summary of Belle sub-detectors and their configuration is shown in Table 3.3.

**Table 3.2. Sub-detectors which measure each particle property.**

Particle	Energy	Momentum	Position	Particle Identification
$e^+, e^-$	ECL	CDC	SVD, CDC	ECL, ACC, TOF, CDC
$\mu^+, \mu^-$		CDC	SVD, CDC	KLM, ACC, TOF, CDC
$\pi^+, \pi^-$		CDC	SVD, CDC	ACC, TOF, CDC (atc)
$K^+, K^-$		CDC	SVD, CDC	ACC, TOF, CDC (atc)
$p, \bar{p}$		CDC	SVD, CDC	ACC, TOF, CDC (atc)
$\gamma$	ECL		ECL	ECL
$K_L$			KLM	KLM

**Table 3.3. Summary of the Belle sub-detector main characteristics.**

Detector type	Detector	Type	$\theta$ coverage (Degrees)/ Configuration	Illustrative performance
Beam pipe		Beryllium double walled	Cylindrical, $r = 20$ mm 0.5 mm Be/2.5 mm He/0.5 mm Be	He gas cooled
Tracking	SVD	Double sided Si strip (3/4 layers)	[17; 150]/ Chip size: $57.5 \times 33.5$ mm <sup>2</sup> , 300 $\mu$ m thick Strip pitch: 25(p)/50(n) $\mu$ m 3 <sup>1</sup> layers: 8/10/14 ladders, $r =$ 3.0 - 5.8 cm 4 layers: 6/12/18/18 ladders, $r =$ 2.0 cm	Single hit resolution: 12 $\mu$ m ( $R \phi$ ) 19 $\mu$ m ( $z$ )
	CDC	Drift Chamber	[17; 150]/ Anode: 50 layers Cathode: 3 layers $r = 8.3 - 86.3$ cm $-77 \text{ cm} \leq z \leq 160 \text{ cm}$	130 $\mu$ m ( $R \phi$ ) 200-1400 $\mu$ m ( $z$ ) $\sigma(dE/dx) \sim$ 7%
Particle ID	TOF	Time of flight scintillator	[34; 130]/ 128 $\phi$ segmentations $r = 120$ cm, 3 m long TSC: 64 $\phi$ segmentations	$\sigma_t = 100$ ps $K/\pi$ separation upto $p < 1.2$ $\text{GeV}/c$
	ACC	Threshold Cherenkov with Silica Aerogel	[17; 127]/ 960 barrel/228 endcap FM-PMT readout	$N_{p.e.} \geq 6$ (Number of photoelectrons) $K/\pi$ separation at $1.2 \text{ GeV}/c < p$ $< 3.5 \text{ GeV}/c$
Calorimeter	ECL	CsI(Tl)	Fwd: [12.4; 31.4]/ $z = -102$ cm Brl: [32.2; 128.7]/ $r = 125$ -162 cm Bwd: [130.7; 155.1]/ $z = 196$ cm	$\frac{\sigma_E}{E} \sim 1.7\%$ (For Bhabha events)
	EFC	BGO crystals 14 layers	$2 \times 1.5 \times 12 \text{ cm}^3$ Segmentation 32 in $\phi$ , 5 in $\theta$	$\sigma_E$ $= (7 - 10)\%$
Solenoid	Magnet	Superconducting		1.5 Tesla
Muon and $K_L$ detector	KLM	Resistive Plate Counters (RPC)	[20; 155]/ 14 layers (5 cm Fe + 4 cm gap) Each gap has 2 RPCs	$\sigma_\theta = \sigma_\phi$ $= 30 \text{ mrad}$ for $K_L$

<sup>1</sup> Untill 2003, Belle used 3 layer SVD.

### 3.4 Trigger system

In Belle experiment, we need to record events which are due to the decay of  $B$  mesons. But, in addition, there are events where  $e^-$  and  $e^+$  are scattered elastically, events where  $e^-$  and  $e^+$  collide with residual gas in the beam pipe, etc. Since it is meaningless to record all such events, it is necessary to have a system that detects when an actual event has occurred and takes the decision in a short time. That is the trigger system. Belle uses the following information to generate a trigger signal:

- Information on the number and position of charged particles detected by CDC.
- Information on energy detected by ECL.
- Information on  $\mu$  particles detected by KLM.

The trigger system is subdivided into three different stages: the hardware Level-1 trigger (Ushiroda *et al* 1999), the online software Level-3 trigger, and the offline software Level-4 trigger. The Level-4 trigger (Hanagaki *et al* 2000) performs the offline processing of the raw data and reduces it by applying a set of minimal selection requirements, such as thresholds of energy deposit and impact parameters. It provides fully reconstructed data sets containing the particle identification information, momenta of reconstructed charged tracks, photon candidates from reconstructed clusters in the ECL etc. for user analysis. Information sent from each detector system is analysed by a system called Global Decision Logic (GDL), and it is judged whether the event is interesting and recorded within about  $2 \mu s$  since the event occurred (200 to 250 events are recorded per second). The decision is sent as a signal to the data collection system.

### 3.5 Data Acquisition System (DAQ)

A system that collects and records a large amount of data measured by Belle detector is an important part of detector system. When receiving the trigger signal, it reads the signal from the detector and converts it to a digital signal so that it can be processed by the computer. Since the data sent from the detector is about 30 KB per event, it is necessary to transfer, process and record data of 10 MB/s. The DAQ system collects the sub-detector information for events specified by the Level-1 trigger. The data sent from each detector is collected for each event by a computer called "event builder" and written to the tape system located at the computer center 3 km away. The 'raw data' coming from the detectors is calibrated and reconstructed usually within 48 hours of the actual data taking and is permanently stored on Data Summary Tape (DST). For user analyses, compact data set ("mini-DST", MDST) is produced, which is approximately 12 KB for one hadronic event.

### 3.6 Computer System and Software

A computer system that analyses the collected data is also important. The raw data sent (digitized) from the detector is first reconstructed into physical particle information (such as position/momentum) after being calibrated for each detector. Belle experiment collected around one Petabyte of raw data during its run. The data has been calibrated, the events reconstructed, and collections of selected events produced. Monte Carlo events (MC) have been generated and reconstructed with the same code used for the detector data. In order to have an optimal signal selection versus background rejection procedure, one needs to understand the behavioral properties and differences between the signal and the background events in the data. It is usually not possible to separate these events in the data itself. On the other hand, any data-driven procedure to optimize signal selection over background rejection is prone to introduce, what is generally termed as, *experimenter's bias*. To avoid such limitations, the Monte Carlo simulation techniques are adopted to generate data-like samples, provided enough input information about the physical processes involved in the decays and the detector performance is known to a good accuracy. MC simulated data is used primarily to develop cuts and reconstruction program techniques in order to test their effect on signal decays and test possible backgrounds. A large amount of MC simulation data is generated to make the analysis more reliable and more precise. The Belle collaboration generates large amount of MC data of several types for different experimental conditions. The signal MC is also used to measure the signal reconstruction efficiency. Apart from collaboration wide samples, users also can produce relatively small samples as required for their individual analyses. Such samples are generated using mathematical models (EvtGen and GEANT), representing the data and all the information about the generation process is available, which can be used to tag and separate the type of events.

The data that Belle can take is 100 TB in raw data and 5 TB in data after reconstruction. To analyse this amount of data, a powerful computer system is necessary. Linux system with high cost performance is adopted for this purpose. Software for analysing data is mostly developed in the high energy industry or developed independently by Belle. As developed outside of Belle, we will simulate using event generator EvtGen (Lange 2001), which simulates what kind of decays are likely to occur in the physical process of collision. This software package can simulate the physical processes of particle decay chain, and is specialised for  $B$  physics decays. A 'decay table' is written to control decays. Users can choose the proper decay properties (particle type, branching ratios) by choosing the parameters of the decay table. The final state produced by the detector will enter the detector simulation. GEANT4 (GEometry AND Tracking) package simulates detector response and particle behaviour through the sub-

detectors. The generated particles are tracked through the detector in the Belle detector simulation (GSIM), based on the GEANT platform. The development language is C++.

In the Belle experiment, all phases in event processing—from online data-taking to offline user analyses—are performed in a unique software framework called as **basf** (Belle AnalySiS Framework). This is “home-made” core software developed within Belle. In this scheme, each program, written in C++, is compiled as a shared object, and it is treated as a module. When one wants to run a program with this framework, the modules defined in one’s script are dynamically loaded. The Belle data were stored using the PANTHER banks event store. In this utility, data transfer between different modules is made and data I/O is manipulated. PANTHER is only software to handle data in any stage of data processing.

### 3.7 Roadmap of Analysis

The analysis tools used to perform the analysis are event generator EvtGen, GEANT4 and ROOT. All phases of the work are carried under the basf framework of Belle. Firstly, a decay file is written for  $B \rightarrow J/\psi\gamma$  and EvtGen software package is used to generate signal Monte Carlo events for the pure signal and we obtain a generator file. The generated file is input to GEANT4 package which simulates the detector response and particle behaviour through the sub-detectors. The generated particles are tracked through the detector in the Belle detector simulation (GSIM), based on the GEANT platform. The simulated file is passed through physics analysis code written in C++ programming language. The output ROOT file is analyzed to obtain histograms, etc., using ROOT software. This process is summarized in the flowchart (Figure 3.24).

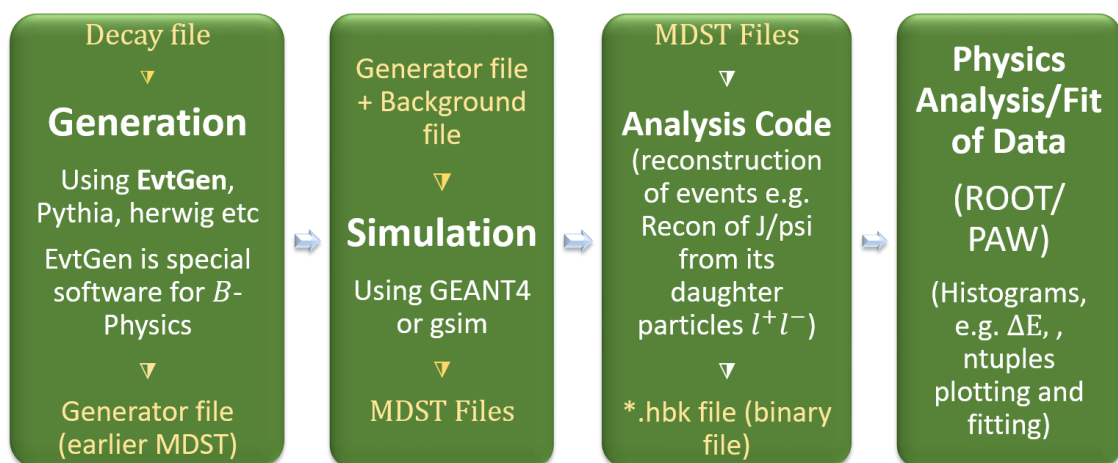


Figure 3.24 Flowchart of the process for carrying out analysis of a decay.

## CHAPTER IV

### RESULTS AND DISCUSSION

Every decay comes with large background and the type and amount of background depends upon the decay under consideration. So, when dealing with a new decay mode, background suppression and signal yield extraction are carried out for the given data. Belle collected 772 million  $B$  meson pairs, which is large enough to carry out analysis of a rare decay. In the present analysis,  $B^0 \rightarrow J/\psi\gamma$  ( $J/\psi \rightarrow l^+l^-$ , where  $l = e/\mu$ ) rare radiative decay is studied. We need to identify the possible backgrounds accompanying the decay and also apply background suppression methods.

#### 4.1 Hadronic Event Selection

There are several processes taking place at large cross sections, along with the desired  $B\bar{B}$  production, at Belle. These events include continuum ( $e^+e^- \rightarrow q\bar{q}$ ), Bhabha scattering ( $e^+e^- \rightarrow e^-e^+$ ) shown in Figure 4.1, two photon events,  $\tau$  pair events ( $e^+e^- \rightarrow \tau^-\tau^+$ ), etc. These events have a high cross-section (cross-section values given in Table 4.1) and so we firstly have to skim these processes out of the event of interest i.e.  $B\bar{B}$  production. Events recorded by Belle are classified into several categories, such as Bhabha events, tau pair, etc., after processing of data. For the analyses of  $B$  and charm mesons, HadronBJ is used which is basically a skim for hadronic events. Using this, the number of  $B\bar{B}$  signals in hadronic data sample are estimated as,

$$N_{B\bar{B}} = N_{on} - \frac{\epsilon_{on} L_{on}}{\epsilon_{off} L_{off}} N_{off} \quad (4.1)$$

where,  $N_{on}(N_{off})$ ,  $L_{on}(L_{off})$  and  $\epsilon_{on}(\epsilon_{off})$  are the number of on resonance (off resonance) or  $q\bar{q}$  (continuum) events, luminosity and the detection efficiency in the on-resonance (off-resonance) data, respectively. Using this relation, the  $B\bar{B}$  events recorded by the Belle detector at  $Y(4S)$  are calculated to be  $772 \times 10^6$  since its operation from June 1999 to June 2010.

**Table 4.1. Production cross-sections ( $\sigma$ ) and selection efficiencies ( $\epsilon$ ) for different processes, as before applying the HadronB selection criteria.**

Process $e^+e^- \rightarrow$	$B\bar{B}$	$q\bar{q}$	$\tau^+\tau^-$	QED	$\gamma\gamma$
$\sigma(nb)$	1.1	3.3	0.93	37.8	11.1
$\epsilon(\%)$	99.4	83.8	24.0	0.2	0.8

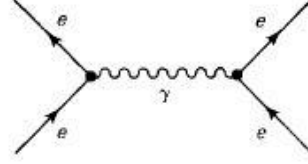


**Figure 4.1 Feynman diagram for Bhabha scattering ( $e^+e^- \rightarrow e^-e^+$ ).**

The following HadronBJ skimming criteria is taken into account to select events with  $B$  mesons. To remove the background, firstly we have to execute the event selection. HadronBJ events are selected mainly on the basis of visible energy and track multiplicity. Charged tracks of hadronic events must be greater than three and should originate close to interaction region, i.e  $|dr| < 2.0$  cm,  $|dz| < 4.0$  cm and  $p_T > 0.1$  GeV/c, where  $p_T$  is the transverse momentum and  $dr$  and  $dz$  represent impact parameters normal to interaction point in the x-y plane and along the z-axis, respectively. These selections remove much of the beam background and  $\gamma\gamma$  events. Further selection criteria applied to remove more beam gas background are:

- A photon candidate within the CDC acceptance ( $17^\circ < \theta < 150^\circ$ ) is defined to have ECL clusters with energy  $E > 100$  MeV having no match to CDC tracks.
- The visible energy  $E_{vis}^*$ <sup>2</sup>, which is the sum of the good track momenta and good photon energies is required to be at least  $0.2\sqrt{s}$ . Figure 4.2 shows distribution of  $E_{vis}^*$  for signal Monte Carlo, where  $s$  is the square of centre-of-mass (CM) energy.
- $E_{sum}^*$  is defined as the energy sum of ECL clusters in the central barrel section and is required be within  $0.1 < E_{sum}^*/\sqrt{s} < 0.8$ .
- The vector sum of z momenta of all good tracks and good photons is required to be  $|p_z| < 0.5 \sqrt{s}$ .
- The vertex of primary event is required to be within a cylinder defined by  $r < 1.5$  cm in the x-y plane, and  $|z| < 3.5$  cm.
- In the barrel region of the detector, the number of ECL clusters,  $N_{CLUSTER} > 1$ .
- The heavy jet mass, HJM, defined as the invariant mass of particles found in perpendicular hemispheres of the event thrust axis, is required to be greater than 0.25 times  $E_{vis}$  to effectively remove  $\tau$  pair events. HJM distribution for signal MC is shown in Figure 4.2. The average cluster energy must be:  $E_{SUM}^{ECL}/N_{CLUSTER}^{ECL} < 1.0$  GeV.

These selection criteria retain 79.5% of continuum events and 99.1% of  $B\bar{B}$  signal events while it reduces the contamination from non-hadronic processes to less than 5%.

For our analysis, the charged tracks are required to have  $|dz| < 4.0$  cm,  $|dr| < 0.4$  cm and  $0.4 \text{ rad} < \theta < 2.43 \text{ rad}$ , where  $dz$  is the z component of the track's closest approach

---

<sup>2</sup> The observables referred with asterisk denote measurements taken in CM frame.



with respect to the origin and  $\theta$  is polar angle of the track, in order to remove charged particle tracks that are poorly measured or do not come from the interaction region. The  $dr$  and  $dz$  distributions from experimental data are shown in Figure 4.3.

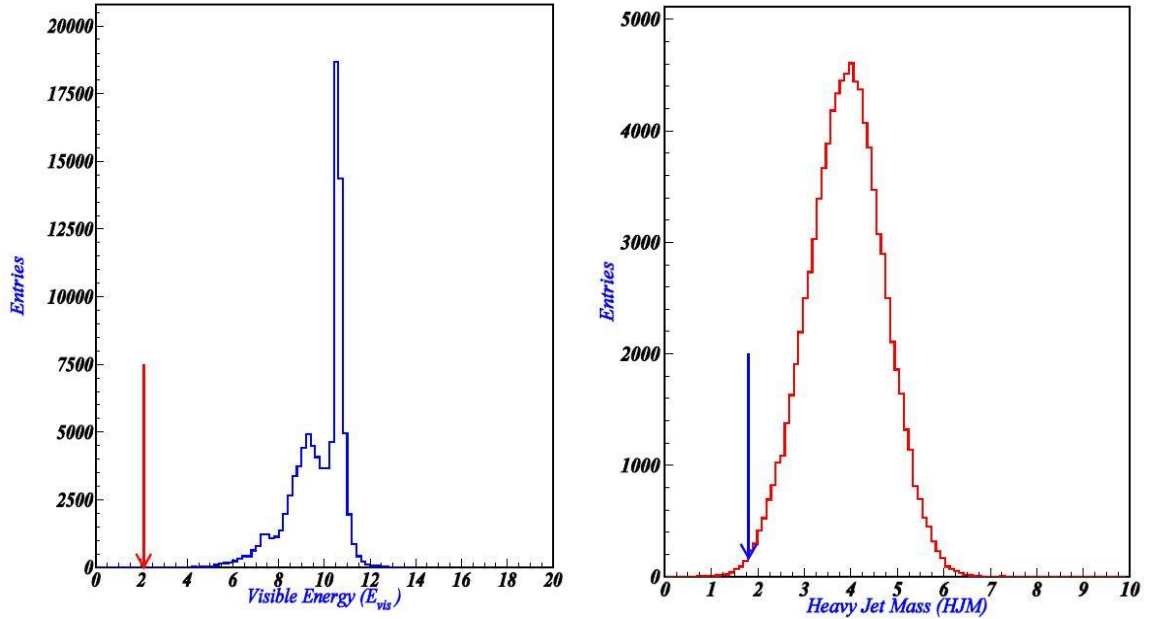


Figure 4.2. Visible Energy ( $E_{vis}^*$ ) (left) and Heavy Jet Mass (HJM) (right) distributions for signal MC. The arrows indicate the cuts applied.

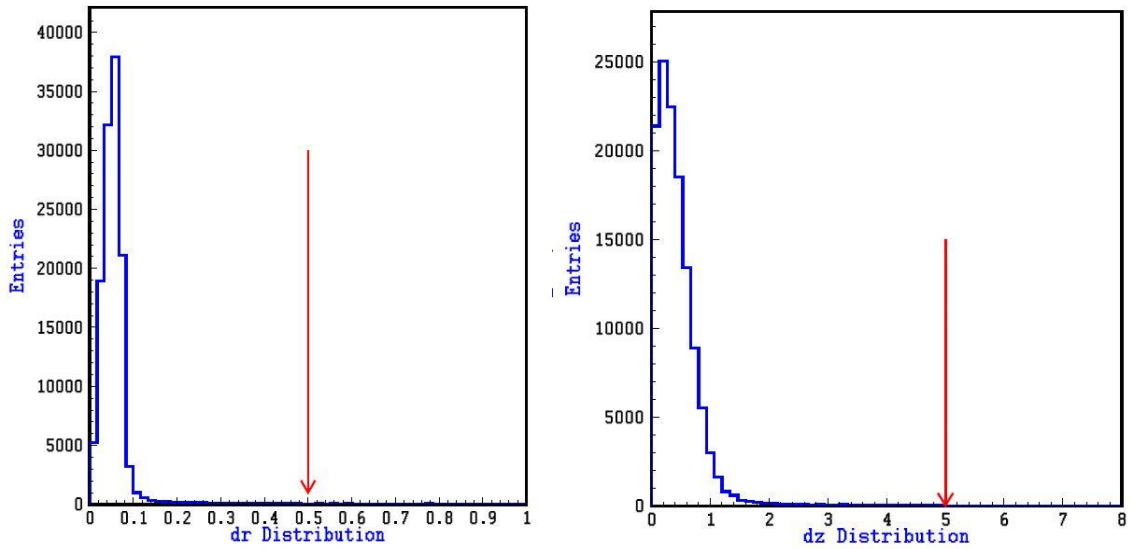


Figure 4.3. The  $dr$  (left) and  $dz$  (right) distributions from experimental data. The arrows indicate the cuts applied for event selection.

## 4.2 Continuum Background Suppression

For the analysis of  $B$  decays, kinematical constraints from  $e^+e^-$  collision at  $\sqrt{s}=10.58\text{ GeV}$  are used. In addition to this, ‘event shape’ information, i.e. the phase-space

distribution of decay particles detected in the event, is crucial to discriminate the background. A specific  $B$  decay can have a large number of background sources like continuum, hadronic or combinatorial background, some of which could be dominant, depending upon the decay channel under consideration. Thus background suppression is crucial issue in the analysis techniques.

After kinematic selection, additional background rejection is obtained by exploiting differences in the angular distributions of the final state particles. The distribution is dependent upon the spin and polarization of the particles involved in the decay chain. This information can be quantified as under:

#### **Variables related to $B$ meson direction:**

The spin-1  $Y(4S)$  decaying into two spin-0  $B$  mesons results in a  $\sin^2 \theta_B$  angular distribution, where  $\theta$  is taken with beam axis. Whereas,  $e^+e^- \rightarrow q\bar{q}$  events, the spin-1/2 fermions  $q$  are light and are produced with a large initial momentum, so they result in two back to back jets of light hadrons distributed following a  $1 + \cos^2 \theta_B$  distribution. This helps in rejecting the continuum background,  $q\bar{q}$ , using variable  $\theta_B$ .

*The Fox-Wolfram moments:* These are mathematical tools to parameterize the phase-space distribution of momentum and energy in an event (Fox and Wolfram 1978). The  $k^{th}$  order Fox-Wolfram moment ( $H_k$ ) for a collection of  $N$  particles with momenta  $p_i$  is defined as

$$H_k = \sum_{i,j}^N |\vec{p}_i| |\vec{p}_j| P_k(\cos \theta_{ij}) \quad (4.2)$$

where  $\theta_{ij}$  is the angle between  $p_i$  and  $p_j$ , and  $P_k$  is the  $k^{th}$  order Legendre polynomial. For particles with vanishing masses,  $H_0 = 1$ ; that is why the normalized ratio  $R_k = H_k/H_0$  is often used, which takes values close to zero (one) for odd (even) values of  $k$ , for events with two strongly collimated jets. These are powerful means to discriminate between events with different topologies.

The jet like backgrounds from continuum background events  $e^+e^- \rightarrow q\bar{q}$  ( $q = u, d, c$  or  $s$ ) are suppressed using the event shape variable,  $R_2 < 0.5$ , where  $R_2$  is the ratio of second to zeroth order Fox-Wolfram moments.  $R_2$  is defined as

$$R_2 = \frac{H_2}{H_0} \quad (4.3)$$

Therefore  $R_2 \rightarrow 1$  for narrowest two-jet event. While in the case of spherical events like  $B$  decays,  $R_2 \approx 0$ . These two types of events are shown in figure 4.4. The cut on  $R_2$  is optimized using the figure-of-merit (FoM), defined by  $S/\sqrt{(S + B)}$ , where  $S(B)$  is the number of signal

(background) events within signal region. Figure 4.5 shows the  $R_2$  distribution for signal Monte Carlo and the experimental data.

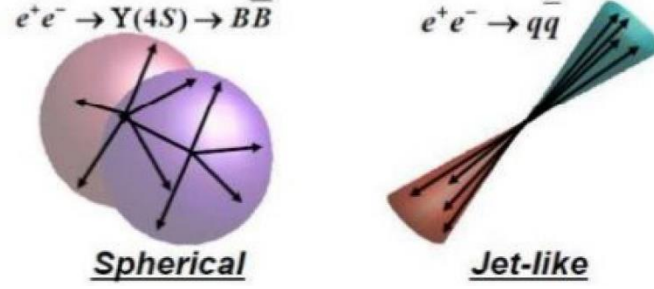


Figure 4.4 Spherical events from the decay of  $B\bar{B}$  at rest and jet like events from continuum  $e^+e^- \rightarrow q\bar{q}$ .

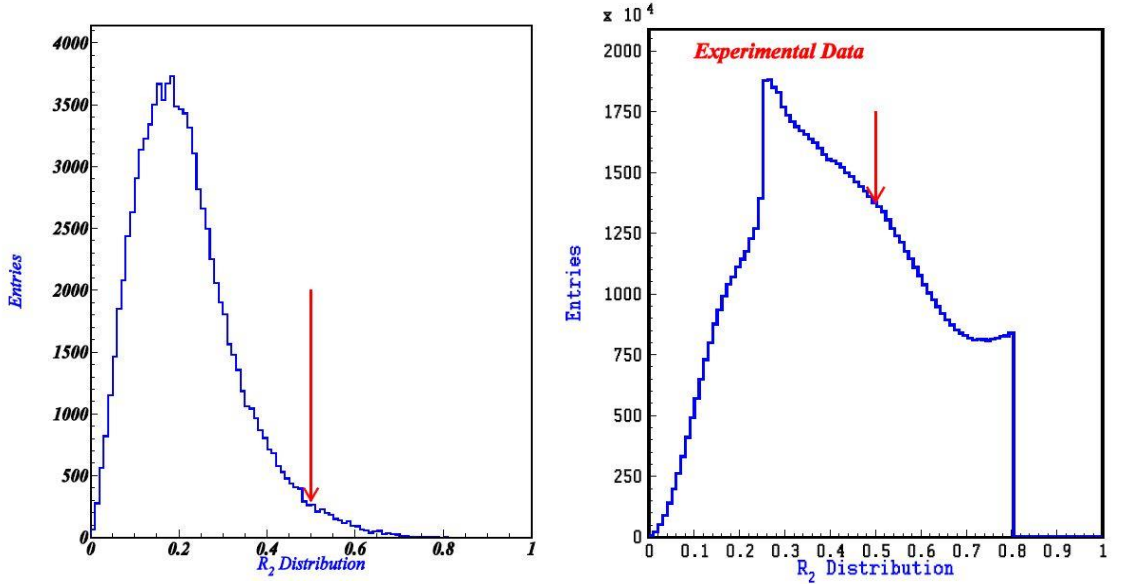


Figure 4.5.  $R_2$  distribution for signal MC (left) and experimental data (right). The arrows indicate the cuts applied for event selection.

### 4.3 Monte Carlo Data

The signal MC means events generated for the decay mode of interest e.g.,  $B \rightarrow J/\psi\gamma$ . Signal MC events are generated with EvtGen (Lange 2001) event generator and the response of the Belle detector is precisely simulated by GEANT4 program (Agostinelli *et al* 2003). In any given event sample  $Y(4S)$  decays to two  $B$  mesons and only one of them will decay via signal mode while the other  $B$  meson will decay generically (to any mode). General events in the detector are simulated based on the known branching fractions and cross-sections. To calculate the reconstruction efficiency for the decay, 100,000 events are generated. The decay model used for  $Y(4S) \rightarrow B\bar{B}$  is VSS (vector to scalar-scalar) and for the decay  $B \rightarrow J/\psi\gamma$ , PHOTOS (Barberio, Eijk, and Was 1991) SVP\_HELAMP (scalar to vector and photon) is

adopted.  $J/\psi \rightarrow l^+l^-$  is modelled by PHOTOS VLL (vector to lepton-lepton). Also, background, which comes from detector noise and beam, is added to these events.

#### 4.4 Particle Identification (PID)

The particle identification is the main step towards efficient reconstruction of particle. Separate groups inside the Belle collaboration have studied the detector response and developed specific particle identification likelihoods to identify electrons, muons and to discriminate between pions, kaons and protons. Excellent PID capabilities are needed for separating the final state particle's momentum and energy and also, the particles have to be reconstructed from the detector recorded hits. The key reconstruction techniques for charged particles and showers are described in the following sub-sections.

##### 4.4.1 Charged particle identification

Belle uses the data collected from all of its sub-detectors for the PID selectors, which are based upon applying cuts to the variable relevant to the particle type (e.g. Cherenkov angle for  $K/\pi$  separation,  $E/p$  ratio for electrons, and so on). CDC provides the  $dE/dx$  measurement of a charged track. ACC provides the number of Cherenkov photons which helps in separation for higher momenta. A TOF counter measures the time-of-flight between the interaction point and counter for a charged particle, which is used to evaluate velocity of the particle. For electron identification (Hanagaki *et al* 2002), ECL information is combined with CDC and ACC. The KLM (Abashian 2002a) is employed for muon identification.

A charged particle leaves track in CDC, which is why track-segment-hit-patterns are first looked for, in order to reconstruct charged final state particles. Axial wire hits provides projection of tracks on  $r - \phi$  plane and the stereo wire hits provide z-positions of the track. Track parameters (position and momentum) are obtained by the fitting based on the Kalman filter technique (Kalman and Bucy 1961), which minimizes the effect of multiple coulomb scattering and non-uniformity of the magnetic field in the CDC. Then, all of the hit points are connected and fitted to a helix to obtain a particle's momentum and position. The reconstructed charged particle trajectory so obtained is then extrapolated towards the SVD hits to improve the resolution of track parameters. The track momenta are also calibrated by a scaling constant so as to match the reconstructed invariant mass of  $J/\psi \rightarrow \mu^+\mu^-$  with the world averages. The calibrations are made for every run, typically after a few months of data taking. The fluctuations in current supplied to the solenoid magnet mainly causes a change in the calibration constant and amounts to the correction of  $O(10^{-3})$ . The estimated errors of track parameters are also calibrated by a scaling constant using the cosmic ray events.

- **Measurement of  $dE/dx$  by CDC**

The  $dE/dx$  measurements by CDC enables us to distinguish hadrons and electrons. The averaged  $dE/dx$  as a function of momentum is shown in the Figure 4.6. From the distribution, the separating power is higher in the lower momentum region and this feature is supplementary to the ability of  $E/p$ . Another discriminant is light yield in ACC, used for the electron identification for the elimination of kaons. Each sub-detector provides a probability for a particle to be of a certain type. This probability is associated to likelihood functions  $\mathcal{L}_k$  that tell if the measured properties of charged track in question correspond to a true  $k$ -particle. Information about charged particle identification, e.g. pions and kaons, is obtained by combining information from the CDC, TOF and ACC. The likelihood for a particle to be of type  $f$  is obtained by multiplying the likelihoods from the subdetectors:

$$\mathcal{L}_f = \mathcal{L}_f^{CDC} \cdot \mathcal{L}_f^{TOF} \cdot \mathcal{L}_f^{ACC} \quad (4.4)$$

The PID at Belle is based on likelihood ratios. The joint information from the CDC, ACC and TOF are combined into likelihood ratio for particle identification. For hadron identification, likelihoods for a candidate are based on  $dE/dx$  information from the CDC ( $\mathcal{L}_\alpha^{CDC}$ ), the number of photons from the ACC ( $\mathcal{L}_\alpha^{ACC}$ ) and time of flight from the TOF ( $\mathcal{L}_\alpha^{TOF}$ ). Then, the likelihood ratios

$$\mathcal{L}(\alpha:\beta) = \frac{\mathcal{L}_\alpha^{CDC} \mathcal{L}_\alpha^{TOF} \mathcal{L}_\alpha^{ACC}}{\mathcal{L}_\alpha^{CDC} \mathcal{L}_\alpha^{TOF} \mathcal{L}_\alpha^{ACC} + \mathcal{L}_\beta^{CDC} \mathcal{L}_\beta^{TOF} \mathcal{L}_\beta^{ACC}} \quad (4.5)$$

are calculated and are used for identification. For example, particles with  $\mathcal{L}(K:\pi)$  exceeding (beneath) a chosen value are classified as kaons (pions). The cut value applied to these likelihood ratios are optimized according to the analysis.

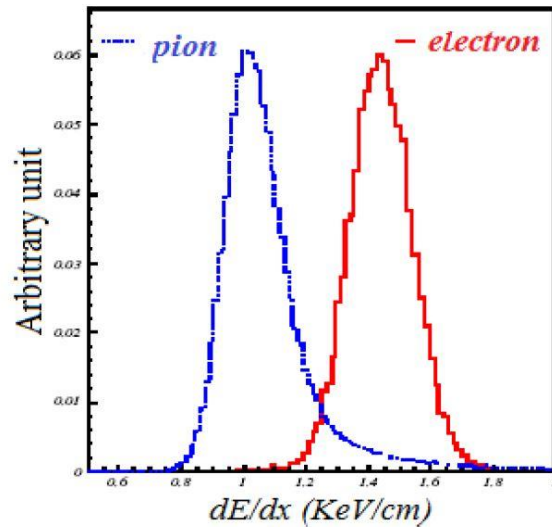
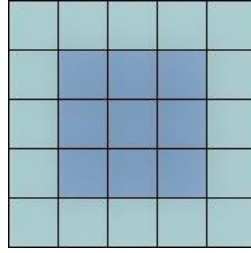


Figure 4.6. Energy loss distribution  $dE/dx$  for electrons and pions.

#### 4.4.2 Shower reconstruction

Photon or electron cause electromagnetic shower at the CsI(Tl) crystal in the ECL, then its energy is measured. An electromagnetic shower spreads over several crystals that are neighboring each other. Therefore, such a group of crystal hits, which is called cluster has to be found to reconstruct a shower. First, a local maximum energy crystal, whose energy deposit exceeds 10 MeV, is picked up as a “seed crystal”. The surrounding crystals of  $5 \times 5$  matrix is the basis of the shower reconstruction. To check the matching among the reconstructed showers and tracks, a track is extrapolated up to the calorimeter crystal front face. When the extrapolated track goes across a CsI crystal front face, the shower including the hit crystal, where the extrapolated track arrived, is regarded as an associated shower with the charged track. Among the showers that are not associated with any charged tracks, all the reconstructed ones that exceed 0.5 GeV are accepted. Below 0.5 GeV, to recognize a photon, the following criteria is required; having at least 20 MeV, shower width is less than 6 cm and  $E_9/E_{25}$  is greater than 0.75, where, shower width is the lateral spread of the shower calculated as the energy-weighted distance between crystal hits and the shower centre.  $E_9/E_{25}$  means the ratio of energies contained by  $3 \times 3$  and  $5 \times 5$  crystal matrices surrounding the seed crystal, as shown in Figure 4.7.



**Figure 4.7. Picturing  $E_9/E_{25}$ ;  $E_9$  corresponds to the total detected energy of inner 9 cells and  $E_{25}$  to all 25 cells.**

#### 4.4.3 Electron Identification

To form likelihood ratios for electron identification, ECL information ( $E/p$ , matching of the positions of the track, transverse shower shape and the energy cluster) is used in addition to  $\mathcal{L}_\alpha^{CDC}$  and  $\mathcal{L}_\alpha^{ACC}$ . Since hadrons and muons do not produce showers in the ECL and lose only a small portion of their energy by means of ionisation, the information from the ECL, compared with momentum measurements provided by the CDC enables the identification of electrons. Discriminating variables that utilize information from these sub-detector systems to identify electrons are as follows:

- **Track to cluster matching  $\chi^2$**

The projected electron track is required to match the position of an ECL cluster. Figure 4.8 shows the difference in  $\phi(\Delta\phi)$  and  $\theta(\Delta\theta)$  between a cluster position and a position of an

extrapolated track.  $\sigma_{\Delta\phi}$  and  $\sigma_{\Delta\theta}$  are the widths obtained by fitting the  $\Delta\phi$  and  $\Delta\theta$  distribution of electrons with Gaussian. The matching condition is decided by measuring a chi-square, defined as

$$\chi^2 \equiv \left( \frac{\Delta\phi}{\sigma_{\Delta\phi}} \right)^2 + \left( \frac{\Delta\theta}{\sigma_{\Delta\theta}} \right)^2 \quad (4.6)$$

The  $\chi^2$  distributions for charged pions and electrons are shown in Figure 4.9. For each charged track, a cluster that gives the minimum  $\chi^2$  and that have the  $\chi^2$  less than 50, is taken for the matched cluster.

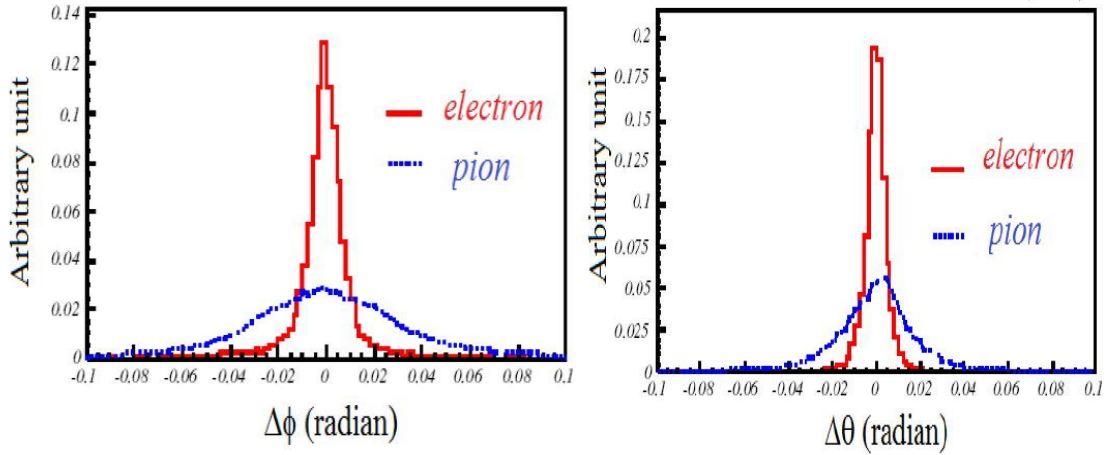


Figure 4.8.  $\Delta\phi$  (left) and  $\Delta\theta$  (right) distributions for electrons and charged pions.

- **$E/p$  determination**

$E/p$  is the ratio of energy measured by the ECL to the momentum measured by the CDC. Electrons, on average, deposit all of their energy in the calorimeter. In contrast, hadrons deposit only a small fraction of their energy, and this fraction fluctuates greatly. Consequently,  $E/p$  tends towards one for electrons but is less than one for hadrons, as demonstrated in Figure 4.10.

- **$(E_9/E_{25})$  Shower Shape**

Electrons and hadrons showers behave differently in both longitudinal and transverse directions in the crystals since hadrons typically provoke more than one shower. These differences are shown in Figure 4.11; the peak of pions evident at 1 represents high momentum pions acting as minimum ionising particles.

In order to eliminate kaons for electron identification, ACC light yield is incorporated. Figure 4.12 shows the electron identification efficiency measured with  $e^+e^- \rightarrow e^+e^-e^+e^-$  data and the fake rate for charged pions from  $K_S^0 \rightarrow \pi^+\pi^-$  decays as a function of momentum. The hadron fake rate is less than 1% and electron identification efficiency is greater than 90% for  $p_{lab} > 1$  GeV/c.

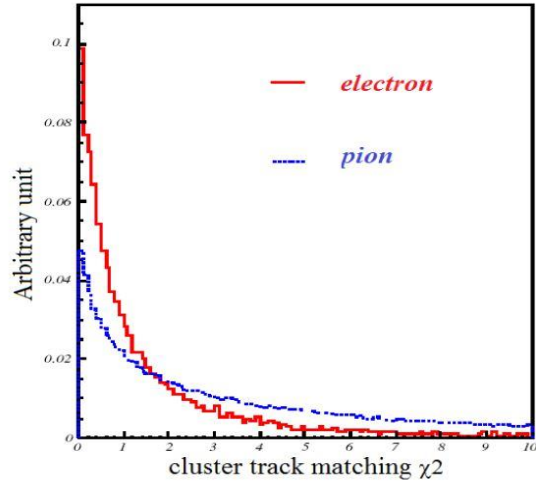


Figure 4.9. Cluster track matching  $\chi^2$  distribution for electrons and pions.

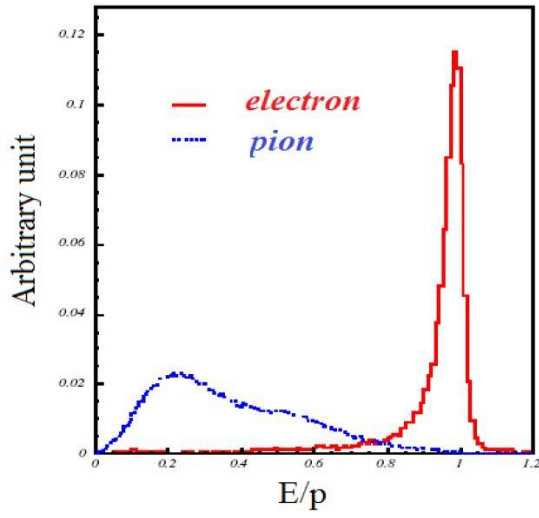


Figure 4.10.  $E/p$  distribution for electrons and charged pions.

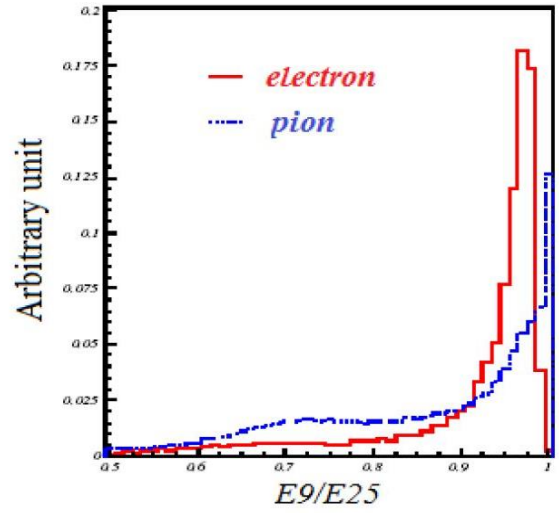


Figure 4.11.  $E_9/E_{25}$  distribution for electrons and pions.

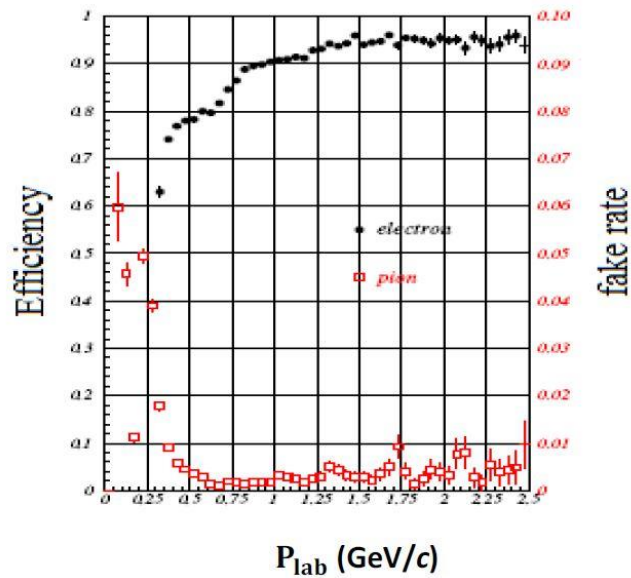


Figure 4.12. Electron identification efficiency (circles) and fake rate for charged pions.



#### 4.4.4 Muon identification

Muons are distinguished from other charged particles, electrons and hadrons, as they penetrate much further in the KLM due to lesser bremsstrahlung energy losses and the fact that they do not interact strongly. Muon deposits its energy by energy loss (ionization and atomic excitation) as it is massive lepton. Electrons, being less massive, totally deposit energy in the ECL and hardly reach the KLM and as a result can be differentiated from muons. For muon identification, KLM hits are matched to the extrapolated CDC track hits ( $K_L$  doesn't leave track in CDC), using the difference  $\Delta R$  between the expected and measured range of the track, and the statistic  $\chi^2$  constructed from the transverse deviations of all hits related to the track, normalized by total hits. The probability density distribution of  $\Delta R$  and  $\chi^2$  is obtained by Monte Carlo simulation. Likelihoods for the  $\pi^\pm, \mu^\pm$  and  $K$  hypotheses are formed based on PDFs (probability density functions) in  $\Delta R$  and  $\chi^2$ . The density  $p(\Delta R, \chi^2)$  is defined by two probability distribution functions,  $P_\mu^{\Delta R}, P_\mu^{\chi^2}$  and is given by

$$p(\Delta R, \chi^2) = P_\mu^{\Delta R} \times P_\mu^{\chi^2} \quad (4.7)$$

Based on this probability density, we obtain likelihood  $\mathcal{L}_\mu$ . If the muon likelihood ratio a track is greater than 0.1, the track is identified as muon, where the muon likelihood ratio is defined as

$$\mathcal{R}_\mu = \mathcal{L}(\mu) / (\mathcal{L}(\mu) + \mathcal{L}(\pi) + \mathcal{L}(K)). \quad (4.8)$$

A track is extrapolated from the CDC to the KLM and corresponding associated KLM hits are investigated; a track is re-fitted with those associated KLM hits, presuming that a track goes through only with the energy loss and multiple scattering effects.

#### 4.5 Reconstruction Procedure for $B \rightarrow J/\psi \gamma$

$B$  meson reconstruction is carried out from its decay particles (daughters and granddaughters) depending upon their stability (lifetime) and identification (in the detector) as they are most stable and can be easily identified in the detector.

##### 4.5.1 Reconstruction of $J/\psi$

$J/\psi$  mesons decay into oppositely charged lepton pairs  $e^+e^-$  or  $\mu^+\mu^-$ , from which we reconstruct back  $J/\psi$ . Electron and muon pairs are selected from the charged tracks after applying electron likelihood ( $\mathcal{L}_e$ ) larger than 0.01 and muon likelihood ( $\mathcal{L}_\mu$ ) larger than 0.1, respectively. The bremsstrahlung photons,  $\gamma_s$ , emitted by either electron or positron within 50 mrad of the initial momentum are added to the invariant mass  $M_{ee}$ . Monte Carlo distribution for  $J/\psi$  signal reconstructed from muon and electrons decay modes are shown in Figure 4.13

(a) and Figure 4.13 (b) respectively. For  $J/\psi$  reconstructed from muons, the mass window is  $3.03 \text{ GeV}/c^2 < M_{\mu\mu} < 3.13 \text{ GeV}/c^2$ . For  $J/\psi$  reconstructed from electron-positron, as we can still miss some photons, we have asymmetric invariant mass window for  $M_{ee(\gamma)}$ ; the region selected is  $2.94 \text{ GeV}/c^2 < M_{ee(\gamma)} < 3.13 \text{ GeV}/c^2$ . Helicity angle,  $\theta$ , is defined as the angle between the  $l^+$  (one of the charged daughters of  $J/\psi$ ) and the negative of the  $B$  flight direction in the  $J/\psi$  rest frame. The helicity plots of  $J/\psi$  from dimuons and dielectrons are shown in Figure 4.13 (c) and (d) respectively. Kinematic mass and vertex-constrained fits are applied to reconstructed  $J/\psi$  candidates to improve momentum and vertex resolution. Fits to invariant mass distribution of  $J/\psi$  from dimuons and dielectrons from Monte Carlo data are shown in Figure 4.14 and from real data are shown in Figure 4.15.

To calculate the signal yield, fitting of  $J/\psi \rightarrow e^+e^-$  and  $J/\psi \rightarrow \mu^+\mu^-$  distributions are made and the resultant signal peak of  $J/\psi$  consists of Crystal Ball function (Gaiser 1982) and for combinational background Chebyshev polynomial of order three. In the ECL, there appears a tail in the line allowed by the Crystal Ball function. This tail appears because of leakage of photon shower.

For the dielectrons case, the invariant mass of  $J/\psi$  comes out to be  $1.20 \pm 0.26 \text{ MeV}/c^2$  more in Monte Carlo than in experimental data ( $3095.70 \pm 0.25$  vs.  $3094.50 \pm 0.06 \text{ MeV}/c^2$ ).

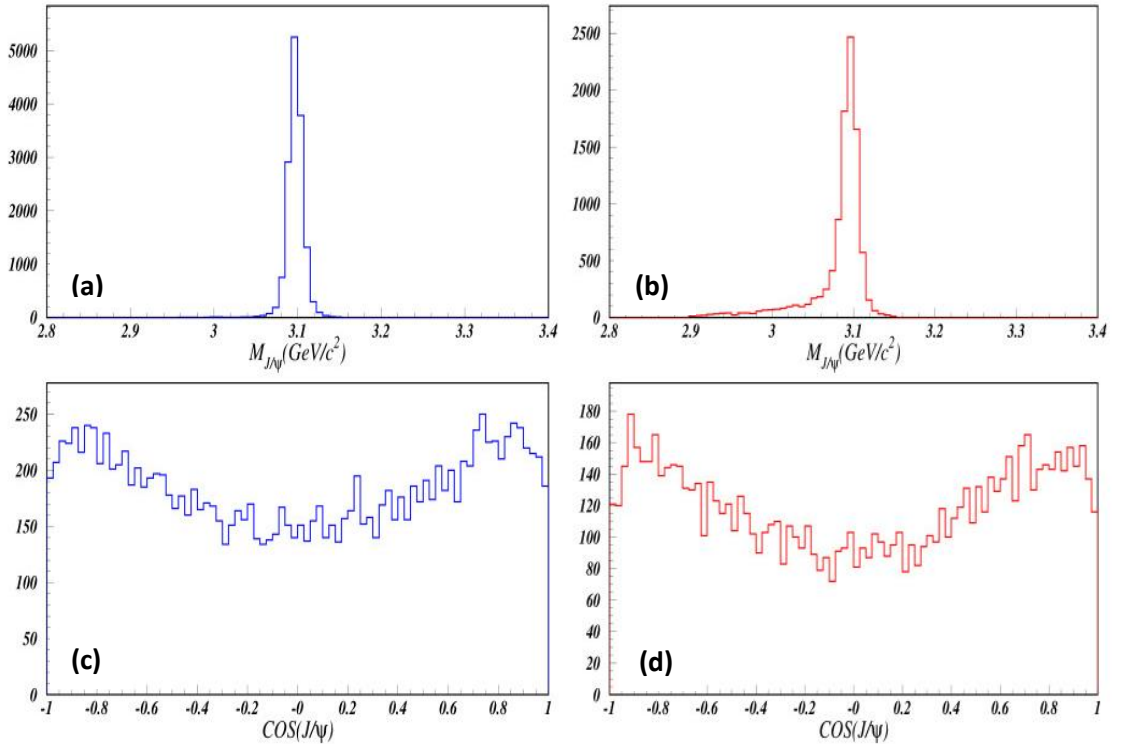


**Figure 4.13.** MC distribution of  $J/\psi$  reconstructed from  $\mu^+\mu^-$  (a) and  $e^+e^-$  (b); helicity ( $\cos \theta$ ) distribution of  $J/\psi$  from  $\mu^+\mu^-$  (c) and  $e^+e^-$  (d). Vertical axis shows number of events.

The width of the signals are in fair agreement ( $10.43 \pm 0.25 \text{ MeV}/c^2$  for MC vs.  $10.42 \pm 0.06 \text{ MeV}/c^2$  for experimental data). For dimuons case, the MC invariant mass of  $J/\psi$  is close to the experimental mass ( $3097.46 \pm 0.13$  vs.  $3096.78 \pm 0.04 \text{ MeV}/c^2$ ) whereas the Monte Carlo width is a bit narrower than in data ( $8.32 \pm 0.12$  vs.  $9.46 \pm 0.04 \text{ MeV}/c^2$ ).

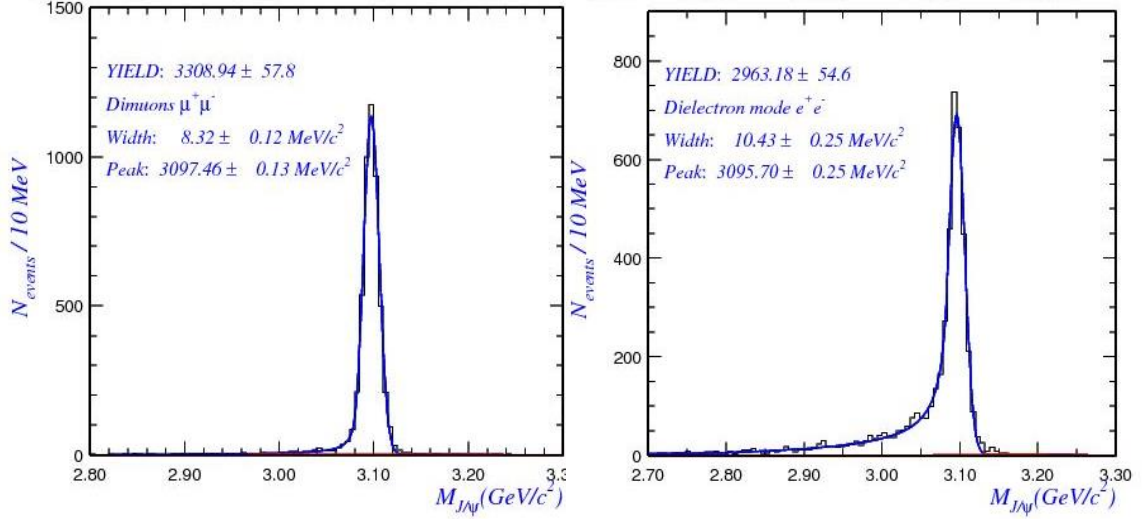


Figure 4.14. Chi square fit to Monte Carlo distribution of  $J/\psi$  reconstructed from  $\mu^+\mu^-$  (left) and  $e^+e^-$  (right) using fit functions Crystal Ball and Chebyshev polynomials of order three.

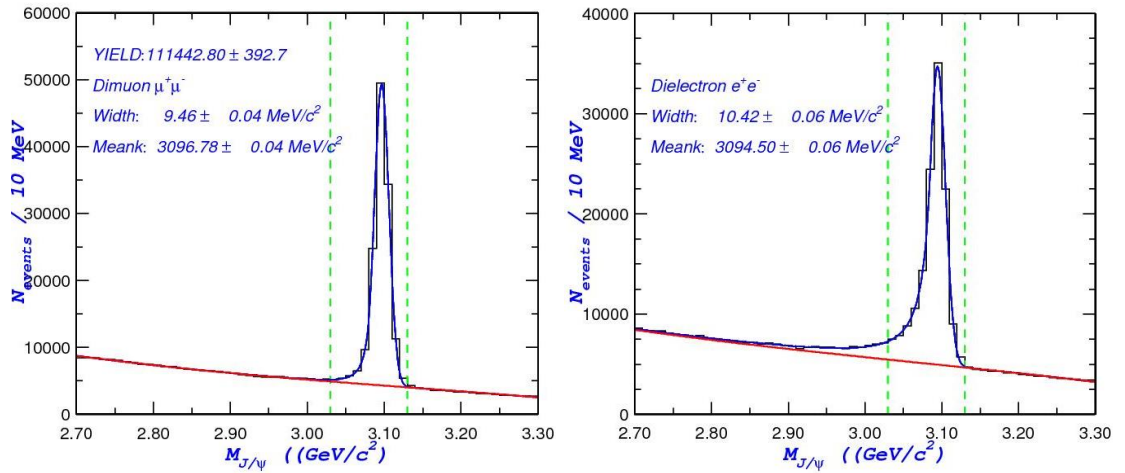


Figure 4.15. The fit to invariant mass distribution for  $J/\psi \rightarrow \mu^+\mu^-$  (left) and  $J/\psi \rightarrow e^+e^-$  (right) from experimental data. The blue and red curves show the signal and the 3rd order Chebyshev polynomial background respectively. The edges of mass windows are indicated by dotted lines.

#### 4.5.2 Standard $\gamma$ Selection Criteria

To select pure  $\gamma$  candidates from reconstructed ECL clusters, following cuts are applied to those clusters:

- Energy cut:  $E_\gamma \geq 1.0 \text{ GeV}$

- ECL match = 0
- Straight  $E_9/E_{25} \geq 0.95$

To reduce the systematic uncertainty, photon candidates detected in the end cap region are rejected. High energy initial state radiations can be suppressed by this selection. We require that the angle of photon candidate against beam axis ( $\theta_\gamma^{lab}$ ), polar angle, is from  $33^\circ < \theta_\gamma^{lab} < 128^\circ$ . When the high momentum  $\pi^0$  and  $\eta$  decay into two photons with asymmetric energies, photons which have higher energy can be background of prompt photon. To suppress the  $\gamma$  coming from  $\pi^0$  or  $\eta$ , we use Koppenburg's (Koppenburg 2004) veto criterion, i.e. probability of photon coming from  $\pi^0$  or  $\eta$ :  $P_{\pi^0} < 0.25$  and  $P_\eta < 0.25$ .

#### 4.5.3 Reconstruction of $B$

$J/\psi$  and  $\gamma$  are combined to form  $B$  candidate. Kinematic parameters used for selecting  $B$  mesons in  $\Upsilon(4S)$  are beam energy constrained mass ( $M_{bc}$ ) and energy difference ( $\Delta E$ ), where  $\Delta E$  is defined as

$$\Delta E = \sum_i E_i^* - E_{beam} \quad (4.9)$$

where  $E_i^*$  is the CM energies of the daughters of  $B$  candidate and  $E_{beam} = \frac{\sqrt{s}}{2}$  is the CM beam energy. The  $\Delta E$  distribution is shown in Figure 4.16.  $M_{bc}$  is defined as

$$M_{bc} = \sqrt{(E_{beam}^2 - \sum_i |\vec{p}_i^*|^2)} \quad (4.10)$$

Where  $\vec{p}_i^*$  is the magnitude of CM 3-momentum of the  $B$  meson decay products. All these parameters are defined in the CM frame of  $\Upsilon(4S)$ . The signal region of  $B$  meson lies within the range of  $5.27 < M_{bc} < 5.29 \text{ GeV}/c^2$  and  $-0.2 < \Delta E < 0.08 \text{ GeV}$ .

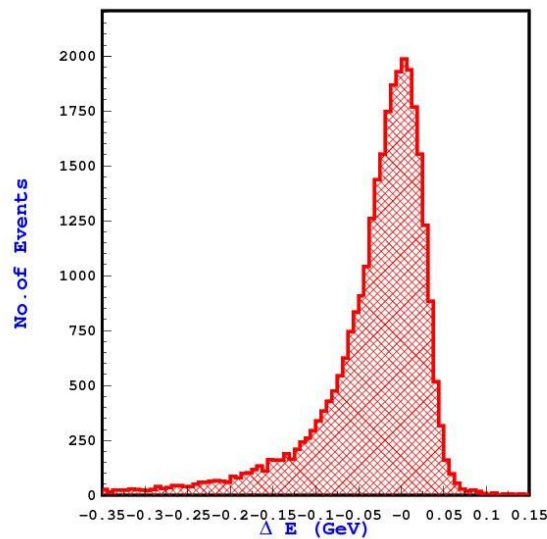


Figure 4.16. The fit to  $\Delta E$  distribution for signal Monte Carlo events.

### Modified $M_{bc}$

$M_{bc}$  resolution is affected by low gamma energy resolution, hence we have used modified  $M_{bc}$ , defined as below:

$$M'_{bc} = \sqrt{E_{beam}^2 - \left( \vec{P}_{J/\psi} + \frac{\vec{P}_\gamma}{|P_\gamma|} \sqrt{E_{beam} - E_{J/\psi}} \right)^2} \quad (4.11)$$

Modified  $M_{bc}$  has an improved resolution as compared to normal  $M_{bc}$ , as shown in Figure 4.17. For the rest of this thesis, modified  $M_{bc}$  will be simply referred by  $M_{bc}$ .

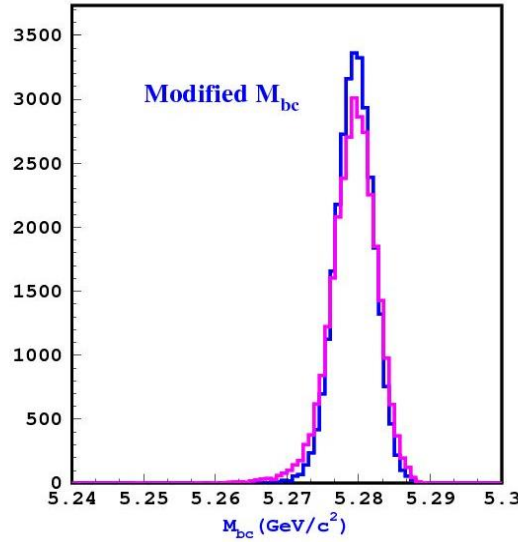


Figure 4.17. The  $M_{bc}$  (red) and modified  $M'_{bc}$  (blue) distribution for signal Monte Carlo.

### Fitting Procedure

To enhance the separation power to extract signal, another fit variable, helicity is chosen such that the distribution of signal and background signals differ significantly. To extract the signal yield, a 3D unbinned extended maximum likelihood (UEML) fit to the variables  $\Delta E$ ,  $M_{bc}$  and  $\cos \theta_{J/\psi}$  (helicity) is used, where helicity angle,  $\theta_{J/\psi}$ , is defined as the angle between  $l^+$  (one of the charged daughters of  $J/\psi$ ) and the negative of the  $B$  flight direction in the  $J/\psi$  rest frame. For the fit, likelihood is defined as

$$\mathcal{L}_{fit} = \frac{e^{-\sum_j N_j}}{N!} \cdot \prod_i^M \left( \sum_j N_j \times \mathcal{P}_j(M_{bc,i}, \Delta E_i, \cos \theta_{J/\psi_i}) \right) \quad (4.12)$$

where  $M$  is the total number of events and  $\mathcal{P}_j(M_{bc,i}, \Delta E_i, \cos \theta_{J/\psi_i})$  is the probability density function (PDF) of the component  $j$  (signal, continuum, and rare  $B$  backgrounds) with number of events  $N_j$ . The correlation between the fit variables are found to be small, and hence the PDF for each of the components can be described as a product of one-dimensional PDF over the fit variables.

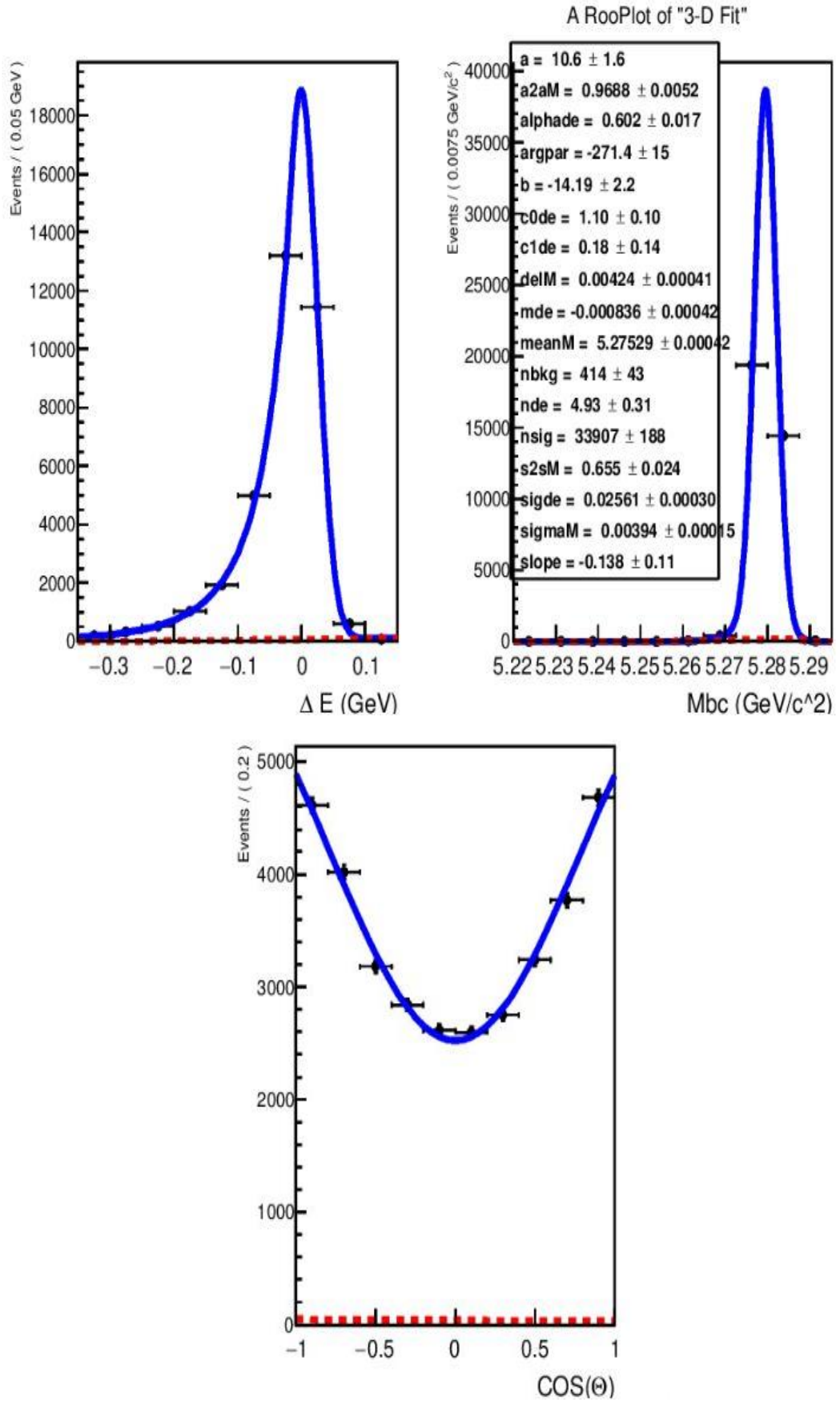


Figure 4.18 Projections of 3D fit for signal Monte Carlo 100,000 events using variables  $\Delta E$ ,  $M_{bc}$  and  $\cos \theta$  (helicity).

## Signal Shape

The signal candidates are obtained in the fitted region selected as:  $-0.35 < \Delta E < 0.15 \text{ GeV}$  and  $5.24 < M_{bc} < 5.30 \text{ GeV}/c^2$ . The signal PDF's obtained from signal Monte Carlo corresponding to 100,000 events are:  $\Delta E$  distribution is described by a sum of Crystal Ball function (Gaiser 1982) and a Chebyshev polynomial of order two.  $M_{bc}$  is modelled using double Gaussian + ARGUS background function (Albrecht H *et al* 1987) and helicity of  $J/\psi$  is modelled by  $a - b \sin^2 \theta$ . The fit to the signal MC is shown in Figure 4.18 and the obtained parameters of the fit are listed in Table 4.2.

**Table 4.2 Parameters obtained by fitting signal MC samples.**

$\Delta E$	$M_{bc}$	$\cos \theta$
$\mu = -0.000836 \pm 0.00042$	$\mu = 5.27529 \pm 0.00042$	$a = 10.6 \pm 1.6$
$\sigma = 0.02561 \pm 0.00030$	$\sigma = 0.00394 \pm 0.00015$	$b = -14.19 \pm 2.2$
$\alpha = 0.602 \pm 0.017$	$\Delta M = 0.00424 \pm 0.00041$	
	Ratio of areas ( $a2aM$ ) = $0.9688 \pm 0.0052$	
	$\sigma_2/\sigma_1$ ( $s2sM$ ) = $0.655 \pm 0.024$	

### 4.5.4 Reconstruction efficiency

After applying all the selection criteria, the reconstruction efficiency is determined from the signal MC using the following relation

$$\epsilon = \frac{N_{fit}}{N_{gen}} \times 100 \quad (4.13)$$

where  $N_{fit}$  is the yield obtained ( $33907 \pm 188$ ) in the signal region obtained from the 3D fit to signal MC events and  $N_{gen}$  represents the total number of generated events. Thus, the reconstruction efficiency is

$$\epsilon(B \rightarrow J/\psi\gamma) = 33.9 \pm 0.19\%$$

## 4.6 Background Study

The background events are the events that appear alongside the signal regions. It is required to suppress the background harming the signal events to calculate the branching fraction properly. It is also required to study the background events separately to reduce it further. The main background contribution in  $B^0 \rightarrow J/\psi\gamma$  decay mode is expected to arise from inclusive  $B$  decays to  $J/\psi$ . To study this type of background, a large simulated MC sample of  $B^0 \rightarrow J/\psi X$  events is used, which corresponds to almost 100 times the integrated luminosity

of the experimental data sample, where  $X$  can be any particle. The  $J/\psi$  mass sidebands study in experimental data is also performed to study non- $J/\psi$  background and found that these types of events are negligible.

#### 4.6.1 Types of background

In order to estimate the background source, officially generated  $J/\psi$  inclusive MC sample is used, which includes signal as well as possible backgrounds known at the time of its generation. Some PDFs used for modelling are: bifurcated Gaussian distribution, which is a Gaussian with a different value of  $\sigma$  on either side of the mean; the Crystal Ball lineshape distribution which consists of a Gaussian signal peak matched to a power law tail. It contains a parameter that determines the crossover point from Gaussian distribution to the power law tail distribution. The various backgrounds are classified as under:

##### Continuum Background

The other background in present analysis is due to continuum events, i.e. events coming from light-quark pair production ( $e^+e^- \rightarrow u\bar{u}, d\bar{d}, s\bar{s}, c\bar{c}$  processes). In  $B\bar{B}$  production,  $B$  meson decay products are distributed spherically. On the other hand, the lighter quarks in continuum events are created with large initial momentum, and these results in disintegration of two jets of light quarks. To find the contribution from continuum background, we analyzed on-resonance Monte Carlo data whose luminosity is 100 times that of experimental data. Scatter plots ( $\Delta E$  vs.  $M_{bc}$ ) for  $e^+e^- \rightarrow cq$  is shown in Figure 4.19, and that of on-resonance  $e^+e^- \rightarrow uds$  background in Figure 4.20. Then, we analysed  $125\text{ fb}^{-1}$  experimental off-resonance data and obtained scatter plot as shown in Figure 4.21. After comparing these data sets, it is clear now that there is no continuum background threat in the present decay mode  $B \rightarrow J/\psi\gamma$ . So, we see that there is not much background in the signal region and continuum can be easily removed by applying  $R_2$  cut.

##### Peaking Background

It is noted from the plots of background of  $\Delta E$  and  $M_{bc}$  distribution that the peaking background is dominated by  $B^0 \rightarrow J/\psi \pi^0$  ( $\pi^0 \rightarrow \gamma\gamma$ ) decay mode,  $B^0 \rightarrow J/\psi K_L$  ( $K_L \rightarrow 3\pi^0$  or  $6\gamma$ ) and  $B^0 \rightarrow J/\psi \eta$  ( $\eta \rightarrow \gamma\gamma$ ). To suppress these backgrounds, we veto these photons that when combine with another photon of energy  $E_\gamma > 60\text{ MeV}$  and form a  $\pi^0(\eta)$  candidate.

The Second category of background comes from  $B \rightarrow J/\psi K_S$  and  $B \rightarrow J/\psi K_L$  corresponding to  $165.26 \pm 2.74$  events. 3D fit projections to various backgrounds is shown in Figure 4.22, where the color coding is green- $\eta$ , light blue- $\pi$ , black- $K_L, K_S$  and yellow-other backgrounds. As it is clear from Figure 4.22, these components of background have distinct



characteristics in  $\Delta E$  distribution but have similar  $M_{bc}$  distributions. The different backgrounds are modelled by different PDFs, details of which are given in Table 4.3.

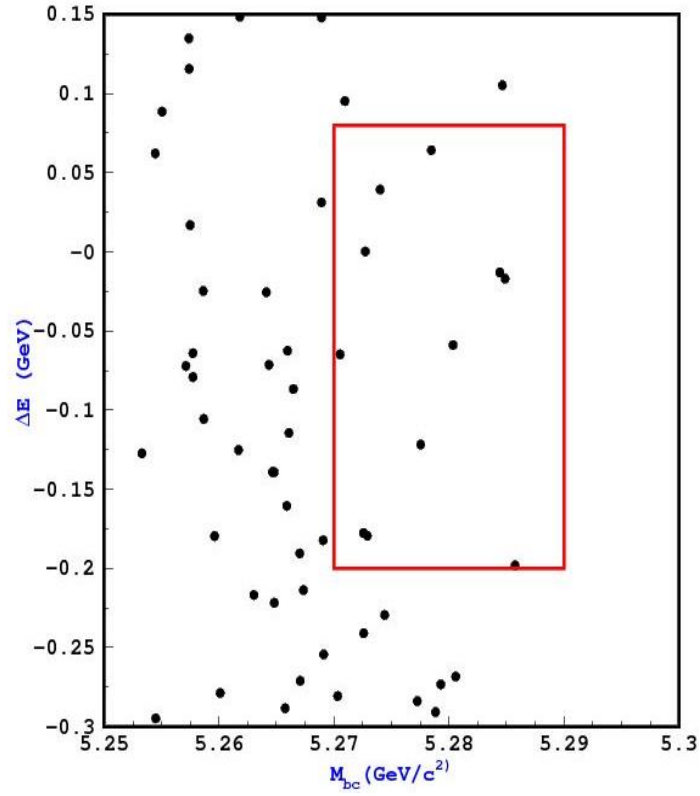


Figure 4.19. On-resonance charmed background  $e^+e^- \rightarrow cq$ .

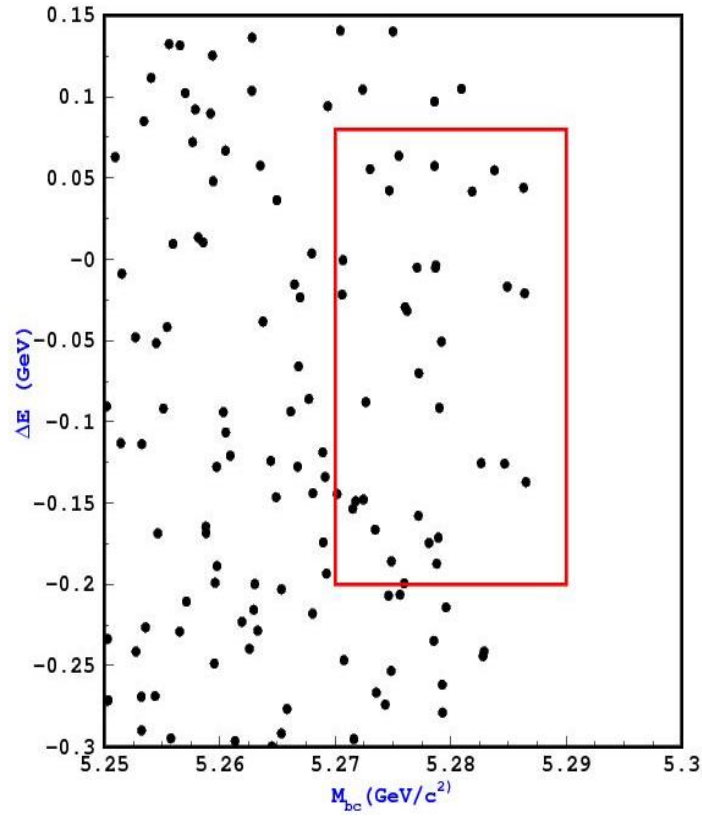


Figure 4.20. On-resonance  $e^+e^- \rightarrow uds$  background.

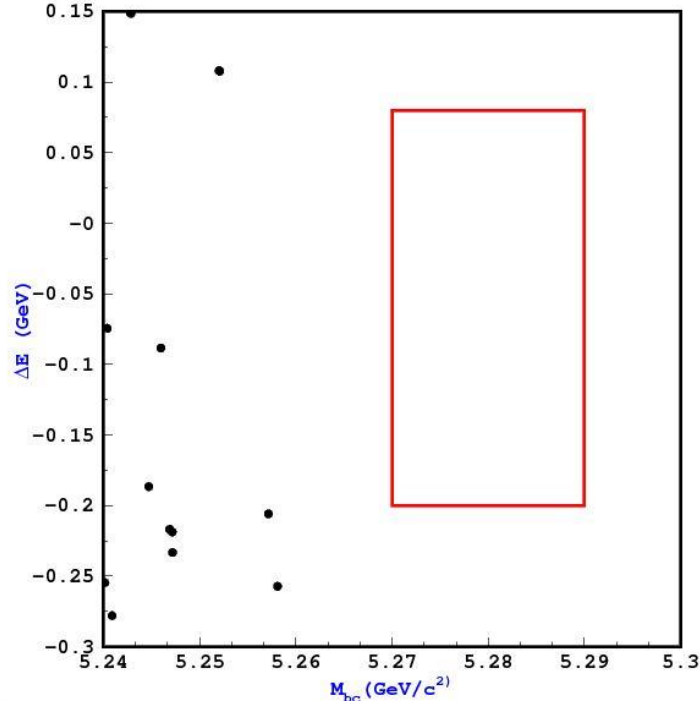


Figure 4.21. Continuum background from real data taken at 60 MeV below 10.58 GeV (off-resonance).

### Combinatorial Background

The third category of background for  $B^0 \rightarrow J/\psi\gamma$  decay mode is the combinatorial background (or rest backgrounds). The  $\Delta E$  and  $M_{bc}$  distribution does not have any peaking structure from this background and is modelled by using Chebyshev polynomial of order four for  $\Delta E$  distribution and in  $M_{bc}$ , it is modelled by ARGUS background.

Table 4.3. Details of parameters used to model various backgrounds.

Background Type	$\Delta E$	$M_{bc}$	$\cos \theta$
$B \rightarrow J/\psi\pi^0$	Sum of two Gaussians + Bifurcated Gaussian	Sum of two Gaussians + Bifurcated Gaussian	$a - b \sin^2 \theta$
$B \rightarrow J/\psi\eta$	Bifurcated Gaussian	Bifurcated Gaussian	$a - b \sin^2 \theta$
$B \rightarrow J/\psi(K_S + K_L)$	Sum of two Bifurcated Gaussians	Crystal Ball + Bifurcated Gaussian	$a - b \sin^2 \theta$
Rest backgrounds	4 <sup>th</sup> order Chebyshev polynomial	ARGUS	$a - b \sin^2 \theta$

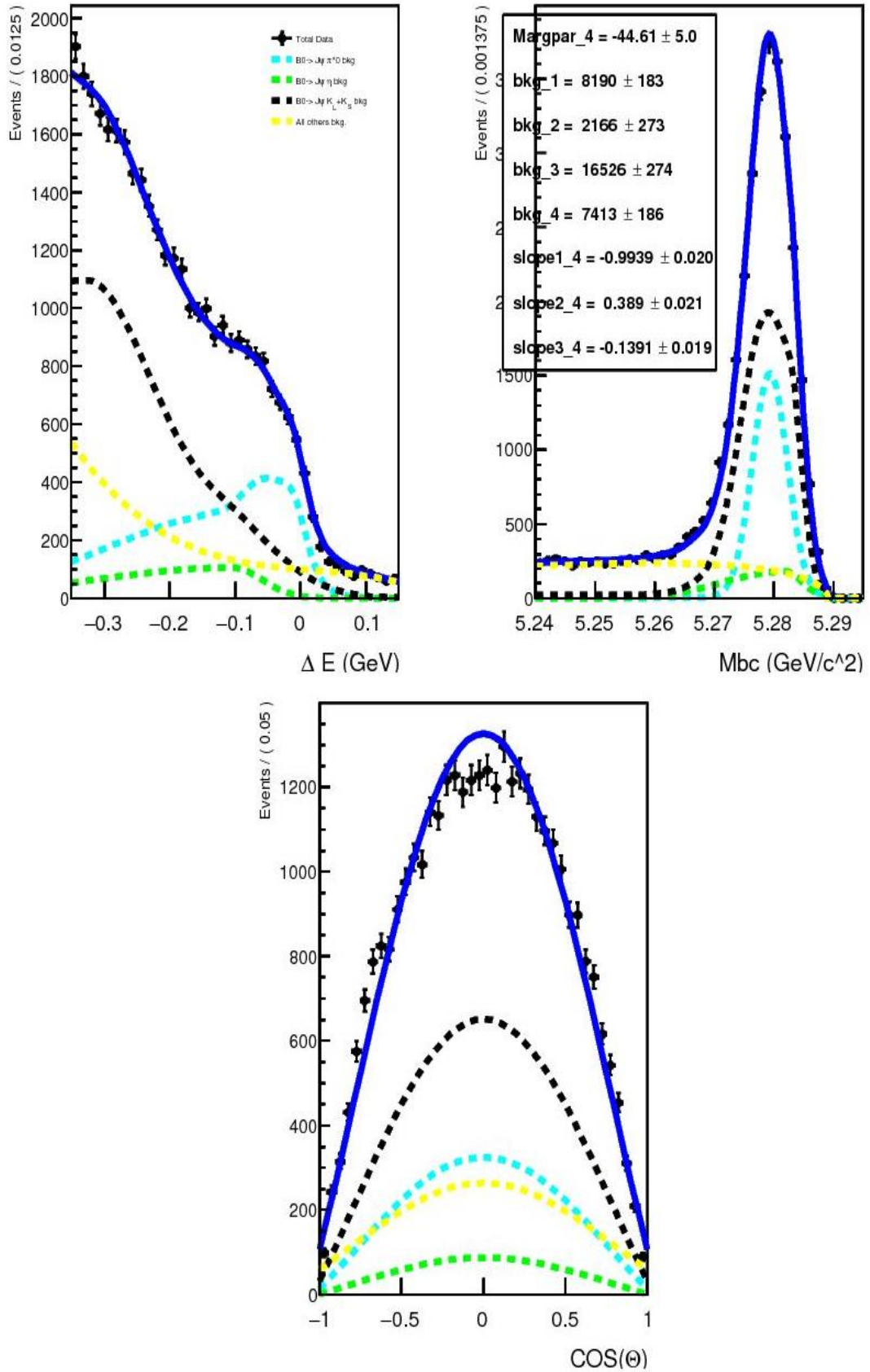


Figure 4.22. A 3D fit for different backgrounds Monte Carlo using variables  $\Delta E$ ,  $M_{bc}$  and  $\cos \theta$  (helicity). Color coding: green- $\eta$ , light blue- $\pi$ , black- $K_L, K_S$  and yellow-other backgrounds.

## 4.7 Conclusion

For the study of rare decay  $B \rightarrow J/\psi\gamma$ , we investigated the shapes of various backgrounds. The peaking backgrounds in the signal region are  $B \rightarrow J/\psi\eta$  and  $B \rightarrow J/\psi\pi^0$  corresponding to  $103.56 \pm 3.29$  events. Whereas,  $B \rightarrow J/\psi K_S$  and  $B \rightarrow J/\psi K_L$  are not peaking in  $\Delta E$  but are peaking in  $M_{bc}$  signal region. Helicity shape of  $J/\psi$  is different for signal and backgrounds and hence it is a powerful tool to extract the signal. Continuum study has been performed and we found that no threat from continuum in our signal region. The reconstruction efficiency obtained for signal  $B \rightarrow J/\psi\gamma$  from the 3D fit is  $33.9 \pm 0.19\%$ .

## CHAPTER V

### SUMMARY

The study performed in this thesis uses data collected by Belle detector at KEKB  $e^+e^-$  asymmetric collider during its long run (1998-2010) with  $e^-$  and  $e^+$  circulating with energies 8 GeV and 3.5 GeV respectively, producing a Lorentz boost of 0.425. The data used for this analysis is collected at centre-of-mass (CM) energy  $\sqrt{s} (= \sqrt{4E_{e^+}E_{e^-}}) = 10.58$  GeV, which is equal to the mass of  $\Upsilon(4S) = b\bar{b}$  resonance, which upon forming instantaneously decays into  $B\bar{B}$  pairs, and which further decay via various possible modes very quickly, within the innermost detector. The decay products move through the detector layers. The finally detected particles in the detector sub-layers are  $e^\pm, \mu^\pm, \pi^\pm, K^\pm, p, \bar{p}, \gamma$ . Belle collected  $772 \times 10^6$   $B\bar{B}$  pairs and this provides huge statistics for performing the analysis of a rare decay.

$B$  mesons are a bound state of  $b$  quark and a light anti-quark ( $u$  or  $d$ ), e.g.,  $B^0$  constitutes  $d\bar{b}$ . They have spin  $J = 0$ , isospin  $I = 1/2$  and negative parity ( $P = -1$ ). Mass of  $B^0$  is  $5.279 \text{ GeV}/c^2$  and lifetime is approximately  $1.5 \times 10^{-12} \text{ s}$ .  $B$  mesons contain quarks of the third generation and thus their decays offer great opportunity to measure the CKM matrix elements  $V_{cb}, V_{ub}, V_{ts}$  and  $V_{td}$  which describe the couplings of the third generation of quarks to the quarks of first and second generations.

In this thesis,  $B \rightarrow J/\psi\gamma$  decay mode is studied, which is a very rare decay and is sensitive probe of physics beyond the SM. Charmonium ( $J/\psi$ ) meson is the bound state of  $c$  and  $\bar{c}$  quarks.  $J/\psi$  is a vector meson with spin 1 and photon ( $\gamma$ ) also has spin 1. So the decay is a pseudoscalar to vector-vector ( $S \rightarrow VV$ ) kind. In the annihilation decay  $B \rightarrow J/\psi\gamma$ , potential sign of New Physics comes from the possibility of (V+A) charged current admixture (Lu, Wang and Yang 2004)) to the standard (V-A) current. Also, CKM suppressed decay mechanisms involving possibility of non-spectator intrinsic charm in the  $B$  meson (Brodsky and Gardner 2002) points towards NP. Our main motive behind this study is to search for this decay mode as it has not been seen yet. BaBar first sought the radiative decay at PEP-II, SLAC from a dataset of 123 million  $\Upsilon(4S) \rightarrow B\bar{B}$  decays. They found no evidence for the signal and they placed an upper limit of  $\mathcal{B}(B^0 \rightarrow J/\psi\gamma) < 1.6 \times 10^{-6}$  at 90% confidence level (Aubert 2004). LHC group also performed a study on this decay using data collected by the experiment at  $\sqrt{s} = 7$  and 8 TeV corresponding to integrated luminosity of  $3 \text{ fb}^{-1}$ . They also set an upper limit which agrees with limit given by BaBar. As Belle has collected large amount of data of  $772 \times 10^6$   $B\bar{B}$  pairs, we have a good opportunity to use this to find an evidence of the decay or to put a precise upper limit.

The analysis tools used to perform the analysis are event generator EvtGen (Lange 2001), GEANT4, ROOT. EvtGen is a software that can simulate the physical processes of particle's decay, and is specialised for  $B$  physics. This is used to generate signal Monte Carlo (MC) events. GEANT4 package simulates detector response and particle behaviour through the sub-detectors. To calculate the reconstruction efficiency for the decay, 100,000 events are generated. The decay model used for  $Y(4S) \rightarrow B\bar{B}$  is VSS (vector to scalar-scalar) and for the decay  $B \rightarrow J/\psi\gamma$ , PHOTOS (Barberio, Eijk, and Was 1991) SVP\_HELAMP (scalar to vector and photon) is adopted.  $J/\psi \rightarrow l^+l^-$  is modelled by PHOTOS VLL (vector to lepton-lepton). Also, background, which comes from detector noise and beam, is added to these events. The generated particles are tracked through the detector in the Belle detector simulation (GSIM), based on the GEANT platform. The simulated file is passed through physics analysis code written in C++ programming language. The output ROOT file is analyzed to obtain histograms, etc., using ROOT software.

We used the identified tracks of final state particles ( $e^\pm, \mu^\pm, \gamma$ ) to reconstruct the signal.  $J/\psi$  decays into oppositely charged lepton pairs ( $e^+e^-$  or  $\mu^+\mu^-$ ). Leptons are selected by starting with charged tracks satisfying  $|dz| < 4.0$  cm, where  $dz$  is the track's closest approach to the interaction point along the beam direction and  $|dr| < 0.4$  cm, to remove charged particle tracks that are poorly measured or do not come from the interaction region. For electron identification, the ratio between the charged track's momentum and the associated shower energy ( $E/p$ ) is the most powerful discriminant. Other information including  $dE/dx$  and the shower shape are also used. Muons are identified by requiring an association between KLM hits and an extrapolated track in CDC. Tracks of both leptons must be positively identified as such. In the  $e^+e^-$  mode, electrons may emit photons by bremsstrahlung, and hence, ECL clusters that lie within  $50$  mrad of the track's initial momentum vector are incorporated in for computing the invariant mass  $M_{e^+e^-}$ . Photon candidates should not have a charged track associated to them, and the cluster shape must be consistent with that of electromagnetic shower. The invariant masses of  $e^+e^-$  and  $\mu^+\mu^-$  combinations are required to fall in the ranges  $3.03 \text{ GeV}/c^2 < M_{\mu\mu} < 3.13 \text{ GeV}/c^2$  and  $2.94 \text{ GeV}/c^2 < M_{e^+e^-} < 3.13 \text{ GeV}/c^2$ , respectively, where  $M_{l^+l^-}$  is the invariant mass of a lepton pair.

The energy difference,  $\Delta E = E_B^* - E_{beam}^*$ , the beam-constrained mass  $M_{bc} = \sqrt{E_{beam}^{*2} - p_B^{*2}}$  and helicity ( $\cos \theta$ ) of  $J/\psi$  are used for signal extraction, where  $E_{beam}^*$  is the beam energy (run dependent),  $p_B^*$  and  $E_B^*$  are the momentum and energy, respectively, of the reconstructed  $B$  mesons in the CM frame. Helicity shape of  $J/\psi$  is different for signal and backgrounds and hence it is a powerful tool to extract the signal. Reconstruction of  $B^0$  from  $J/\psi$  and  $\gamma$  is carried out using  $\Delta E$  in the range  $-0.20 < \Delta E < 0.08 \text{ GeV}$  and  $5.27 < M_{bc} <$

$5.29 \text{ GeV}/c^2$ , where  $M_{bc}$  is the modified beam-energy-constrained mass, since its resolution is better than simple  $M_{bc}$ . For signal yield extraction, a 3D unbinned extended maximum likelihood fit to the variables  $\Delta E$ ,  $M_{bc}$  and  $\cos \theta_{J/\psi}$  (helicity) is performed, where helicity angle,  $\theta_{J/\psi}$ , is defined as the angle between  $l^+$  (one of the charged daughters of  $J/\psi$ ) and the negative of the  $B$  flight direction in the  $J/\psi$  rest frame. The signal candidates are obtained by applying the cuts:  $-0.35 < \Delta E < 0.15 \text{ GeV}$  and  $5.24 < M_{bc} < 5.30 \text{ GeV}/c^2$ . The signal PDF's used to model shapes of signal variables as:  $\Delta E$  distribution is fitted by a sum of Crystal Ball function (Gaiser 1982) and a Chebyshev polynomial of order two.  $M_{bc}$  is modelled using double Gaussian + ARGUS (Albrecht H *et al* 1987) and  $\cos \theta$  is modelled by  $a - b \sin^2 \theta$ . The reconstruction efficiency is calculated to be  $33.9 \pm 0.19\%$ .

For background study, large sample of  $B \rightarrow J/\psi X$  inclusive MC sample is used, which corresponds to almost 100 times the integrated luminosity of the experimental data sample, where  $X$  can be any particle. Continuum background ( $e^+e^- \rightarrow u\bar{u}, d\bar{d}, s\bar{s}, c\bar{c}$  processes) study is performed. In  $B\bar{B}$  production,  $B$  meson decay products are distributed spherically. On the other hand, the lighter quarks in continuum events are created with large initial momentum, and these results in disintegration of two jets of light quarks. We found that there is no threat from continuum and it is sufficient to apply  $R_2 < 0.5$  ( $R_2$  is the ratio of second to zeroth Fox-Wolfram moments) to remove it. The peaking background is dominated by  $B^0 \rightarrow J/\psi \pi^0$  ( $\pi^0 \rightarrow \gamma\gamma$ ) and  $B^0 \rightarrow J/\psi \eta$  ( $\eta \rightarrow \gamma\gamma$ ) decays. Other major background is  $B^0 \rightarrow J/\psi K_L$  ( $K_L \rightarrow 3\pi^0$  or  $6\gamma$ ). To suppress these backgrounds, we veto these photons that when combine with another photon of energy  $E_\gamma > 60 \text{ MeV}$  and form a  $\pi^0(\eta)$  candidate, using Koppenburg's (Koppenburg 2004) veto criterion, i.e. probability of photon coming from  $\pi^0$  or  $\eta$ :  $P_{\pi^0} < 0.25$  and  $P_\eta < 0.25$ . The peaking backgrounds  $B \rightarrow J/\psi \eta$  and  $B \rightarrow J/\psi \pi^0$  correspond to  $103.56 \pm 3.29$  events. Whereas,  $B \rightarrow J/\psi K_S$  and  $B \rightarrow J/\psi K_L$  are not peaking in  $\Delta E$  but are peaking in  $M_{bc}$  signal region.

## REFERENCES

- Aad G *et al* ATLAS Collaboration (2012) Observation of a new particle in the search for the Standard Model Higgs boson with the ATLAS detector at the LHC. *Phy Lett B* **716**:1.
- Aaij R *et al* (2015) Search for the decays  $B^0 \rightarrow J/\psi\gamma$  and  $B_s^0 \rightarrow J/\psi\gamma$ . *Phys Rev D* **92**: 112002.
- Abachi S *et al* (1995) Search for high mass top quark production in  $p\bar{p}$  collision at  $s=1.8$  TeV. *Phys Rev Lett* **74**:2422-26.
- Abashian A *et al* (2000) The  $K_L/\mu$  detector subsystem for the BELLE experiment at the KEKB factory. *Nucl Instrum Meth A* **449**:112-24.
- Abashian A *et al* (2002) (Belle Collaboration) The Belle Detector. *Nucl Instrum Meth A* **479**:117-232.
- Abashian A *et al* (2002a) Muon identification in the Belle experiment at KEKB. *Nucl. Instrum. Meth. A* **491**: 69-82.
- Abe F *et al* CDF Collaboration (1995) Observation of top quark production in  $\bar{p}p$  collisions with the collider detector at Fermilab. *Phys Rev Lett* **74**: 2626-31.
- Abe K *et al* Belle Collaboration (2001) Observation of  $CP$  violation in the neutral  $B$  meson system. *Phys Rev Lett* **87**:091802.
- Agostinelli S *et al* (2003) GEANT4 - a simulation toolkit. *Nucl Instrum Meth A* **506**:250-303.
- Akai K *et al* (2018) SuperKEKB Collider. *Nucl. Instrum. Meth. Phys. Res. A*
- Albrecht H *et al* (1987) Observation of  $B^0 - \bar{B}^0$  Mixing. *Phys Lett B* **192**:245-52.
- Anderson C D (1933) The positive electron. *Phys Rev* **43**:491-94.
- Andrews D *et al* (1980) Observation of a fourth upilon state in  $e^+e^-$  annihilations. *Phys Rev Lett* **45**:219.
- Ansari R *et al* UA2 Collaboration (1987) Measurement of  $W$  and  $Z$  production properties at the CERN  $pp$  collider. *Phys Lett B* **194**:158-66.
- Aubert B *et al* BABAR Collaboration (2001) Observation of  $CP$  violation in the  $B^0$  meson system. *Phys Rev Lett* **87**:091801.
- Aubert B *et al* BABAR Collaboration (2004) Search for the decay  $B^0 \rightarrow J/\psi\gamma$ . *Phys Rev D* **70**: 091104.
- Aubert J J *et al* (1974) Experimental observation of a heavy particle  $J$ . *Phys Rev Lett* **33**:1404-06.
- Augustin J E *et al* (1974) Discovery of a narrow resonance in  $e^+e^-$  annihilation. *Phys Rev Lett* **33**:1406-08.
- Barberio E, van Eijk B, and Was Z (1991) PHOTOS: A Universal Monte Carlo for QED radiative corrections in decays. *Comput. Phys. Commun.* **66**: 115-128.



- Barish B *et al* (1996) Measurement of the  $B$  semileptonic branching fraction with lepton tags. *Phys Rev Lett* **76**:1570.
- Bartel W *et al* (1982) Upper limit on beauty lifetime and lower limit on weak mixing angles. *Phys Lett B* **114**:71-5.
- Behrends S *et al* (1983) Observation of exclusive decay modes of  $b$ -flavored mesons. *Phys Rev Lett* **50**:881.
- Beringer J *et al* (2012) Review of Particle Physics. *Phys Rev D* **86**:45-57.
- Bigi I I and Sanda A I (1984)  $B^0$ - $\bar{B}^0$  mixing and violation of  $CP$  symmetry. *Phys Rev D* **29**:1393-8.
- Brodsky S J and Gardner S (2002) Evading the CKM hierarchy: Intrinsic charm in  $B$  decays. *Phys Rev* **65**: 054016.
- Buchmuller W, Peccei R D and Yanagida T (2005) Leptogenesis as the origin of matter. *Ann Rev Nucl Part Sci* **55**:311-55.
- Carosi R *et al* (1990) A measurement of the phases of the  $CP$  violating amplitudes in  $K^0 \rightarrow 2\pi$  decays and a test of  $CPT$  invariance. *Phys Lett B* **237**:303-12.
- Carter A B and Sanda A I (1981)  $CP$  Violation in  $B$ -meson decays. *Phys Rev D* **23**:1567-79.
- Chao Y *et al* Belle Collaboration (2004) Evidence for Direct  $CP$  Violation in  $B^0 \rightarrow K^+\pi^-$  decays. *Phys Rev Lett* **93**:191802.
- Chatrchyan S *et al* CMS Collaboration (2012) Observation of a new boson at a mass of 125 GeV with the CMS experiment at the LHC. *Phys Lett B* **716**:1.
- Christenson J H, Cronin J W, Fitch V L and Turlay R (1964) Evidence for the  $2\pi$  Decay of the  $K_2^0$  Meson. *Phys Rev Lett* **13**:138-40.
- Danby G *et al* (1962) Observation of high energy neutrino reactions and the existence of two kinds of neutrinos. *Phys Rev Lett* **9**:36.
- Eichten E *et al* (2008) Quarkonia and their transitions. *Rev Mod Phys* **80**:1161-93.
- Fernandez E *et al* (1983) Lifetime of particles containing  $b$  quarks. *Phys Rev Lett* **51**:1022.
- Feynman R P (1948) Space-time approach to non-relativistic quantum mechanics. *Rev Mod Phys* **20**:367-87.
- Fox G C and Wolfram S (1978) Observables for the analysis of event shapes in  $e^+e^-$  annihilation and other processes. *Phys Rev Lett* **41**:1581.
- Gaiser J E (1982) Charmonium spectroscopy from radiative decays of the J/psi and psi prime: Appendix-F. Pp 178. PhD Thesis. SLAC-R-255, United States.
- Gell-Mann M (1964) A schematic model of baryons and mesons. *Phys Lett* **8**:214-15.
- Glashow S L (1961) Partial-symmetries of weak interactions. *Nucl Phys* **22**:579-88.

- Goldhaber G (1992) From the  $\psi$  to charmed mesons: Three years with the SLAC-LBL detector at SPEAR. *Proc of the Third International Symposium: The History of Particle Physics "The Rise of the Standard Model"*, Stanford, CA. June 25 LBL-32514 UC-414 Lawrence Berkeley Laboratory, University of California, CA.
- Hanagaki K *et al* (2000) The Level 4 Software Trigger at BELLE. *Belle Internal Note* 299.
- Hanagaki K *et al* (2002) Electron identification in Belle. *Nucl. Instrum. Meth. A* **485**: 490-503.
- Herb S W *et al* (1977) Observation of a dimuon resonance at 9.5 GeV in 400 GeV proton-nucleus collisions. *Phys Rev Lett* **39**:252-55.
- Higgs P W (1966) Spontaneous symmetry breakdown without massless bosons. *Phys Rev* **145**:1156.
- Hirano H *et al* (2000) A high-resolution cylindrical drift chamber for KEK B-Factory. *Nucl Instrum Meth A* **455**:294-304.
- Iijima T *et al* (2000) Aerogel Cherenkov Counter for the BELLE detector. *Nucl Instrum Meth A* **453**:321-25.
- Ikeda H *et al* (2000) A detailed test of the CsI(Tl) calorimeter for BELLE with photons beam of energy between 20 MeV and 5.4 GeV. *Nucl Instrum Meth A* **441**:401-26.
- Innes W R *et al* (1977) Observation of structure in the Y region. *Phys Rev Lett* **39**:1240.
- Islam M M and Rosen J (1969) High energy  $pp$  scattering and proton substructure. *Phys Rev Lett* **22**:502.
- Kawasaki T (2002) The Belle silicon vertex detector. *Nucl Instrum Meth A* **494**: 94101.
- Kichimi H *et al* (2000) The BELLE TOF system. *Nucl Instrum Meth A* **453**:315-20.
- Kobayashi M and Maskawa T (1973)  $CP$  violation in the Renormalizable theory of weak interaction. *Prog Theor Phys* **49**:652-57.
- Kodama K *et al* DONUT collaboration (2001) Observation of tau neutrino interactions. *Phys Lett B* **504**:218-24.
- Koppenburg P (2004) Internal Belle Note 665.
- Kurokawa S and Kikutani E (2003) Overview of the KEKB Accelerator. *Nucl Instrum Meth A* **499**:1-7.
- Lange D J (2001) The EvtGen particle decay simulation package. *Nucl Instrum Meth A* **462**:152-55.
- Lu G, Wang R and Yang Y D (2004) The rare radiative annihilation decays  $\bar{B}_{s,d}^0 \rightarrow J/\psi\gamma$ . *Eur Phys Jour C* **34**:291
- Nakamura K *et al* Particle Data Group (2010) Review of particle physics. *Nucl Part Phys* **37**:075021.

- Nambu Y (1979) QCD and the String Model. *Phys Lett B* **80**:372-76.
- Neddermeyer S H and Anderson C D (1937) Note on the nature of cosmic-ray particles. *Phys Rev* **51**:884.
- Oddone P (1987) Detector considerations. *Proc. of UCLA Linear-Collider BB Factory Concep. Design.* pp 423-446.
- Perepelitsa D V (2008) Sakharov conditions for baryogenesis. Columbia University Department of Physics.
- Perl M L *et al* (1975) Evidence for anomalous lepton production in  $e^+e^-$  annihilation. *Phys Rev Lett* **35**:1489-92.
- Peruzzi I (1983) Measurement of the  $b$  lifetime with MAC. *Invited talk at Como Workshop "Search for heavy flavours"* Como, August 27-30, LNF-83/76(P). Laboratori Nazionali di Frascati, Frascati, Italy.
- Reines F and Cowan Jr C L (1953) Detection of the free neutrino. *Phys Rev* **92**, 830.
- Rubakov V A and Shaposhnikov M E (1996) Electroweak baryon number non-conservation in the early universe and in high-energy collisions. *Phys Usp* **39**:461-502.
- Sakharov A D (1967) Violation of  $CP$  Symmetry,  $C$  asymmetry and baryon asymmetry of the universe. *Pisma ZH Eksp Teor Fiz* **5**:32-35.
- Sakurai J J (1994) *Modern Quantum Mechanics*. Pp. 61, revised edition. Addison-Wesley Publishing Company, California.
- Salam A (1968) Elementary particle physics: Relativistic groups and analyticity. I: Svartholm N (ed). *Eighth Nobel Symposium. Stockholm: Almquist and Wiksell*. Pp 367.
- Schwinger J (1954) The theory of quantized field VI. *Phys Rev* **94**:1362-84.
- Street J C and Stevenson E C (1937) New evidence for the existence of a particle of mass intermediate between the proton and electron. *Phys Rev* **52**: 1003.
- Toge N *et al* (1995) KEKB  $B$ -factory design report. *KEK Report* **95-7**.
- Toker O *et al* (1994) VIKING, a CMOS low noise monolithic 128 channel frontend for Si-strip detector readout. *Nucl Instrum Meth A* **340**: 572-79.
- Tomonaga S (1946) On a relativistically invariant formulation of the quantum theory of wave fields. *Prog Theor Phys (Kyoto)* **1**:27-42.
- Ushiroda Y (2003) Belle silicon vertex detectors. *Nucl Instrum Meth A* **511**:6
- Ushiroda Y *et al* (1999) Development of the central trigger system for the BELLE detector at the KEKB factory. *Nucl Instrum Meth A* **438**:460-71.
- Weinberg S (1967) A model of leptons. *Phys Rev Lett* **19**:1264-66.

- Wolfenstein L (1983) Parametrization of the Kobayashi-Maskawa matrix. *Phys Rev Lett* **51**: 1945.
- Yamamoto Y *et al* (2010) Beam commissioning status of superconducting Crab Cavities in KEKB. *Conf. Proc.* C100523, MOOCMH03.
- Yang C N and Mills R L (1954) Conservation of isotopic spin and isotopic gauge invariance. *Phys Rev* **96**:191.
- Yukawa H (1934) On the interaction of elementary particles. *PTP* **17**:48.
- Zweig G (1964) An SU(3) Model for strong interaction symmetry and its breaking. *CERN Report No.* 8182-TH-401.

## **VITA**

**Name of the student** : Titiksha Dua  
**Father's name** : Mr. Bharat Bhushan Dua  
**Mother's name** : Mrs. Sunita Dua  
**Nationality** : Indian  
**Date of birth** : 20-03-1995  
**Permanent Home Address** : B-34, 3979/1, Post Office St. Durga Puri,  
Haibowal Kalan, Ludhiana, Punjab

## **EDUCATIONAL QUALIFICATION**

**Bachelor degree** : B.Sc. (Non-Medical)  
**University and year of award** : Panjab University, Chandigarh  
2016  
**%age** : 76.70%  
**Master's degree** : M.Sc. (Physics)  
**University and year of award** : Punjab Agricultural University, Ludhiana  
2019  
**OCPA** : 7.88/10.00  
**Title of Master's Thesis** : Branching ratio measurement for rare  
annihilation decay  
**Awards/Distinctions/Scholarships/  
Fellowships** : Received Merit Certificate in Fine Arts during  
Master's degree program.

### **Publications in Conferences:**

Titiksha and Kumar R (2017) “Prospects of SuperKEKB and present status of CKM angles”. 5<sup>th</sup> IAPT-National Student Symposium on Physics held at Punjab University, Chandigarh during November 10-12.

Titiksha and Kumar R (2018) “Silicon Vertex Detector for Belle II experiment”. 21<sup>st</sup> Punjab Science Congress held at Punjab Agricultural University during February 7-9.

### **Conferences Attended:**

Attended “4<sup>th</sup> IAPT-National Student Symposium on Physics” held at held at Punjab University, Chandigarh during November 4-6, 2016.

Attended “20<sup>st</sup> Punjab Science Congress” held at IET, Bhaddal during February 7-9, 2017.

Attended “5<sup>th</sup> IAPT-National Student Symposium on Physics” held at held at Punjab University, Chandigarh during November 10-12, 2017.

Attended “**Belle Analysis Workshop (BAW)-2017**” held at Malviya National Institute of Technology, Jaipur during November 29- December 2, 2017.

Attended “21<sup>st</sup> Punjab Science Congress” held at Punjab Agricultural University during February 7-9, 2018.

Attended “6<sup>th</sup> IAPT-National Student Symposium on Physics” held at held at Punjab University, Chandigarh during October 10-12, 2018.